STUDIES ON MAGNETICALLY CONSTRICTED ANODE PLASMA SOURCE

By

SAMIRSINH GANPATSINH CHAUHAN

PHYS06201104008

INSTITUTE FOR PLASMA RESEARCH, BHAT

GANDHINAGAR 382428, INDIA

A thesis submitted to the
Board of Studies in Physical Sciences

In partial fulfillment of the requirements
for the degree of

DOCTOR OF PHILOSOPHY

of

HOMI BHABHA NATIONAL INSTITUTE
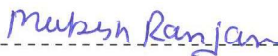

April 2017

Homi Bhabha National Institute

Recommendations of the Viva Voce Committee

As members of the Viva Voce Committee, we certify that we have read the dissertation prepared by **Mr. Samirsinh Ganpatsinh Chauhan** entitled "STUDIES ON MAGNETICALLY CONSTRICTED ANODE PLASMA SOURCE" and recommend that it may be accepted as fulfilling the thesis requirement for the award of Degree of Doctor of Philosophy.

--- Date : 07/ 08/ 2017

Chairman : Dr. Mainak Bandyopadhyay

--- Date : 07/ 08/ 2017

Guide/ Convener : Dr. Mukesh Ranjan

--- Date : 07/ 08/ 2017

Examiner : Dr. Suraj Kumar Sinha

--- Date : 07/ 08/ 2017

Co-Guide : Prof. S. Mukherjee

--- Date : 07/ 08/ 2017

Member : Dr. N. Ramasubramanian

--- Date : 07/ 08/ 2017

Member : Dr. G. Ravi

Final approval and acceptance of this thesis is contingent upon the candidate's submission of the final copies of the thesis to HBNI.

I hereby certify that I have read this thesis prepared under my direction and recommend that it may be accepted as fulfilling the thesis requirement.

--- Date : 07/ 08/ 2017
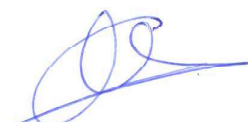
Guide : Dr. Mukesh Ranjan   **Place:** IPR, Gandhinagar

STATEMENT BY AUTHOR

This dissertation has been submitted in partial fulfillment of requirements for an advanced degree at Homi Bhabha National Institute (HBNI) and is deposited in the Library to be made available to borrowers under rules of the HBNI.

Brief quotations from this dissertation are allowable without special permission, provided that accurate acknowledgement of source is made. Requests for permission for extended quotation from or reproduction of this manuscript in whole or in part may be granted by the Competent Authority of HBNI when in his or her judgement the proposed use of the material is in the interests of scholarship. In all other instances, however, permission must be obtained from the author.

Samirsinh Chauhan

DECLARATION

I, hereby declare that the investigation presented in the thesis has been carried out by me. The work is original and the work has not been submitted earlier as a whole or in part for a degree/diploma at this or any other Institution/University.

Samirsinh Chauhan

List of Publications arising from the thesis

Journal:

1. **Droplet shaped anode double layer and electron sheath formation in magnetically constricted anode**

   S. Chauhan, M. Ranjan, M. Bandyopadhyay, S. Mukherjee. *Phys. Plasmas* **23**, 01352, (2016).

2. **Observation of mode transition and low-frequency oscillations in magnetically constricted anode**

   S. Chauhan, M. Ranjan, M. Bandyopadhyay, S. Mukherjee. *Phys. Plasmas* **23**, 123524, (2016).

3. **Plasma fireball: A unique tool to fabricate structured nanodots**

   S. Chauhan, T. Barman, M. Bhatnagar, M. Ranjan, S. Mukherjee. *Rev. Sci. Instrum.* **88**, 063507 (2017)

Conferences Presentations:

1. **Reverse polarity planar magnetron plasma source**

   S. Chauhan, M. Ranjan, S. Mukherjee. *Sokendai Asian Winter school, AWS 2013*, Toki, Japan.

2. **Plasma mode switching in inverted polarity DC planar Magnetron**

   S. Chauhan, M. Ranjan, S. Mukherjee. 29th *Symposium on plasma science and technology, PLASMA - 2014* Kottayam, Kerala, India.

3. **Stability and operation of large anode fireball in magnetically constricted anode**

   S. Chauhan, M. Ranjan, M. Bandyopadhyah, S. Mukherjee. 43rd *IEEE International Conference on Plasma Science (ICOPS), June 19-23, 2016*, Banff, Alberta, Canada.

4. **Experiments with anode stops in magnetron anode plasma device**

   S. Chauhan, M. Ranjan, M. Bandyopadhyah, S. Mukherjee. *European Physical Society (EPS)* 43rd *Conference on plasma physics, July 4-8, 2016*, Leuven, Belguim.

Samirsinh Chauhan

In loving memory

of

Bapu

(my Grandfather)

Late Shri. Gulabsinh Parbhusinh Chauhan

09/11/1926 - 10/10/2014

His love and support made my life gratifying. He passed away during my Ph.D. tenure, he would have been proud today to see me graduate. His cheerful memories will last forever with me and my family.

ACKNOWLEDGEMENTS

Contents

SYNOPSIS

Plasma is a collection of charged particles, which shows collective behaviour. As a whole plasma has overwhelming tendency to stay neutral. In low temperature plasma (mostly!) the electrons and ions are not in thermal equilibrium with each other. Electrons usually have very large temperature as compared to room temperature ions. This along with a very low mass of electrons makes it highly mobile species in the plasma. The highly mobile electrons tend to shield any perturbation introduced in plasma. In fact, if we introduce externally biased electrode inside the plasma, it will shield its potential within a very thin region known as the sheath. The sheath is a thin space charge region near any surface in contact with the plasma, it controls the flux of charged particles to that surface. Any floating surface in plasma would quickly charge negative due to agile electrons. A floating surface will set its negative potential to equalize the electron and ion flux. Such sheath has an excess of ions in it, and is known as ion sheath. Ion sheath has potential lower than plasma potential and it attracts ions and repel electrons. Due to very high velocity of the electrons this is the usual scenario in practically every sheath in the plasma. Nevertheless any surface in contact with plasma can be biased positive, self-consistently or externally, provided it can take all the electrons that hit it. Such scenario is usually encountered in positively biased Langmuir probe. The resulting electron flux and hence current at such potential is known as electron saturation current in the probe terminology. The electron flux at positively biased electrode depends mainly on plasma density and electron temperature. To limit this current to the acceptable values, these electrodes are usually kept small in dimension.

Though electron sheath is a known phenomena in plasma physics, exact nature of it is still debated [1, 2]. This electron sheath can have accelerating voltage for electrons large enough to ionize the gas in the sheath region. Such sheath can

breakdown into the bright glowing quasi-neutral plasma region, known as fireball [3, 31, 36, 37, 39–41] . This fireball is separated from the rest of the plasma by a double layer. Conde *et.al.*[39] numerically showed that the electron sheath can breakdown into double layer type structure due to ionization in the sheath. The fireballs are complicated structures and are not understood in detail. Such fireballs are generally small within 1 or 2 *cm* diameter [3, 4]. Stenzel *et.al.* [31] produced large inverted fireball under very low pressure conditions, but they used grid-cage to sustain the fireball. Gruenwald *et.al.* [5] showed that a Langmuir probe can be implemented by cutting a hole in the grid. This hole needs to be smaller in comparison to cage size. Double layer forms at the fireball or fire rod boundary [3, 4], whose potential drop is close to the ionization energy of the background gas. The streaming electrons from the bulk plasma produce the additional ionization in the sheath, electrons produced due to this ionization are quickly absorbed by the anode, whereas ions flow out of the fireball much slowly.

An experimental study is presented here to create and study a rather large size droplet shaped fireball using a sputter magnetron like anode design. The device produces dense localized plasma region in region of weak magnetic field. We took cylindrical vacuum chamber of 30 *cm* in diameter and 40 *cm* in length and mounted an anode on it. Design of the anode consists of the copper electrode with magnets in the center and periphery, which creates inhomogeneous, localized, magnetic field on the surface of the anode. Permanent magnets of the NdFeB type, 15 *mm* in diameter are used. These magnets are provided water cooling for safety against excessive heating during operation. Sixteen discrete magnets are used in the periphery and one in the center. The strength of the magnets near the poles is approximately 2200 *gauss*. The detailed description of the system is given elsewhere [6]. This anode is biased positive with respect to grounded chamber, which acts as the cathode of the system. The system is evacuated to base pressure better than 5×10^{-5} *mbar* before introducing the Argon gas. Discharge

is struck at elevated pressure and the pressure is then reduced to required values for different experiments. Magnetic field on the surface of the anode is measured using standard Hall probe technique and is reported in ref [6] in detail. Magnetic field quickly drops in magnitude as we move away on from the anode. This makes the fireball produced in the discharge essentially magnetic field free. Standard Langmuir probe techniques were used to obtain the plasma parameters. The single Langmuir probe is made of tungsten with a diameter of 0.7 mm and length 7 mm. In the fireball regions both probe measures similar plasma density within the errors of measurements. However, the electron temperature is better estimated from single Langmuir probe. The emissive probe made up of 0.125 mm diameter tungsten wire loop is used for plasma potential measurements. The emissive probe can measure plasma potential reliably in variety of conditions [7, 8]. The floating potential technique is used for determination of the plasma potential.

It was found that the discharge operates in the two stable modes depending on the background pressure. In low pressure, the discharge remains in so called C-Mode. The C-Mode (Central-Mode) the fireball takes shape of droplet and attached with the anode at its center. In this mode discharge current sees moderate rise with increasing discharge voltage. Upon increasing pressure above certain critical value, the anode glow (Fireball) jumps to peripheral region. This mode is termed as P-Mode (Peripheral-Mode) discharge. In this P-Mode the discharge current increases more rapidly with the discharge voltage. This distinct power-law is clearly seen in the discharge I-V characteristics. In the intermediate pressure, we can see the glow transition from one mode to another with hysteresis. This transition is sudden in nature. Both modes did not appear simultaneously in our experiments. The central mode is studied under various discharge conditions. Important results are discussed and conclusions are made. The C-Mode plasma is measured to have the double layer at the visible boundary. This double layer potential is 15.6 V, which is close to Argon (working gas) ionization potential.

The measurements are facilitated by the fact that the fireball is formed mainly in weak magnetic field region. The fireball's dimension depends on the background pressure. The main dimensions are measured and qualitatively discussed. The size of fireball is determined by the particle balance, the high pressure makes ionization efficient and hence similar ionization can be achieved in lower volume. That is why the fireball shrinks in dimensions at elevated pressures.

The mechanism of the discharge is further discussed in detail. The source of electrons in our case is the cathode of the discharge, which is grounded chamber. The electrons diffuse to the anode, however, they encounter the strong inhomogeneous magnetic field. This magnetic field restricts the electrons from reaching anode except at the pole regions, where magnetic field connects with the anode. This is similar to solar wind hitting the poles of the earth. This is in stark contrast to sputter magnetron in which the electrons originated on the cathode (anode in our case) and gets trapped in the $\vec{E} \times \vec{B}$ drift. In our case, the plasma potential remains below the anode potential. This can only happen in the case of a very small electrode, in which case the electron sheath is warranted at the anode. Ballrud *et.al.* [9] have suggested that for an electron sheath the condition $\frac{A_E}{A_w} \leq \sqrt{(2.3\frac{m_e}{m_i})}$ should hold. It was verified that this does not hold for our entire anode area. Taking the effect of the magnetic field into account, it was shown that the said condition can be satisfied. This supports our observation of electron sheath and fireball on a relatively larger anode.

In Argon discharge, increasing the pressure above critical (5×10^{-2} $mbar$) value, makes the C-Mode unstable and triggers sudden transition to the P-Mode plasma.[10] We have observed such transition for the first time, however, the reason for the transition could not be traced beyond qualitative arguments. The increased pressure increases the width of the plasma contact with the anode. This is due to the enhanced cross-field diffusion due to increased collisions at elevated pressures. The key factor here is the electron-neutral collisions. The increased diffusion makes

the plasma penetrate in otherwise inaccessible magnetic fields. As the background pressure is increased the plasma contact width increase and approaches the diameter of the central magnet. Since there are no magnetic field lines beyond the magnet diameter which intersect the anode, the plasma cannot make contact beyond the diameter of the central magnet. And when the pressure increases beyond the above mentioned critical limit the anode fireball makes a sudden transition. This transition is marked by a sudden increase in discharge current. The increase in discharge current may be associated with the increased anode contact area and increased overall surface area of the now annular fireball. When we take the area of the fireball we must consider the area that is parallel to the anode, the fireball boundary near the anode is restricted by strong magnetic field.

The P-Mode plasma is accompanied by low frequency oscillations in the range of few kHz. These oscillations are may be due to the increased ionization in a reduced volume. Further these oscillations are may be similar to the breathing oscillations of plasma thruster, which are explained as the predator prey cycle in the high ionization region. We have measured oscillations in the light emission from the anode fireball and cathode glow. The oscillation in light appears only in the anode glow region, no such oscillations are observed in the cathode glow or the bulk plasma, this is in contrast to the global nature of the floating potential oscillations. The frequency of the oscillation and the waveform matches very well with each other suggesting their common origin. The discharge current also carries similar oscillations.

The thesis is organized in different chapters as outlined below.

Organization of the thesis

Chapter-1 : *Introduction.* Brief introduction of glow discharge and anode region will be given. Detailed literature survey of anode region of glow discharge will be discussed. Fireball and its properties will be presented. Motivation of the

present thesis work will be outlined.

Chapter-2 : *Physics of anode layer and fireball.* For physically small anodes the electron sheath becomes viable. This electron sheath is unstable above certain critical voltage and breakdowns in the fireball. Physics of such near anode phenomena in the DC glow discharge will be qualitatively discussed. Various types sheath formations at the anode will be presented. The basic of the plasma sheath will be revisited from a perspective of the fireball formation. Previous theoretical models will be discussed and attempt will be made to clearly represent those ideas in simple terms. Various constrains on the design of the experiments will be explained. The behaviour of plasma in magnetic field will be presented, including particle drifts and diffusion across magnetic field.

Chapter-3: *Experimental set-up and diagnostics.* In this chapter, the experimental setup used for the study of constricted anode plasma source is presented. A detailed description of vacuum chambers, power supplies, pumping system and anode design etc. will be provided. The magnetic field near anode measured with hall probe will be given, main features of the magnetic field will be highlighted. The hall probe technique will be very briefly mentioned. The experimental procedure to produce the plasma will be explained and various difficulties and workaround will be presented. Various relevant electric probe (e.g. Single Langmuir probe, Double probe, Emissive probe) based diagnostics will be discussed. The methodology to derive the plasma parameters from various probes will be discussed in detail. The emissive probe technique will be presented and a case will be made that the floating potential technique of the emissive probe can be effectively used for measurement of the plasma potential. The coordinate system to be used in rest of the thesis will be introduced at this point. Typical plasma parameters will be elaborated.

Chapter-4: *Anode double layer and electron sheath formation.* This chapter contains main results of the experiments. It deals primarily with the dynamics of the C-Mode discharge. The discharge current voltage characteristics are discussed. The potential structure of the fireball is presented. It is shown that the double layer potential of the fireball is very close to the ionization potential of the Argon gas used in the experiments. The plasma potential profile measured with emissive probe is plotted in two mutually perpendicular axis. The plasma potential in both directions remains constant through out the bulk plasma regions and makes rather sharp jump at the visible boundary of the fireball. This explains the brightly glowing fireball, as the electrons are accelerated by this potential. The electrons produce intense ionization inside the fireball bringing plasma density inside the fireball as large as an order of magnitude higher that the bulk region. The effect of the background pressure and discharge voltage on the fire ball is presented. The link is established between visual observation and measured plasma parameters. The existence of the electron sheath is challenged from point of view of the current at the electrode. It is argued that the electron sheath can exist only at the surface drawing more current than the local electron saturation current. It is shown that the full anode surface can not form the electron sheath for our discharge current and plasma density, hence the reduced contact area due to the magnetic field has to be taken into account to explain the observation. It is also shown that the Baalrud's global nonambipolar flow model[9] also hold on similar arguments

Chapter-5 : *Mode transition and oscillations.* In this chapter, the transition from C-Mode to P-Mode is discussed. The qualitative reasoning of the transition is given. It is argued that the background pressure forces plasma into the stronger and wider area near the anode surface. By means of optical images,

the contact area of the plasma on the anode is determined. It is shown that it approaches the diameter of the central magnet and saturates close to it in C-Mode. The P-Mode is induced when the pressure is increased beyond the critical value. The oscillations in the P-Mode is measured in light emission in addition to floating potential and discharge current. The observation that the light emission oscillations are observed only in the anode glow close to the anode suggests the origin of the oscillations in the P-Mode anode glow.

Chapter-6 : *Application of anode fireball.* Application of the device as localized plasma source will be proposed. The nanopatterning of the GaSb is demonstrated at low pressure C-Mode discharge. Experiments with anode stops are discussed, this technique forces the discharge to stay in C-Mode.

Chapter-7 : *Conclusions and future scopes.* Results are summarised in this chapters. Some of the future scopes of the thesis work are discussed. The main results of this thesis are summarized as follow:-

- Our experiments provide a clear demonstration of the formation of the electron sheath and fireball in sputter magnetron like device. The size of a fireball is large and it resides in weak magnetic field regions facilitating measurements.

- The existence of the two mutually exclusive modes of such device is very unique and is observed for the first time to the best of our knowledge.

- Formation of fireball on magnetically constricted anode electrode is demonstrated first time to the best of our knowledge. This device also makes up as a candidate for future basic and applied research. It can be used to test the

recently developing hypothesis of the electron pre-sheath, fireball oscillation etc.

- Diffusion of the plasma in cusp magnetic field is observed and is related to enhanced plasma loss from the cusp at elevated pressures.

Future scope

This thesis work can be extended for studying the plasma diffusion in magnetic field, basic sheath fireball physics, and application such as etching, surface modification, nanopatterning, etc.

List of Figures

Samirsinh Chauhan/Ph.D. Thesis/April, 2017

List of Tables

1

Introduction

Plasma is a collection of charged particles where the motion of each particle is heavily influenced by the other charged particles. The gas of charged particles behaves differently from a neutral gas cloud. The plasma has overwhelming tendency to stay 'neutral'. If charge particles are removed from plasma, it creates a prohibitively large electric field to attract them back. To emphasize this behaviour it is said that the plasma is in a quasi-neutral state. Hence, plasma is also known as the fourth state of matter. It is also the most widely available form of matter in the universe. In fact, 99% of the visible universe is made up of plasma [11]. Stars, Nebulae, interstellar gas etc. are examples of naturally occurring plasma. On earth lightning is an example of naturally occurring plasma. Man-made plasma has revolutionized the technology, especially the semiconductor industry rely heavily on plasma based processing. The hope for nuclear fusion has constantly pushed for a deeper understanding of plasma behaviour.

DC glow discahrge is an example of the most basic plasma produced in larobatory. DC glow discharge is ignited by stray electrons accelerated by a DC potential applied between the two electrodes [12]. The negative electrode is known as cath-

ode, whereas the positive electrode is known as anode. The accelerated electron collides with the background gas and ionizes the atom, which makes another electron available and the chain reaction leads to an avalanche. Once the discharge gap is filled with charged particles, the DC current flows through the Plasma and it can be sustained indefinitely. The DC glow discharge was initially studied in long glass tube and various regions such as cathode dark space, negative glow, positive column, anode dark space etc. were identified. Though positive column is absent along with some of the other features in most of the processing discharges. The identifying characteristic of the DC glow discharge is the large cathode fall. In fact, most of the applied voltage is dropped along the cathode fall. This large cathode fall is well documented [12–19] but the anode fall remains little explored phenomena, this is partly because it is mostly not relevant to the discharge and acts only to balance the current. This however, is not always the case and anode fall can rather be crucial plasma producing region for example in case of very small anode [20]. The region connecting the plasma to the electrodes is called sheath. The sheath in general is the only region in plasma where strong electric field exist, be it anode sheath or cathode sheath.

The sheath is a thin non-neutral region that forms near any surface in contact with the plasma. The sheath regulates the flux of plasma to the surface (or walls) and hence is very important in plasma confinement. Any surface biased to the plasma potential in a quasi-neutral plasma consisting of Maxwell-Boltzmann electrons and cold room temperature ions having temperature $T_i << T_e$ will collect all the particles that hits it. T_e and T_i are electron and ion temperature, respectively. For Maxwell-Boltzmann distribution number of particles hitting any plane surface is given by,

$$J_e = \frac{1}{4} n_e \langle V \rangle \qquad (1.1)$$

here, $\langle V \rangle$ is the average speed. Very high temperature along with very little mass

of electrons makes the flux in equation 1.1 very high for electrons than that of ions. Hence, any surface at plasma potential collects mainly electrons. For the potential below the plasma potential, the electrons are repelled by the surface and the fraction of collected electrons can be given by Boltzmann factor viz. $J = J_0 exp(-\phi/T_e)$ where, ϕ is the potential of the surface measured with respect to the local plasma potential. Now, if a metal electrode is introduced in the plasma and is not connected to any other surface or electrode, since no current is carried by such electrode, it will keep charging negative until the electron flux is reduced and becomes equal to the ion flux. This is achieved by the formation of the sheath near that electrode. Such sheaths have number density of ions in excess and is called ion sheath. This kind of sheath is most common to occur in plasma, which is due to the very high mobility of electrons and are frequently needed to be retarded to maintain local particle balance.

If the electrode surface immersed in the plasma is biased at a potential higher than the local plasma potential, the non-neutral sheath region becomes electron rich. The ions are usually much less energetic and can be completely blocked by potential only a few volts higher than the local plasma potential. Such sheaths are known as electron sheath. The electron sheath has been recently speculated to have more wider influence on the plasma than anticipated earlier [21]. The electron sheath has accelerating region for electrons in contrast to the ion sheath. Electron-rich sheaths have many interesting and unexplored properties. These properties are important for many applications such as electrostatic probes [22], current collectors used in space application [23–26], virtual cathode oscillators [27, 28] and fireballs formed by a biased grid or an electrode in plasma [29–31]. It has been observed that such sheaths are subject to various instabilities like, electron two-stream instabilities, transit-time instabilities [32], high-frequency sheath-plasma oscillations near the electron plasma frequency [33], low frequency potential relaxation instabilities [34, 35] and ionization instabilities in the presence of neutrals

leading to unstable fireballs [3, 31, 34, 36–41]. When the accelerating voltage and hence the electron energy reaches the potential necessary to ionize the background gas (15.7 eV for Argon), the sheath turns into, what has come to be known as *Fireball!* [37].

It has been reported by a number of authors that the positively biased electrode in the plasma forms a bright, generally spherical glow with a sharp boundary [3, 4, 9, 30, 31]. The phenomena is explained as below. The electrons starts accelerating as the potential of the biased electrode is increased. Below the ionization potential the sheath glows due to the excitation of the neutral atoms. When the electrons attain enough energy to ionize, the background gas starts to produce additional electron ion pairs inside the sheath. The electrons so produced are readily absorbed by the positively biased electrode. Due to its inertia the ions are pushed away slowly. Hence, the ions act to neutralize the negative space charge of the electron sheath and produce a new quasi neutral region with different plasma potential than the original plasma. These regions are usually connected by a potential double layer which is visually observed as a sharp boundary of the glow.

There are mainly two ways the fireballs are studied. The primary method is to use an additional separately biased electrode in the plasma [3]. The other is to use a wire cage to accelerate the electrons, the fireball forms inside the cage [31, 32]. Both of the methods rely on the bias potential being larger than the local plasma potential. In the cage however, the grid is highly transparent and hence one does not need to worry about large electron flux which has to be carried as current in the case of electrode immersed in plasma. Formation of the fireball is a very important phenomena as it can determine the global plasma parameters in the system. The fireball can be single most important location for the loss of electrons from the system [3]. Fireball formed on auxiliary electrode has been found to control the global plasma potential of the discharge, taking over the role of primary anode of the discharge [9, 42]. Sometimes the phenomena is also refered as anode spot,

when it occurs localized on rather large sized anode. It was reported to be useful as high current ion source [43]. With this brief understanding of various types of sheath, fireball, which is essential to understand the content of the thesis, the outline of the present thesis is given below.

Outline of the thesis

An experiment is devised to obtain a rather large sized fireball using magnetic field on the surface of the primary anode. Though the anode of the discharge is large, it is magnetically constricted to effectively be very small, which is a requirement for the formation of the electron sheath at the first place. Our experimental device consists of a stainless steel vacuum chamber, 30 cm in diameter and 40 cm long. DC glow discharge is produced by a high voltage power supply connected between the anode and the grounded chamber which acts as the cathode. The anode houses permanent magnets producing strong localized magnetic field. The plasma is formed in the form of bright anode glow, which we have identified as the "inverted droplet" shaped fireball. This fireball has a double layer structure which connects it to the rest of the plasma. The plasma is shaped mainly by the curved magnetic field near the surface of the anode. Background pressure in the system plays a crucial role as it modifies the behaviour of plasma in the magnetic field. In fact, the discharge shows two stable modes of operation depending upon the background pressure. For lower pressure the "inverted droplet" shaped fireball is attached in the center of the anode which is termed as the C-Mode discharge. Increased pressure makes the C-Mode unstable and the anode fireball transforms into an annular shaped glow attached at the periphery of the anode, this type of glow is termed a P-Mode discharge.

The thesis is organized as follows, Chapter 2 introduces to physics of sheath. Types of sheath near the anode are discussed and the condition for having either ion

sheath or electron sheath near the anode is presented. The chapter further examines the scenario of electron sheath with potential drop larger than the ionization potential. It is argued that this electron sheath can produce new quasi-neutral plasma region that results into a fireball. Chapter 3 discusses the experimental system and diagnostics. The vacuum system and subsystems are also explained. Further the typical condition of the discharge is given as well as the basic procedure to obtain the discharge is explained. The construction and operation of Langmuir probe and emissive probe are discussed. Chapter 4 describes the main results regarding the C-Mode plasma. Formation of the fireball and and its peculiar shape is discussed in this chapter. The role of magnetic field is qualitatively discussed. Further, potential structure near the anode is discussed in detail. It is shown that this potential structure requires the formation of electron sheath near the anode. Formation of the electron sheath is questioned and argued to conclude its existence. Variation of the fireball with discharge parameters is discussed to complete the narrative of the discharge. Chapter 5 discusses the formation of P-Mode discharge in the device. Existence of this mode at higher pressure is attributed to the enhanced collisions, which results in the enhanced root width. This mode also show oscillations in the range of few KHz. These oscillations are qualitatively discussed in this chapter. The results of the light emission observed with photodiode are also presented in this chapter. Chapter 6 outlines the possible applications of the device in the field of nanopatterning. Tunability of nanodots with various fireball properties is presented. The contact angle is measured on the surface of the nanopatterned GaSb substrate which shows remarkable hydrophobic behaviour. Some of the initial results from the experiments are discussed which set the basis for future explorations. Chapter 7 presents the conclusions drawn from the thesis and the future scopes.

2

Physics of anode layer and Fireball

Plasma is generally the most positive body in the discharge. This is due to extreme difference between the mobility of electrons and ions. Any surface immersed in the discharge will be quickly charged to a negative potential due to these electrons. In a DC glow discharge the sheath formation at every surface is such that it retards electrons. This is true even at the anode. This kind of sheath is known as ion sheath due to the excess number of ions in the sheath region. However, in certain cases when the anode size is *small* the electron attracting sheath also known as electron sheath, can be formed. The rest of the chapter describes how an electron sheath near the anode can be turned into an ionizing electron sheath, which results in the formation of the fireball.

2.1   DC Glow discharge

DC glow discharge is produced by applying a potential difference between two electrodes. Typically, a few hundred volts of potential difference is required to maintain a DC discharge. These two electrodes can have variety of shape, orienta-

tion and sizes, all of which affect the discharge. The simplest geometry is that of a parallel plate configuration. This consists of two metal electrodes placed at the opposite ends in a long cylindrical glass tube. The typical long tube discharge can be seen to be divided into cathode sheath, cathode glow, negative glow, Crooks dark space, Faraday dark space, positive column, anode glow, and anode dark space etc. For different geometry and operating condition some of the above mentioned feature may not be present. The length of the positive column depends on the distance between the electrodes and it may be absent in many discharges especially the ones used in processing. The cathode sheath however is always present in the DC discharge. It can be seen from potential distribution shown in figure 2.1 that most of the applied DC voltage falls within small distance near the cathode. The accelerated ions hit the cathode and emit secondary electrons with typical yield in the range of $0.1 - 0.2$. These secondary electrons play an important role in carrying the current in cathode sheath, moreover it provides crucial ionization for maintaining the plasma. The detailed discussion of the positive column and the cathode sheath can be found elsewhere [14, 15, 18, 19]. The region of interest for the current work is anode.

2.1.1   Anode

The obvious requirement of the DC glow discharge is the flow of current. The current has to be continuous through all of the regions of the glow discharge, for most of the DC glow discharge the current is carried by the electrons. From basic kinetic theory of gases, for any gas having Maxwell-Boltzmann distribution the number of particles hitting the wall per unit area can be given by

$$J_0 = \frac{1}{4} n \bar{v} \tag{2.1}$$
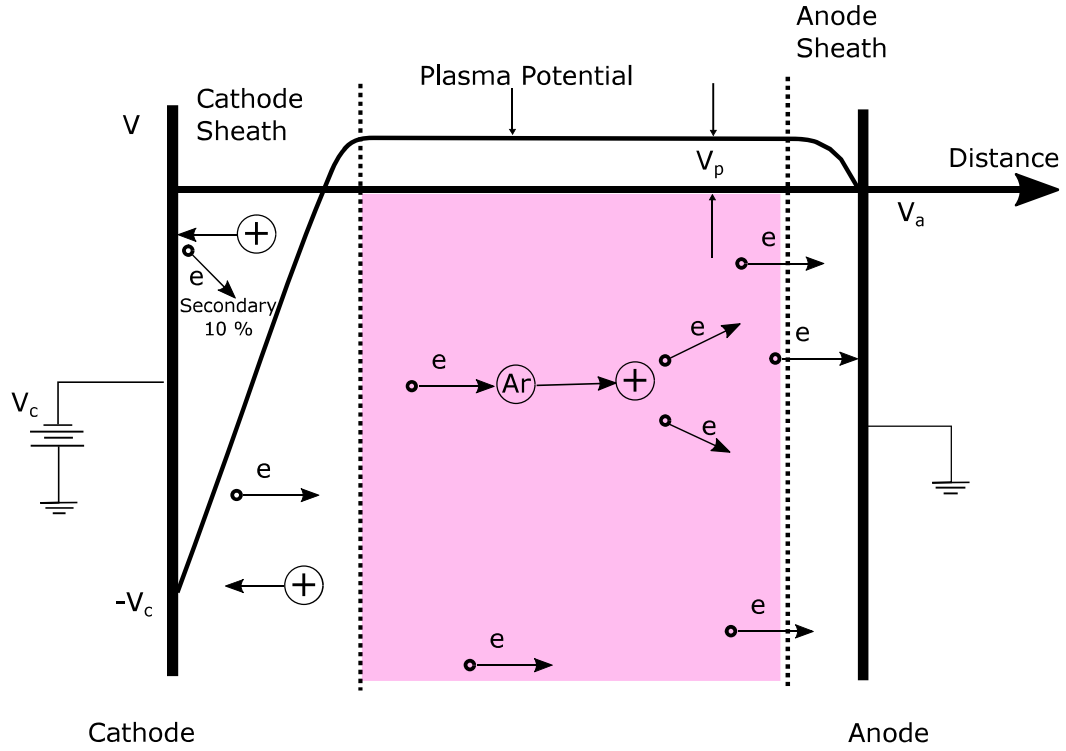
Figure 2.1: *Typical DC glow discharge potential distribution with schematic representation of some of the important processes. The plasma potential V_p is shown with respect to anode potential V_a. Anode is held at ground potential and cathode is biased $-V_c$ with respect to ground. Cathode sheath and anode sheath are shown schematically, the plasma region is shown coloured for the purpose of clarity only.*

where, $\bar{v}$ is thermal velocity of the particle and is given by

$$\bar{v} = \left(\frac{8KT}{\pi m}\right)^{1/2} \tag{2.2}$$

Above equation can be applied to any gas, including electrons and ions as far as they are in thermal equilibrium having Maxwell-Boltzmann distribution. Here K is Boltzmann constant, T is temperature of the particle in consideration, m is the mass of that particle. Above mentioned equations are also valid for electrons and ions of the plasma, and can be used by taking into account the respective mass and temperature of the plasma species. The flux given by equation 2.1 is received by any electrode in contact with the plasma, the floating electrode however is charged negative and the flux reduces accordingly. This flux along with the current carried by the electrode determines the structure of the sheath. The current carried by the electrode depends on the external circuit. The flux in equation 2.1 when multiplied by the area of the anode (A) gives the total electron current ($I_T = J_0 \times A$) at the anode. If the current imposed by the external circuit (i.e. discharge current I_d) is less than this thermal current, some of the electrons are retarded and stopped from reaching the anode in order to satisfy the current continuity. This is most often the case, due to the large mobility of the electrons. Figure 2.1 shows the anode sheath potential for this usual case. In some special cases however, when the thermal electron current is not sufficient to provide the current requirement on that electrode the accelerating region for the electron may form. Such a region is called the *electron sheath*. This kind of sheath is generally observed in small area electrodes such as Langmuir probe. The typical potential profile of such sheath is sketched in figure 2.2. The plasma potential rises as it approaches the electrode which is held at a potential higher than the plasma potential. It is to be realized that for any electrode to be held at or above plasma potential it must carry a current which is at least equal to the local electron saturation current.
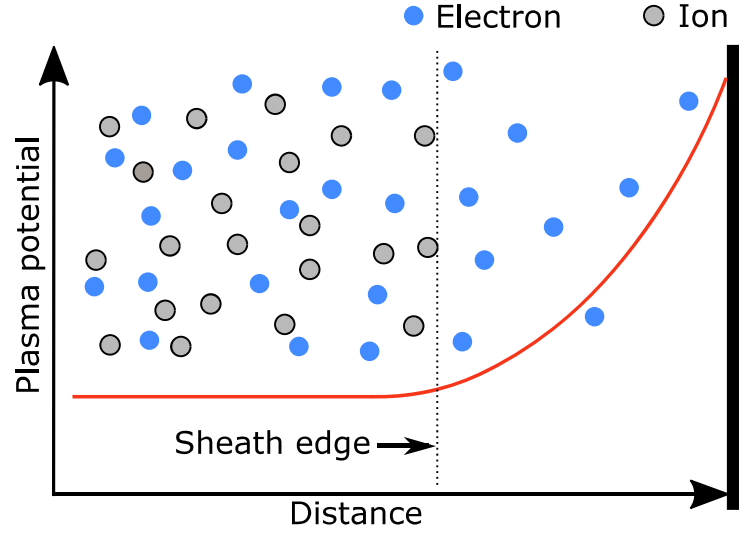
Figure 2.2: *Schematic representation of the plasma potential in an electron sheath. The boundary on extreme right is biased to a positive potential. The dotted vertical line represent the boundary of the sheath, due to very small energy of the plasma ions, they are unlikely to cross this boundary.*

2.2 Sheath

Sheath is a very important aspect of plasma, it controls the flux and the energy of the plasma particles being lost to any solid surface, for example, chamber wall. By controlling the sheath we can control the loss of plasma. Plasma is widely used in industrial application especially surface modification, which is entirely determined by sheath dynamics. Since most of the applications as well as the occurrence of the sheath concerns the ion sheath, it is well studied both experimentally [44, 45] as well as in theory and simulation [46–52]. We will restrict the discussion to collision less sheath, more on collisional sheath can be found in literature [19, 53–59].

2.2.1 Child's Law

The problem of sheath was studied in early 20th century for thermionic emission currents used in vacuum diode [60–62]. The problem consisted of an electron

emitting surface and electron collecting surface, which in case of plasma can be compared with sheath. Sheath boundary emits particles and wall or surface at the end collects it. The so called Child's Law gives the value of maximum current density (J_0) that can be carried by such sheath for given voltage (V) and separation (d).

$$J_0 = \frac{4}{9}\epsilon_0 \left(\frac{2e}{M}\right)^{1/2} \frac{V^{3/2}}{d^2} \tag{2.3}$$

where, ϵ_0 is the permitivity of the free space, M is the mass of particle. The above equation gives the space charge limited emission current for a plane diode. In the derivation it was assumed that the particle originated with zero initial velocity. In the case of plasma sheath it was realized that the sheath has a transition layer with bulk quasi neutral plasma. This transition layer is known as pre-sheath. It was shown mathematically by Bohm [48] that the ions entering the sheath must have a minimum energy given by

$$u_B = \sqrt{\frac{eT_e}{M}} \tag{2.4}$$

where M is mass of ion, T_e is electron temperature in eV and u_B is Bohm velocity. For ions to accelerate to this energy, a certain potential drop in the pre-sheath is needed, equation 2.4 and energy conservation gives this potential drop to be $\phi = T_e/2$. Using this potential and Boltzmann relation the density at the sheath edge can be related to bulk plasma density as $n_s = 0.61n$, where n_s is the density at the sheath edge. This relation is useful in Langmuir probe diagnostics.

Electron sheath and ion sheath can be treated identically, however, exact mechanism by which the random electron velocity changes into the directional velocity in the case of electron sheath is still a topic of research [1, 2].
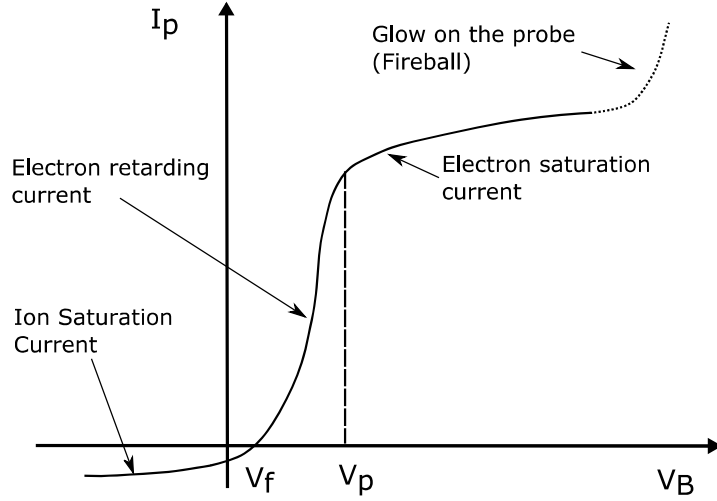
Figure 2.3: *Typical Langmuir probe current voltage characteristics. The bias potential is referenced to the laboratory ground. Three main regions of the probe are shown. For a very high positive potential the probe forms a bright fireball.*

2.2.2   Langmuir Probe

Motivation to discuss Langmuir probe here is two fold, first, it fits as the natural extension of sheath analysis and second, it shows the formation of fireball when biased highly positive. Langmuir probe was one of the earliest technique used to obtain localized plasma parameters. It consists of a small auxilary electrode biased at different voltages to infer the plasma properties. Such an electrode is known as Langmuir probe in honour of Irving Langmuir who first used it and gave a theory to explain the results. The bias voltage of the Langmuir probe is usually measured with the system ground and not with respect to plasma potential due to technical limitations. The usual practice is that the current from the probe to the plasma is termed positive and is followed throughout the thesis. Figure 2.3 shows typical current-voltage characteristics of the Langmuir probe. The probe voltage V_B is measured with respect to the ground, the plasma potential is indicated as V_p in the schematic. The probe characteristic is mainly divided into three parts *viz.* $V_B > V_p$ (electron saturation), $V_f < V_B < V_p$ (Electron retarding) and $V_B < V_f$

(ion saturation) regions. At V_p the probe is at the same potential as the plasma and hence collects all of the electrons that arrive at it. This current can be given by our previous analysis of the sheath. A sheath is inevitable at the so called Langmuir probe, which is actually a metallic electrode immersed in the plasma. This current is known as electron saturation current and is given by

$$I_0 = \frac{1}{4}en_0\bar{v}_e A \qquad (2.5)$$

Where A is the area of the probe. Below the plasma potential the electrons are retarded as the probe becomes negative with respect to the plasma which is sitting at V_p. The reduction in the electron current can be given by the Boltzmann factor and the current for probe bias $V_B < V_p$ is given by

$$I(V_B) = I_0 exp\left(\frac{V_B - V_p}{T_e}\right) \qquad (2.6)$$

where I_0 is the electron saturation current, and T_e is electron temperature in eV. At bias potential $V_B = V_f$ the probe draws no current, at this potential the electron current has been reduced so much that it equals the ion current to the probe. This potential is known as floating potential as it is the potential at which an insulating probe, which cannot draw current would float. Below this so called floating potential, the probe draws the ion current and saturates at ion saturation current. This however, will be discussed later in the thesis.

What happens if the probe is biased above the plasma potential? The usual answer is, it would saturate and would ideally draw the local electron saturation current. This however is not the case when the probe is biased *very high* above the plasma potential. In such cases, the probe develops the glow and the current in the probe is increased many fold, this is due to the increased ionization near the probe. This is another kind of fireball formation. In the next section we will see how electron collecting sheath near the electrode (probe) biased above the plasma

potential can turn into ionizing fireball.

2.3 Fireball

A small auxiliary electrode (e.g. Langmuir probe) when placed inside the plasma and biased at or above the plasma potential, draws electron saturation current. The electron sheath formed on the positively biased electrode accelerates electrons and these energized electrons cause the sheath to glow. When biased above a certain critical potential it develops a bright glow and the current to the electrode rises rapidly. This bright glow is caused by the breakdown of the sheath into the quasi neutral plasma [3] and such structures were called fireball, first by Song et al. [37] and subsequently by others [31, 63–67]. Their operation and stability has been investigated experimentally [31, 32, 37, 64] and theoretically [63, 65, 68, 69].

The electron sheath is a prerequisite for the formation of the fireball. As discussed earlier this is generally achieved by biasing a small electrode above the local plasma potential but this can also happen as a natural consequence of the particle balance in the case of a DC discharge having *small* anode [4]. Electron sheath is usually understood from the Langmuir probe theory where the probe or the surface collects the random flux of the electrons, electron distribution function at the sheath edge is assumed to be half Maxwellian. The electron sheath equivalent of the Bohm criterion is thought to satisfy naturally as the electrons arrive to the sheath with the thermal speed. However, Scheiner et al. [2] have disputed this traditional understanding of the electron sheath. They have shown that the electron sheath is significantly different, complicated and that the pre-sheath may extend much deeper into the plasma than thought earlier. They also argue that the electrons achieve the drift velocity due to the electron pressure gradient instead of the pre-sheath electric field. The distribution function of the electrons at the sheath - pre-sheath boundary is also shown to be shifted (flowing) Maxwellian. This the-

ory has both theoretical and indirect experimental support, however the pressure gradient has not been measured experimentally. Baalrud et al. [9] reported on the conditions required to form a particular type of sheath on any electrode. They solved for the particle balance when a "global non-ambipolar flow" is present. This is the case where all ions are lost to one surface and all electrons to the other. Their results were stated in terms of the area ratio of the surface collecting particles of a particular type. Baalrud et al. [9] and Barnat et al. [1] showed experimentally that this model correctly predicts the type of sheath formation.

The fireball is visually observed as a bright glow with a sharp boundary attached to the positively biased surface. The sharp boundary is due to the presence of a double layer, which separates the fireball from the surrounding plasma. For the surrounding (background) plasma, the fireball acts as a virtual electrode, which basically enhances the collection area of the original electrode. This puts a physical limit over the size of a fireball. Typically, the plasma density inside the fireball is about an order of magnitude higher than the surrounding plasma.

Song et al. [37] observed the fireball on an anode disc biased $40 - 50 \ V$ above the ground potential. As the bias voltage is increased they first observed the luminous sheath which suddenly turned into the fireball over a certain threshold voltage, similar observation is made for the increase in the background pressure. The observations were explained with the help of a spherical double layer formed at the fireball boundary. Formation of the fireball was observed to greatly increase the electron collection ability of the anode. Hence, the fireball acts as a virtual anode which results in the manifold increase of the collection area. They also observed oscillations in the collected current. The oscillations were explained as repetitive formation and loss of the the double layer structure. The rise time and the fall time of the oscillations were shown to be related to the production of the ions due to the ionization and the loss of them due to the potential difference. The diameter of the fireball is shown to be proportional to the inverse of the background

pressure.

Following text explains the physical mechanism behind the formation of the fireball. Electron sheath accelerates the electrons from the bulk plasma to the electrode. Electron sheath starts to glow if accelerated electrons have sufficient energy to excite the gas in the sheath. Furthermore, if the potential is high enough such that the electrons reach the ionization energy before hitting the electrode, they may produce ions due to collisional ionization. The electron produced in the ionization is quickly collected by the positive electrode, however heavy ions take much more time to move away from the electrode. If there are sufficient number of ionization events to balance the charge, the sheath converts into a quasi-neutral plasma region. This newly formed plasma region will have a different plasma potential from the original surrounding plasma, forming a double layer at the boundary. The potential difference of the double layer is usually found to be close to the ionization potential of the gas [3]. Though any potential larger than the ionization potential should theoretically work, however it takes the minimum possible value and stay close to the ionization potential in order to minimize the power. In other word it is the lowest energy state.

Very thin region of the electron sheath, typically a few debye lengths (λ_d), raises the question of the mechanism of neutral gas breakdown. Typical experiments with auxiliary electrode find that the formation of the fireball occurs at a bias potential in the range of $40 - 50\ V$ above the plasma potential [3, 40, 66]. This means that the electron reaches the required ionization energy levels ($\sim 15.7\ eV$ for Argon) very close to the electrode. This rules out the possibility of an avalanche process.

Conde et al. [39] gave the theoretical explanation of the electron sheath breakdown. They showed mathematically that the ionization events in the sheath are sufficient to establish the double layer that results in the formation of the fireball. Their study takes into account the fact that an avalanche is not possible in such a thin region and only considers the positive charge produced by streaming electrons.

Over a critical bias voltage they observed a bifurcated solution, one for electron sheath and other for a double layer like potential profile [39]. No particular instability mechanism was found necessary for the formation of this double layer. It is to be noted that their model does not account for the denser fireball formation that occurs as a result of the double layer.

Baalrud et al. [3] gave a model to explain various features associated with the formation of the fireball. The model relates the critical voltage for formation of the fireball to the inverse of the background pressure. As the ions start to accumulate in the sheath region, they hypothesized that the sudden transition to the fireball happens when the number of electrons in a "Debye cube" equal the number of ions in the same "Debye cube". They also explain the hysteresis observed in the current voltage characteristics. Their model correctly predicts the length of the fireball and also the shape of the fireball for a large disc shaped electrode. The hysteresis in the occurrence of the fireball is related to the local Debye length, which is different in the presence and the absence of the fireball. This leads to the different critical values for the appearance and disappearance of the fireball. One of their important observation is the so called plasma potential locking. When the fireball is present on the electrode it drains a large plasma current such that the global plasma potential starts to follow this auxiliary electrode instead of the original anode of the discharge. Once this is achieved the plasma potential is locked few volts below the bias potential minus the ionization potential of the gas. This puts the limit to which the potential of the biased electrode can be raised above the plasma potential.

Stenzel et al. [32, 70] reported the dynamic behaviour of the so called inverted fireball. In these experiments the fireball is produced using a wire mesh with spacing smaller than the Debye length. When biased positive, the grid develops a continuous electron sheath which accelerates the electrons. The highly transparent grid drains considerably less current than the equivalent solid electrode, hence large

sized fireball can be artificially created. When the grid is in the form of a closed surface e.g. a sphere, the fireball gets trapped inside it. Such fireball presents many interesting features e.g. high frequency oscillations, light oscillations, transit time instability etc. The high frequency oscillations have a period corresponding to the transit time of the electrons through the sphere. The frequency of the oscillations can be tuned by an external resonator circuit. They observed the potential drop between the fireball and plasma to be much higher than the ionization potential, in contrast to the other fireball configurations.

Formation of the fireball was also studied in the presence of the magnetic field [71, 72]. The magnetic field predictably changes the shape of the fireball to a cylindrical one. Cartier and Merlino [71] observed the fireball at the end plate in a long cylindrical vacuum chamber with a non-uniform magnetic field. The fireball was produced by drawing current through the anode of the Argon discharge. The anode was placed at the end of the vacuum chamber in the diverging magnetic field region. The length of the fireball was observed to be a function of the bias voltage, background pressure and the strength of the magnetic field. The fireball had the electric field component in both parallel and perpendicular direction to the magnetic field. They investigated the scaling of the fireball with this component of the electric field and magnetic field. An et al. [72] studied the effect of the external magnetic field on the evolution of the firerod and fireball in Argon and Xenon discharge. The fireball produced using a biased electrode turned into a rod shape above a certain externally applied magnetic field. They observed that there also exists an upper limit for the strength of the magnetic field above which a fireball cannot sustain. The lower limit on the strength of the magnetic field was attributed to the requirement of some weak magnetization of ions, though for the entire range of magnetic field in their experiments, the ions remained only weakly magnetized [72]. A simple model earlier given by Song et al. [37] was used to study the effect of the magnetic field on the shape and size of the fireball. They

incorporated the effect of the magnetic field in the form of modified particle fluxes through various boundaries.

Anode fireball can be used as a source of plasma for many applications. For example, Mujawar et al. [4] obtained a fireball on differentially pumped constricted anode in a DC discharge to be used in a specialized plasma source. The region near the anode showed a steep rise in the electron density. The discharge current was found to be oscillating in the range of $250 - 400 \ kHz$ which is credited to the anode glow instability. Lee et al. [73] have reported the use of such fireball for high current ion beam extraction. A small anode with a hole in the center is used to create the fireball in the RF plasma. A beam current of $204 \ mA/cm^2$ was obtained with the help of the fireball. Nema et al. [74] used a small anode biased highly positive for the formation of the localized plasma near the anode which was used for plasma polymerization. They used a large grounded vacuum chamber as the cathode of the discharge. The small anode concentrates the electric field which creates a localized plasma. The generated plasma is then used for the cathode polymerization of the grounded sample placed in front of the anode. Mayer et al. [75] used the inverted fireball to deposit a diamond like carbon films. The inverted fireball using the closed cage of the fine mesh provided a highly localized plasma. The ambient plasma was created using a hot cathode discharge. The fireball very efficiently ionizes the working gas for the deposition of the DLC (Diamond Like Carbon) film.

2.4 Motivation

Most experiments with the fireball involve the use of an auxiliary electrode in the plasma [3, 37] or a wire cage to trap the fireball [31, 32, 76]. The latter approach has the advantage that it does not have to carry the large current associated with the fireball. So far, most of the experiments performed with the auxiliary elec-

trode show the formation of a rather small sized fireball, typically $\sim 1\ cm$ in length. This structure is therefore difficult to analyse using any of the standard probe technique. Since the formation of the fireball depends upon the ionization in the electron sheath, it is highly sensitive to the neutral density i.e. the background pressure. Lower pressure produces a larger fireball but is difficult to establish. Using magnetic field is another approach, however this introduces additional complications in the probe diagnostics. The use of the cage seems to be ideal but the fireball is trapped inside the cage and hence one has to cut open the cage for the insertion of the probe [5]. This also has some limitations, for example the hole has to be small compared to the dimension of the cage but large enough to provide access to the probe shaft.

Our experiment described in the present thesis consists of the formation of the fireball on rather large electrode, constricted by the magnetic field. The device is based on the cost effective DC sputter magnetron design. The magnetic field affects the narrow channel close to the anode where it helps in increasing ionization. The limit imposed by the plasma on the size of electrode for the formation of the electron sheath is satisfied due to the presence of the magnetic field. The fireball is of a few cm in diameter which is advantageous for probe measurement. Hindrance in probe access due to the presence of grid is avoided. The fireball forms mainly in weak magnetic field region is an added advantage from diagnostics point of view. The fireball is formed on the main electrode rather than the auxiliary one. We report on the plasma density and the plasma potential structure and would explain the results qualitatively.

3

Experimental set-up and Diagnostics

This chapter is mainly divided into two parts, the first section describes the experimental vacuum system, typical operation of the device and power supplies, the second section gives the details of various diagnostics and its implementation. The main components of the device are the vacuum chamber, diffusion pump, power supply, the anode and various diagnostics.

3.1 Experimental device

The experiments were performed in a stainless steel vacuum chamber 30 cm in diameter and 40 cm long. The chamber was electro-polished from inside and made free of sharp edges, this was necessary to suppress possible arcing at high voltages. The schematic of the vacuum chamber is shown in figure 3.1. It consists of a large, 30 cm diameter view port on one side and is pumped via an 'L' section from the other. The view port is designed to give full cross sectional view inside the chamber. It is made from perspex having 1.2 cm thickness, this port is also used to mount a photodiode and is periodically cleaned to maintain suitable visibility.
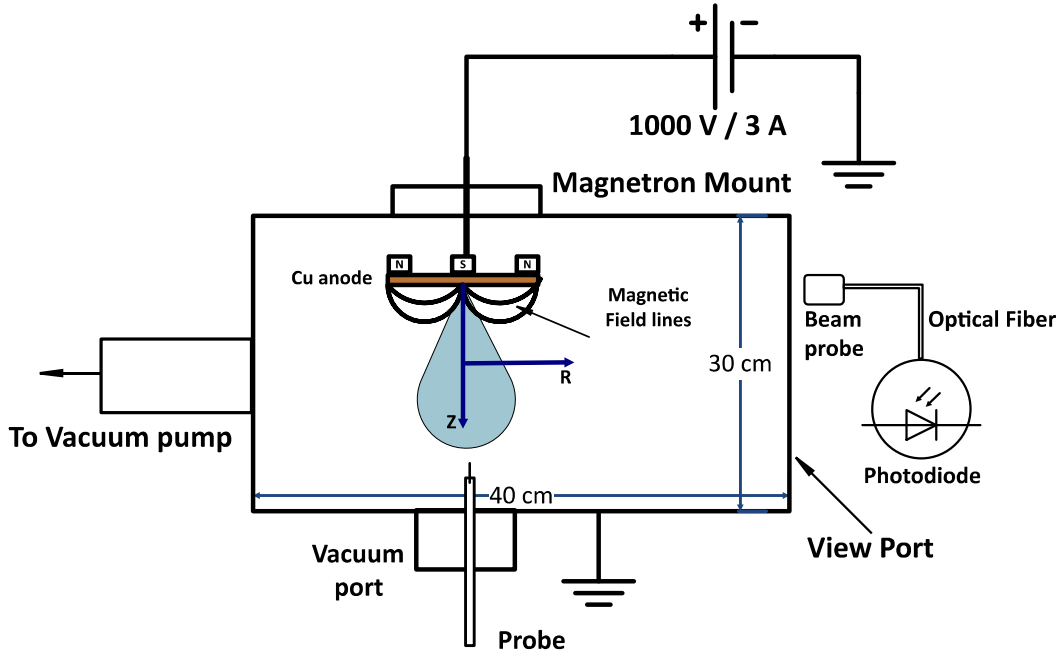
Figure 3.1: *The schematic of the vacuum chamber. The view port is made of perspex, it coves entire right cross section. Probe mounting is shown from the bottom port. Coordinate system for measurement is illustrated with the anode. The wall of the vacuum chamber is grounded and acts as the cathode of the system. The diagram is not to the scale.*

The anode is mounted from the top and the remaining three sides have ports that give access to various probes. The figure 3.1 shows only one of the three port used for probes, *viz.* the bottom port. The port has one access port in the middle. It is designed with 25 KF nipple welded in the central hole, this can easily give access to a variety of probes. All of the three ports are made identical which enable us to easily switch the mounted diagnostics from port to port, for horizontal and vertical measurements. Two of them, including bottom port are used for mounting various probe diagnostics, whereas one is used to mount the pressure gauges. The combination gauge or pirani-penning type is used for monitoring the pressure. Figure 3.2 shows the actual photograph of the experimental device. The working gas used for all of the experiments is Argon, it is fed into the system using either
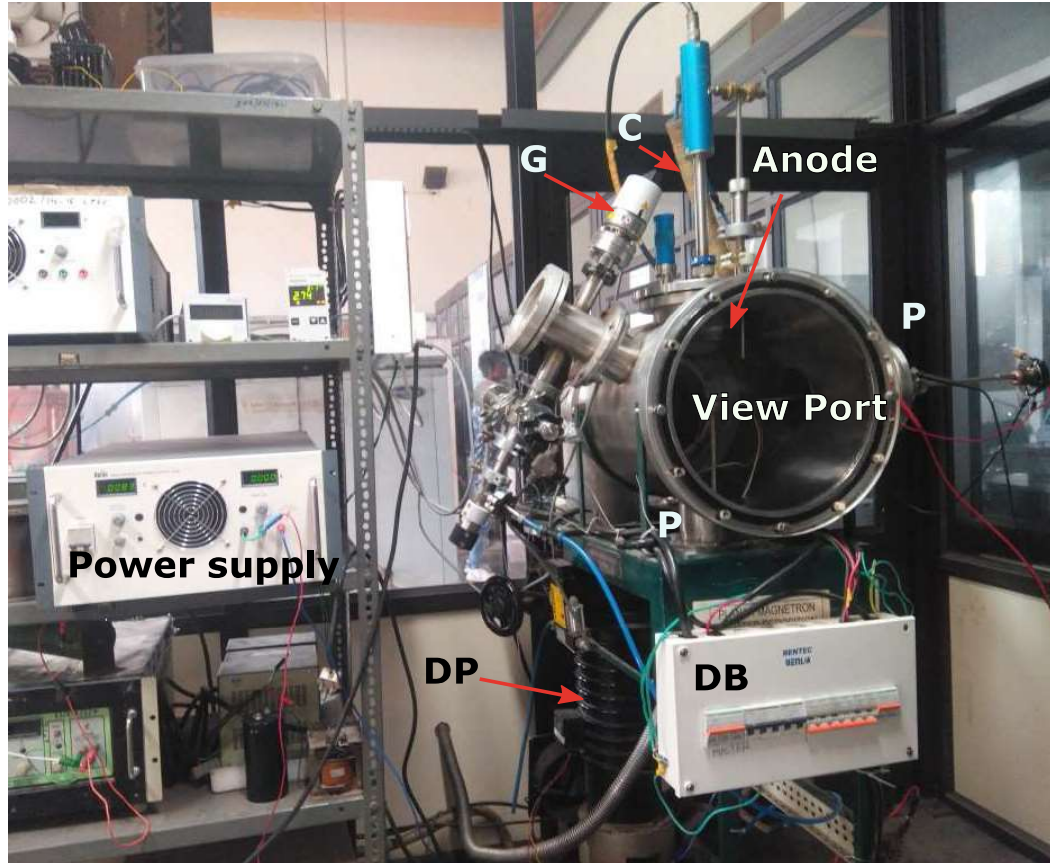
Figure 3.2: *Photograph of the experimental system. The anode is mounted on top flange isolated by an O-ring. The blue shaft of the anode is visible outside the chamber which carries the cooling line as well as the electrical connection to the anode. G - Pressure gauge, C -cooling line, DP - Diffusion pump, DB - Electrical power distribution board, P - vacuum port for probe access.*

a gas dosing valve (for high pressure) or a mass flow controller (for low pressure). The base vacuum of better than 5×10^{-5} *mbar* is achieved using a combination of rotary and diffusion pump. Starting from atmospheric pressure a rotary pump takes 20 minutes to reach a pressure of 1×10^{-2} *mbar*. From this pressure a diffusion pump takes over, a cold diffusion pump takes about 30 minutes to reach maximum pumping, which then goes to base pressure in few minutes. A manual gate valve is installed between the diffusion pump (DP) and the vacuum chamber, in combination with butterfly valve of the rotary pump, this can be used to open vacuum chamber without cooling down the DP. Once the base vacuum is achieved, the gas dosing valve or mass flow controller is turned on to maintain pressure in the range of 1×10^{-3} *mbar* to 1×10^{-1} *mbar* which is the entire pressure range that is explored in the present experiments. Stabilizing pressure in all of the pressure range may not be straight forward, we throttled the diffusion pump to reduce its pumping speed to stabilize pressure in various operating range. The discharge is powered by a 1000 V, 3 A power supply with a series resistor of 1 $k\Omega$ which caps maximum current well below the safety rating and is well above typical discharge current of 10 mA. Negative terminal of the power supply is grounded, hence, the vacuum chamber acts as grounded cathode.

3.2   Anode assembly

Anode is the main component of experimental system, since our goal was to create rather large sized fireball and explore its properties and applications. The use of an auxiliary electrode was not favourable from the application point of view where the simple setup is preferred. There is experimental evidence that the auxialiary electrode takes over as the main anode of the discharge in the presence of the fireball, identified as plasma potential locking by Baalrud et al. [3]. The use of a very small anode usually produces small fireball confined very close to the anode

[4, 34]. Therefore, using a planar sputter magnetron with slight modification in the operation we developed a device which produces a large sized fireball with unique properties. This is due to the magnetic constriction of the anode. Commercial sputter magnetron has magnetic field restricted very close to the surface of the electrode. We use a modified design of the sputter magnetron as the anode for our experiments. Copper electrode, 7.5 cm in diameter and 0.3 cm in thickness is used as the anode. Copper provides an ideal balance as it is highly conductive of heat and electricity and is non magnetic. Arrangement of the magnets on the back side of the anode is shown in the figure 3.3 and figure 3.4. The magnets create well known magnetron type magnetic field on the surface of the anode. The magnets used were of NdFeB type with maximum strength at the pole of about 2500 $gauss$. Diameter of the magnets is 1.5 cm and length is 1 cm, 16 of such magnets were used on the periphery of the anode and one in the center. Peripheral arrangement of the magnet is made convenient with a soft iron back plate. Since the like poles of the magnets are close together it is difficult to assemble them, the soft iron provide the base for the magnets as well as the magnetic coupling which makes the arrangement stable. Besides this, there is a copper housing for the magnets which act as the mould as well as the cooling apparatus (see figure 3.4). The cooling of magnets is provided with de-ionized water, kept below 20 $°C$ and circulated through the copper housing of the magnets. The cooling is necessary due to the localized plasma formation which can heat the central magnet and could deteriorate its magnetic field over long period of operation.

3.2.1 Magnetic field

The magnetic field on the anode was measured using the standard hall probe technique. A three axis hall probe is mounted on an XY translator with accuracy of 0.1 cm. Hence the spatial resolution is limited only by the size of the hall sensor, which comes about 0.5 cm. The probe is moved in a plane so as to measure the
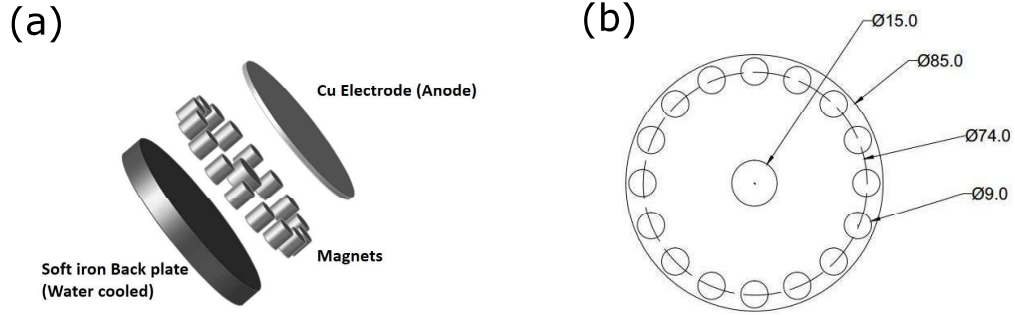
Figure 3.3: (a) The design and placement of magnets, copper anode and back plate. (b) The dimension of the magnets and central anode as well as the location of peripheral magnets. The dimensions are to the scale, all of the numbers are in millimetre. Central magnet has south pole facing the anode and peripheral magnets have north pole facing the anode.

Figure 3.4: Photograph of the magnets arranged in the copper housing.
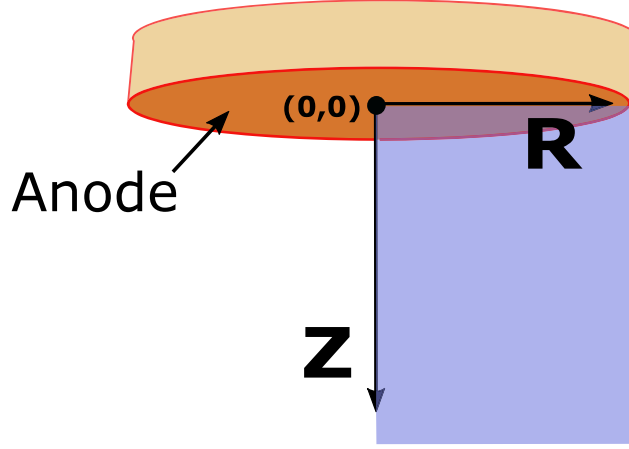
Figure 3.5: *The coordinate system used for measurements through out the thesis. The cylindrical coordinated system is adopted with R being parallel to the anode surface and Z perpendicular. Origin of the coordinate system is at the center of the anode, marked (0,0) in figure. The light blue coloured plane represents the area over which the magnetic field is measured.*

magnetic field in the plane perpendicular to the surface of the anode. Figure 3.5 shows the plane of measurements and the coordinate system used for measurement of all of the parameters in the entire thesis, unless otherwise stated. The magnetic field measured is that of the vacuum case and not in the presence of the plasma. We do not expect the magnetic field to change substantially during the plasma operation since plasma β in our case is $\sim 10^{-6}$ which is $\ll 1$ [11, 77, 78]. The main feature of the magnetic field is that it reduces sharply as we move away in positive $\hat{Z}$ direction. In radial direction the field is very complicated. The field near the anode is highly non-uniform with very steep gradients and curvatures. Magnetic field is measured in the $\hat{R} - \hat{Z}$ plane. The $\hat{R}$ component of magnetic field B_r is termed the parallel magnetic field as it it is parallel to the anode surface. Similarly the $\hat{Z}$ component, B_z is termed perpendicular as it is perpendicular to the anode surface. The measured magnetic field is given in figure 3.6. The contours represent the strength of the magnetic field given by $B = \sqrt{B_r^2 + B_z^2}$ and the local direction of the magnetic field is represented by the lines in a quiver type plot.

The individual component of the magnetic field is given in figure 3.7. Left column
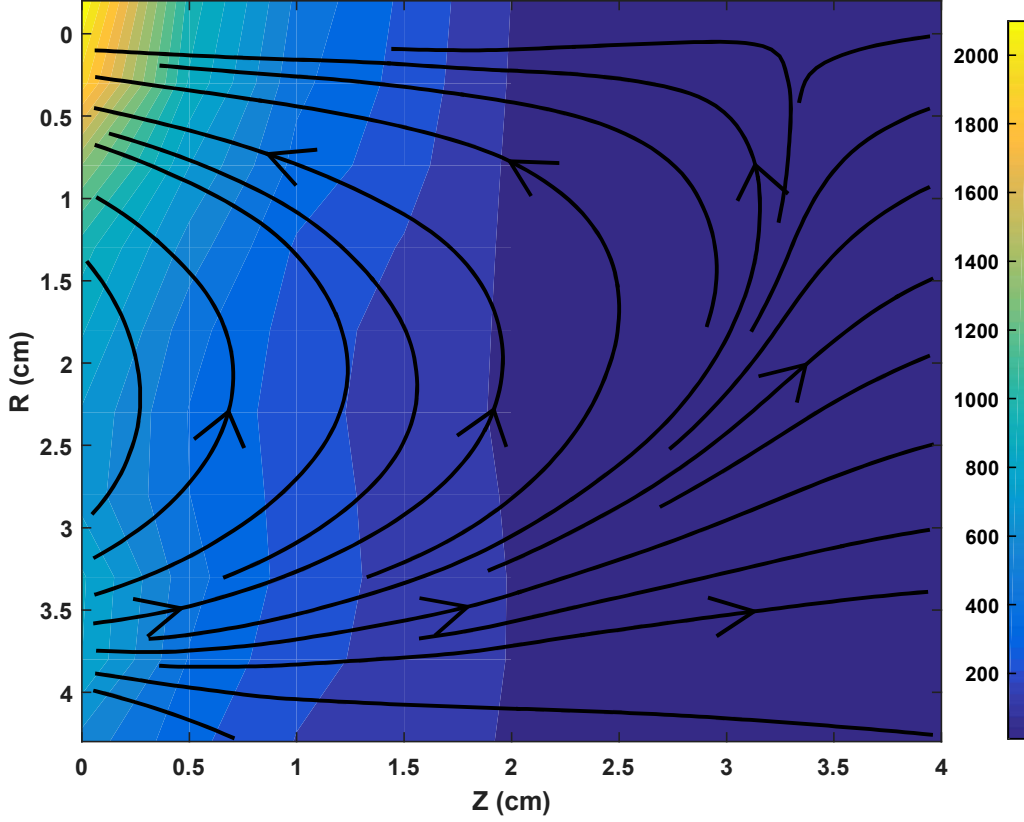
Figure 3.6: *Contour plot of the magnetic field on $R-Z$ plane. The colour coding is magnetic field in gauss as shown in the colour bar. The lines represents the local direction of the magnetic field.*

in figure 3.7 shows the variation along $\hat{R}$ for different Z values, where as the right column shows the variation along $\hat{Z}$ for different R values. The anode is located at the $Z = 0$ plane. Top row in figure 3.7 shows the magnetic field component B_r, it is highly inhomogeneous in R (see top left plot), but not so much in Z direction (see top right plot). It is important to stress the role of this component in the anode glow and the motion of the electrons. The electric field near the anode is expected to be purely along the $\hat{Z}$ direction. B_r is strongest only in between the pole locations at about $R = 2\ cm$, at this location the B_z is weakest making the B_r
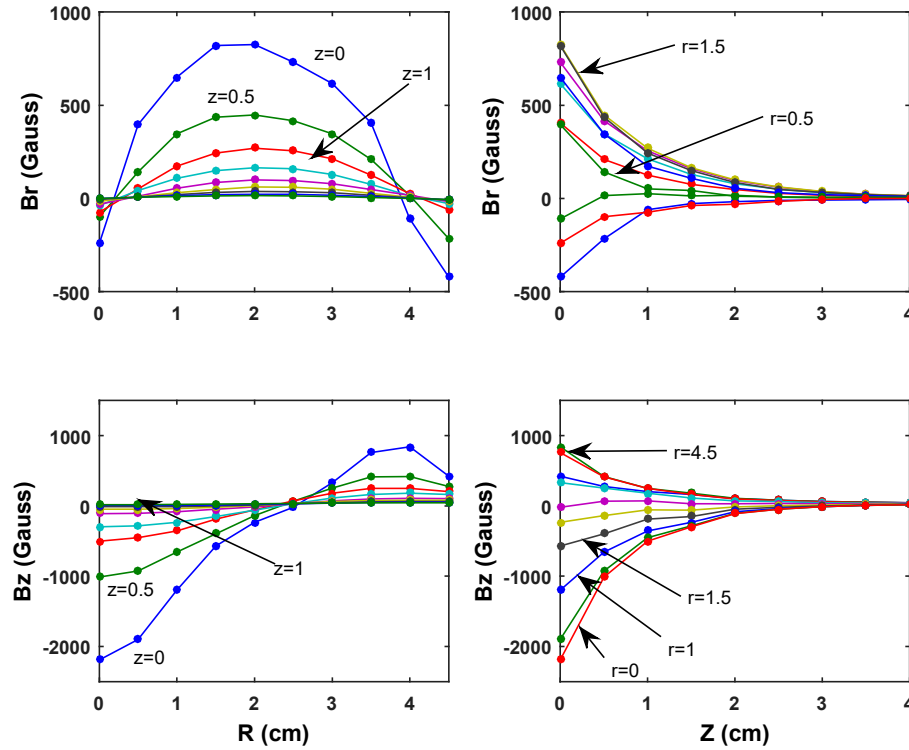
Figure 3.7: B_r and B_z are the component of the magnetic field along R and Z axis respectively. Top and bottom row shows parallel (B_r) and perpendicular (B_z) component, respectively. Left and right column shows variation along R and Z, respectively. Right column shows that both of the components fall rapidly as we move away from the anode. See figure 3.5 for the coordinate system.

dominant. It is to be noted that the pole of the magnets are located at $R = 0 \; cm$ and $R = 3.7 \; cm$ corresponding to the central and peripheral magnets, respectively. Lets take an example of a single electron moving towards the anode in electric field $E(z)$. Motion of the electron will be strongly affected by the $\vec{E} \times \vec{B}$ drift only in between this pole location, say at around $R = 2 \; cm$. At the location of the poles this drift goes to zero. This clearly indicates that an electron approaching from $Z = \infty$ towards the anode for any R except the pole location will be drifted away in the direction of $\vec{E} \times \vec{B}$ which is $\hat{\theta}$ in our case. Hence, these electrons will not reach the anode. The electrons streaming from far at pole location i.e. at $R = 0$ will not encounter any $\vec{E} \times \vec{B}$ drift since the only dominant component at this location is B_z which is parallel to the electric field $E(\hat{Z})$. This leaves only the pole (0,0) of the magnet as the possible location for electron to sink into the anode.

3.3   Discharge procedure

Plasma is produced by applying DC bias between the anode and the grounded chamber. Positive terminal of the power supply is fed to the anode as shown in figure 3.1. This produces bright "inverted droplet" shaped glow near the anode. Discharge is operated from $5 \times 10^{-3} \; mbar$ to $5 \times 10^{-2} \; mbar$ of pressure and typically near 300 V. Discharge current is typically between $1 - 10 \; mA$.

Paschen curve of any discharge device gives breakdown voltage for a given set of experimental conditions. It identifies the minimum ignition voltage for a given set of geometry. For a parallel plate DC discharge, the relation between the breakdown (ignition) voltage (V_d) and the product of pressure and distance (Pd) between the electrode is given by

$$V_d = \frac{BPd}{ln(APd) - ln\left(ln(1 + \frac{1}{\gamma_{se}})\right)} \tag{3.1}$$
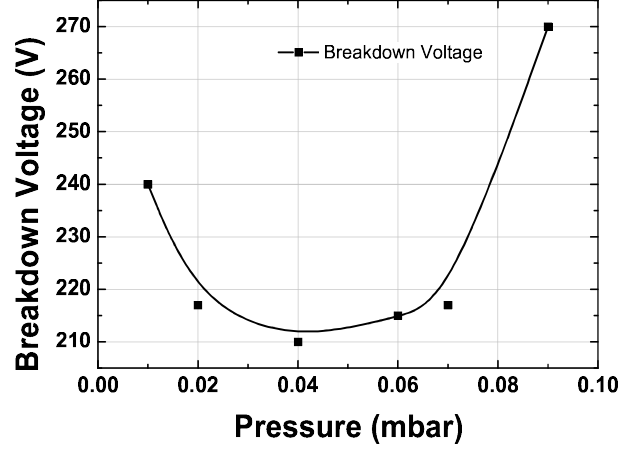
Figure 3.8: *The Paschen curve for our system. The Paschen minimum occur at pressure of 4×10^{-2} mbar.*

where, A, B are constants, γ_{se} is the secondary electron yield, which is constant for a given material. Essentially only the pressure (P) and distance (d) are variables. For a complex geometry the Paschen curve can be determined by varying only pressure, which changes the product Pd. For determining minimum voltage and pressure for breakdown, the Paschen curve for our system is obtained and is shown in figure 3.8.

The ideal pressure to ignite the discharge is found to be $4 - 5 \times 10^{-2}$ mbar. The vacuum chamber is first pumped to base vacuum of 1×10^{-5} mbar, within $35 - 40$ minutes. Then the argon gas is introduced using a gas dosing valve to bring the pressure in the range of 4×10^{-2} mbar, the discharge is obtained by slowly increasing the voltage. Once the discharge is established the pressure is reduced to the desired value. The discharge is formed in the shape of "inverted droplet" near the surface of the anode. Typical plasma density in the bulk region is $1 - 10 \times 10^8$ cm^{-3}, and electron temperature is few eV.

3.4   Diagnostics

3.4.1   Langmuir Probe

We have touched upon this most basic diagnostics earlier in Chapter 2, section 2.2.2. The Langmuir probe is a small, practically cylindrical (or planar or spherical) electrode (e.g. bare wire) introduced into the plasma. This electrode is biased to various voltages and the corresponding current is measured to infer the plasma properties. This measured set of voltage and current of the Langmuir probe is known as current-voltage characteristic of the probe. The two biggest advantages of the Langmuir probe are that it is relatively simple to implement and one can perform highly localized measurements.

Figure 2.3 (page 13) shows typical Langmuir probe characteristics. It can be conveniently divided in three regions depending on what type of particles are collected by the probe. We have already seen in earlier chapter, the concept of Plasma potential (V_p), floating potential (V_f), electron saturation current (I_{es}) and ion saturation current (I_{is}). We have also discussed in brief the three regions and the Boltzmann factor which decides the probe current in the electron retarding region ($V_B < V_p$). The bias voltage of the probe V_B is always measured with respect to the laboratory ground or one of the electrode of the discharge. The standard Langmuir probe theory predicts completely flat electron and ion saturation current, however both currents do not completely saturate, again due to the complicated sheath dynamics. Below we discuss the equations of the current in all three regions and its explanation.

V_p is the plasma potential with respect to the laboratory ground potential. When the probe is biased at that potential there exist no electric field between the probe and the plasma. Any particle that arrives at the probe is collected. Since the random flux of electrons is very high compared to ions (see chapter 2) all of

the current at this potential or higher consists of electron current. This current is conventionally shown as positive probe current. Ideally for any bias voltage above this potential the current should remain constant however this usually does not happen, and the current keeps on increasing weakly with bias voltage. This is due to the increase in the sheath thickness which ultimately determines the collection area. The electron saturation current is given by

$$I_p = I_{es} = enA\sqrt{\frac{KT_e}{2\pi m}} \tag{3.2}$$

where A is the probe area, n is plasma density, e is elementary charge, K is the Boltzmann constant, T_e is electron temperature, m is the mass of electron.

For probe bias below the local plasma potential, the probe becomes negative with respect to the plasma and retards the incoming electrons. For Maxwell-Boltzmann distribution of velocity, the number of electrons repelled is proportional to the Boltzmann factor and the current to the probe is given by

$$I_e(V_B) = I_{es}exp\left(\frac{-e(V_P - V_B)}{KT_e}\right) \tag{3.3}$$

This is one of the most important region of the Langmuir probe characteristics, which is usually first to be evaluated. One can see that the current in this region depends on the electron temperature. Upto now we have neglected the contribution of the ion current, however, as V_B is reduced the electron current reduces exponentially and becomes comparable to ion current. For a certain voltage below the plasma potential, both ion and electron current become equal and cancel each other, at this instance no current flows through the probe. This potential is known as floating potential of the probe since an insulating probe which cannot carry current will float at this potential.

Further negative biasing of the probe will result in a well developed ion sheath

since most of the electrons are now repelled and the collected current is due to the ions. As we have seen in Chapter 2, the ion sheath requires a pre-sheath which accelerates the ions to Bohm velocity, which is the minimum velocity it requires to enter the sheath. We have already seen in Chapter 2, section 2.2.1 that the density at the sheath edge is reduced by a factor of 0.61. Considering this the ion current can be written as

$$I_p = I_{is} = 0.61 e n A \sqrt{\frac{KT_e}{M}} \tag{3.4}$$

where M is the mass of ion. This equation can be effectively used to obtain plasma density (n), since a quasi neutral plasma has equal number of electrons (n_e) and ions (n_i), $n_i = n_e = n$. All of the above equations hold for collisionless sheath only, which is satisfied in our case. Also the application of Bohm criterion for ion current is applicable only to planar sheath, this can hold for cylindrical Langmuir probe only if the sheath thickness 'd' is much smaller than the radius of the Langmuir probe 'r_p'. Hence the condition of applicability of plane sheath theory in cylindrical Langmuir probe is $(r_p/\lambda_d) >> 1$, where λ_d is the debye length and is a measure of the sheath thickness. Figure 3.9 shows two cases of r_p/λ_d. Our analysis in present thesis assumes the case (a) in figure 3.9. The discussion of many other ion collection theories for thick sheath can be found in many references [22, 79–81].

Electron temperature and plasma density calculation

Electron temperature is usually the first quantity we obtain from Langmuir probe I-V characteristic. This is because it is relatively straight forward and is usually accurate if the distribution function of electrons is isotropic Maxwellian. We have seen that the electron probe current below the plasma potential is an exponential function of the probe bias divided by the electron temperature. The main issue that arises here is to determine the current due to the electrons only. Since the probe near and above the floating potential collects both electrons and ions, we
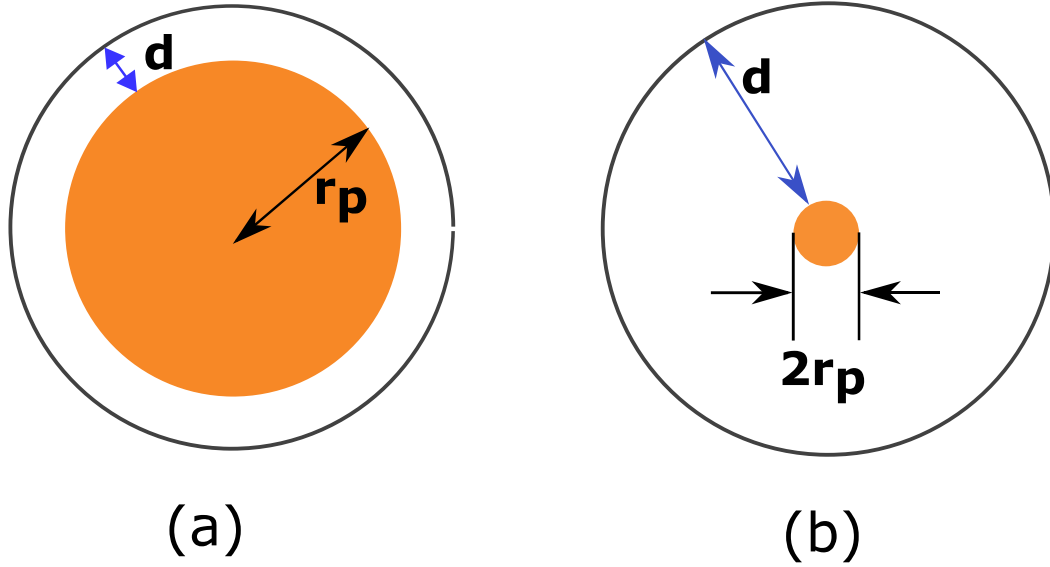
Figure 3.9: *(a) Thin sheath limit, the Bohm current is applicable and is reliable to calculate plasma density (b) The sheath is cylindrical and the ion collection was originally explained by Langmuir, the theory is known as OML.*

have to carefully determine the contribution of ions and subtract it from the probe characteristics. This can be done with various theories and can determine the accuracy of measured electron temperature. The ion current can be estimated using OML, ABR, or thin sheath approximation. Since in our case, the thin sheath approximation is applicable we can use the Bohm current to subtract from the I-V of Langmuir probe. However the ion saturation current is not strictly constant due to the expansion of the sheath. To a reasonable extent, the ion current can be approximated by a linear fit to the ion region and extrapolating it and subtracting from the I-V, gives the electron current of the probe.

Once we have electron current it can be seen from equation 3.3 that the natural logaritm of the curve will give straight line for electron retarding region, i.e. upto the plasma potential. Taking plasma potential as reference ($V_p = 0$) and taking log of equation 3.3,

$$ln(I_e) = \frac{eV_B}{KT_e} + constant \tag{3.5}$$
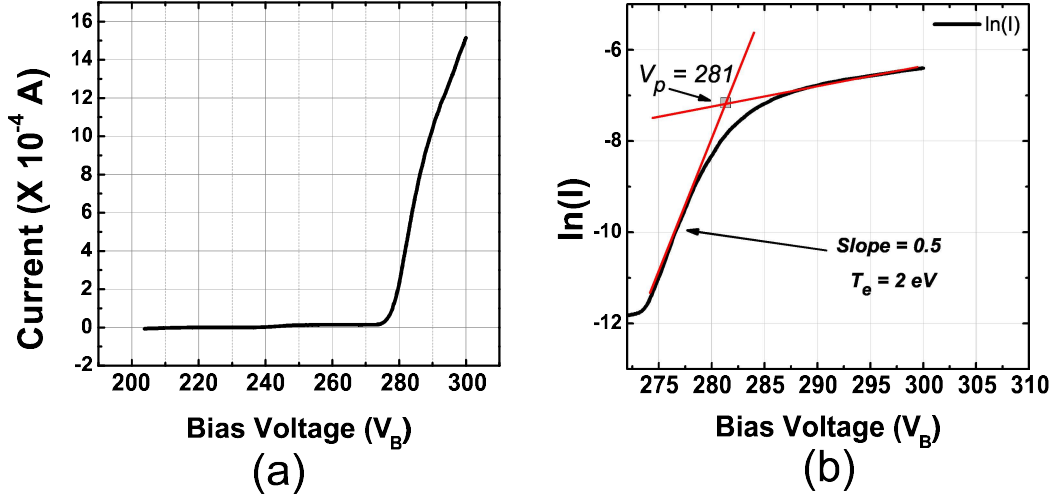
Figure 3.10: *Sample Langmuir probe I-V curve. (a) Raw data, the knee of plasma potential is not clearly distinguishable. (b) Semi-log plot of Langmuir probe data. The knee is now easily identifiable. T_e is obtained readily from the slope of linear region between floating potential and plasma potential.*

This is a linear equation of $y = mx + c$ type, here x is V_B in our case and m is e/KT_e. Hence the inverse of slope in the linear region of the $ln(I_e)$ vs V_B curve directly gives the electron temperature in eV.

Once T_e is known the plasma density n is readily obtained from equation 3.4 which is applicable in the thin sheath limit.

Plasma potential and Floating potential

The floating potential (V_f) is easily obtained from original Langmuir probe I-V characteristic by observing the voltage at which zero current occur. To avoid the inaccuracy in the case of small ion saturation current it is advisable to plot the square of the probe current with respect to the probe voltage, this will enable us to clearly identify the location of the floating potential. Plasma potential (V_p) can be identified as a knee in the well obtained Langmuir probe I-V characteristics. However, it is easier to identify the plasma potential in the $ln(I)$ vs V_B plot. In this plot we can extrapolate the linear regions of electron retarding and electron

saturation and the cross section of the lines is the plasma potential. The current at plasma potential is electron saturation current. Another method to identify the plasma potential is the inflection point method. In this the first or second derivative of the probe current with respect to bias voltage is taken, the inflection point of the first derivative is the location of plasma potential, alternatively the zero crossing of the second derivative gives the plasm potential. There are uncertainties in the determination of plasma potential by using these various methods hence it is advisable to use emissive probe for the measurement of the plasma potential.

Effect of the magnetic field

In the presence of magnetic field, Langmuir probe becomes considerably difficult to analyze. The magnetic field causes the electrons and ions to gyrate and allow them to move only along the magnetic field lines. The motion of the particles is restricted to gyro or larmor radius of the particles r_L, it is this length which is compared with typical probe dimension r_p. For $r_L >> r_p$ the unmagnetised version of the Langmuir probe is applicable. Ion larmor radius is usually much larger than the electron larmor radius, hence the effect of magnetic field on ion current can usually be neglected. Electrons, though affected by magnetic field, are repelled according to the Boltzmann factor $(exp(-e(V_p - V_b)/kT_e))$. Hence in many cases where ion larmor radius is larger than the probe dimension, the usual Langmuir probe analysis suffice. In the case of magnetised plasmas where ion larmor radius is smaller than the probe dimension the magnetized sheath and pre-sheath may exist. In such cases the projection of Langmuir probe in the direction of magnetic field is taken as effective area to calculate the plasma density. In our case the fireball mostly forms in magnetic field free region and most of the measurements are performed in weak ($\sim$ 10 $gauss$) or no magnetic field region.

Practical formulae for calculating electron and ion gyro radius is given below,

$$r_{ce} = \frac{3.37\sqrt{E}}{B_0} \ cm \ (E \ in \ eV, \ B_0 \ in \ gauss) \tag{3.6}$$

$$r_{ci} = \frac{144\sqrt{EA_R}}{B_0} \ cm \ (A_R \ in \ amu) \tag{3.7}$$

where, r_{ce} and r_{ci} are electron and ion gyro radius in cm, respectively. A_R is the mass of ions in amu, B_0 is the magnetic field in $gauss$ and E is the energy of the particle (perpendicular to magnetic field) in eV. Using the above mentioned formulae for ionizing ($16 \ eV$) electrons and room temperature ($0.026 \ eV$) ions, their gyro radius comes out to be 1.3 and 14.4 cm, respectively. Since both gyro radius at measurement location are much bigger then the probe dimension ($0.7 \ mm$) the condition $r_L >> r_p$ holds, hence the effect of the magnetic field is neglected for Langmuir probe measurements.

3.4.1.1 Double Langmuir probe

As shown previously in figure 3.10, our plasma potential is very high compared to the laboratory ground, this happens because we have the cathode of the discharge grounded and the anode is floating positive. This requires a sweeping voltage for Langmuir probe measurements to be of the order of discharge voltage. In such a scenario a double Langmuir probe is convenient to use. The maximum current that a double Langmuir probe can carry is limited to ion saturation current and hence large electron saturation current is avoided.

The initial use of the double Langmuir probe was by Johnson and Malter [82]. The double Langmuir probe is an isolated system of two identical Langmuir probes biased with respect to each other. The advantages and limitations of such system are well documented in the literature [82–84]. Theory of Double Langmuir Probe (DP) can be easily understood from our understanding of the ion and electron
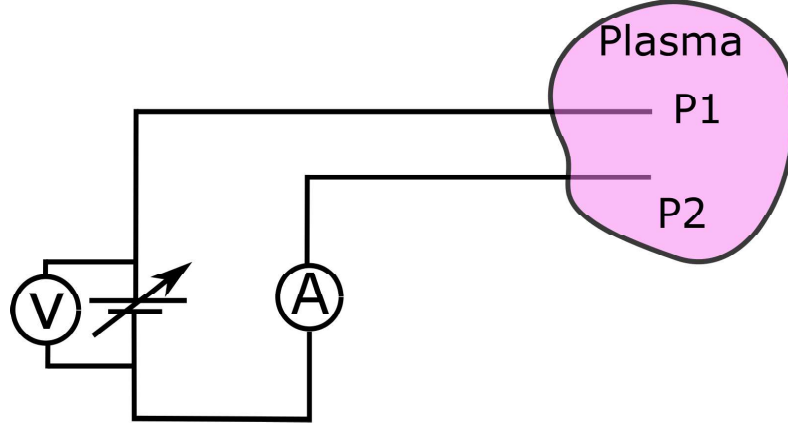
Figure 3.11: *Circuit diagram of a typical Double Langmuir Probe. The voltage source is completely floating. P1 and P2 are two probes immersed into the plasma.*

current to the single Langmuir probe. Figure 3.11 shows the typical double probe circuit. The sweeping voltage used in the circuit is completely floating from plasma and laboratory ground. In the double probe, the current from one probe must equal the current from second, hence the current is always limited to the ion saturation value. Using this condition,

$$I_{P1} = -I_{P2} \tag{3.8}$$

where, I_{p1} and I_{p2} are the current through probe 1 and 2, respectively . The current in the double Langmuir probe can be written as,

$$I = I_{is} tanh\left(-\frac{eV_d}{2KT_e}\right) \tag{3.9}$$

where, V_d is the voltage of a probe with respect to the other probe. From above equation the electron temperature can be calculated as below,

$$\left(\frac{dI}{dV_d}\right)_{V_d=0} = \frac{eI_{is}}{2KT_e} \tag{3.10}$$

$$\frac{KT_e}{e} = T_e(eV) = \frac{I_{is}}{2} \times \frac{1}{\text{slope at } V_d = 0} \tag{3.11}$$

Once T_e is obtained with above equation, it is straight forward to obtain plasma density using equation 3.4. As the whole Double probe system is floating, it cannot be used to obtain plasma potential or floating potential. Since the Double probe system does not require well defined voltage reference or reference electrode it is much more versatile and is not affected by changes in the discharge voltage. The measurement of Double probe is also immune from possible large electron saturation current and is highly repetitive.

3.4.1.2   Designing of the Langmuir probe

To design a good Langmuir probe system one should consider the range of parameters they want to measure. The plasma density in particular is a preliminary deciding factor. The most essential factor is the ratio of probe radius to sheath thickness (r_p/d), the sheath thickness is usually a few debye lengths (λ_d) wide, hence the ratio is often written as r_p/λ_d. To use the thin sheath approximation, $r_p/\lambda_d > 1$ is preferred. However this becomes difficult to satisfy for low density $(\sim 10^8 \ cm^{-3})$ plasmas. The practical formula for debye length is $\lambda_d = 740\sqrt{T_e/n_e} \ cm$, where T_e is in eV and n_e is in cm^{-3}. For $n_e = 10^8 \ cm^{-3}$ and $T_e = 4 \ eV$ the debye length $\lambda_d = 1.4 \ mm$, if Langmuir probe radius is kept larger than that, it may collect a large electron current and would drain the plasma. Hence to minimize the disturbance the Langmuir probe needs to be smaller and the large sheath (due to large debye length) would require the OML or ABR analysis of the Langmuir probe data. For higher plasma density $n_e > 10^9 \ cm^{-3}$ the debye length falls below $0.4 \ mm$. Our expected density is of the order of $10^9 \ cm^{-3}$ in the bulk plasma and as high as $10^{10} \ cm^{-3}$ in a localized fireball region. We have chosen the Langmuir probe diameter of $0.7 \ mm$, which satisfies the $r_p/\lambda_d \geq 1$ for our density range and the thin sheath approximation (figure 3.9(a)) is applicable. The length of the Langmuir probe is taken as $7 \ mm$ to avoid the end effects. Total area of Langmuir probe is taken as $A = 2\pi r l + \pi r^2$, where r and l are radius and length of the
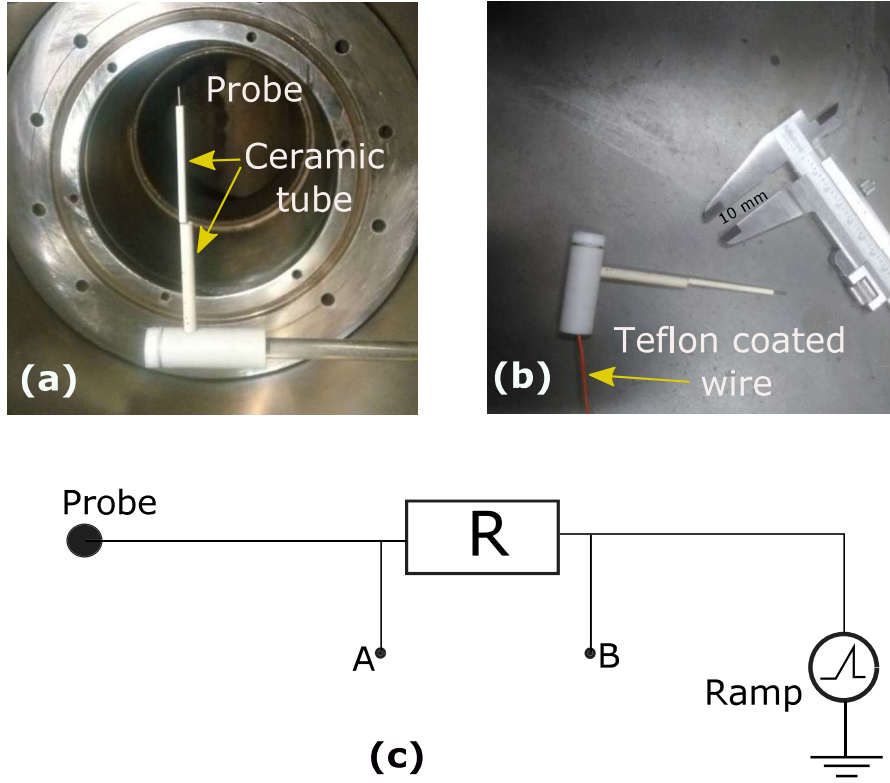
Figure 3.12: *(a) and (b) are photos of the actual Langmuir probe constructed of Tungsten. In (a) the probe can be moved horizontally. (c) Circuit diagram, the resistor R is floating and a four channel floating oscilloscope is used to measure the current through the probe.*

Langmuir probe, respectively.

Tungsten (W) is used as the tip of the Langmuir probe as it is less prone to sputtering and does not melt or deform at high temperature. Tungsten is difficult to machine and weld, the wire was cut, shaped and fixed in a small ceramic tube. The connection is taken out by a copper wire inside the ceramic tube, which runs through the SS pipe, which is connected to a vacuum port. The Langmuir probe can be moved in and out to measure the plasma properties. Figure 3.12 shows the Langmuir probe mounted on a port. Before every measurement the Langmuir

probe is sputter cleaned by biasing it extremely negative.

The double Langmuir probe is similar in design, except two identical probe tips are fixed in a double bore ceramic tube. The circuit diagram is shown in figure 3.11. Care has to be taken that the sheath of one probe does not overlap that of the other probe. Rest of the fabrication remains similar, except that two wire connect two identical Langmuir probes through SS pipe and vacuum feed through.

3.4.2   Emissive Probe

Emissive probe is extensively used for the measurement of plasma potential. It can measure plasma potential reliably in various conditions e.g sheath, double layer e.t.c., where the conventional Langmuir probe is prone to errors [7, 8]. The emissive probe consists of a thin wire, usually tungsten, which is heated to very high temperature sufficient to induce thermionic emission of electrons.

The principle of operation of emissive probe is simple, it will emit electrons only when biased negative with respect to the local plasma potential. Comparing the I-V traces of cold and emitting probe will enable us to identify the potential where their current differ which is the local plasma potential. Since the emission from the probe depends directly on the local plasma potential, it is not affected by the flow of plasma or the electron temperature.

Temperature limited emission current can be given by,

$$I_{e0} = A T_w^2 \ S \ exp\left(\frac{e\phi_w}{T_w}\right) \tag{3.12}$$

where, A is Richardson's constant, ϕ_w is the work function of the wire, T_w is the temperature of the wire and S is surface area of the wire. This current flows when the probe is biased negative with respect to the plasma however all of the emission is halted above the plasma potential. Considering this simple assumption will help us in understanding the I-V traces of the emissive probe.
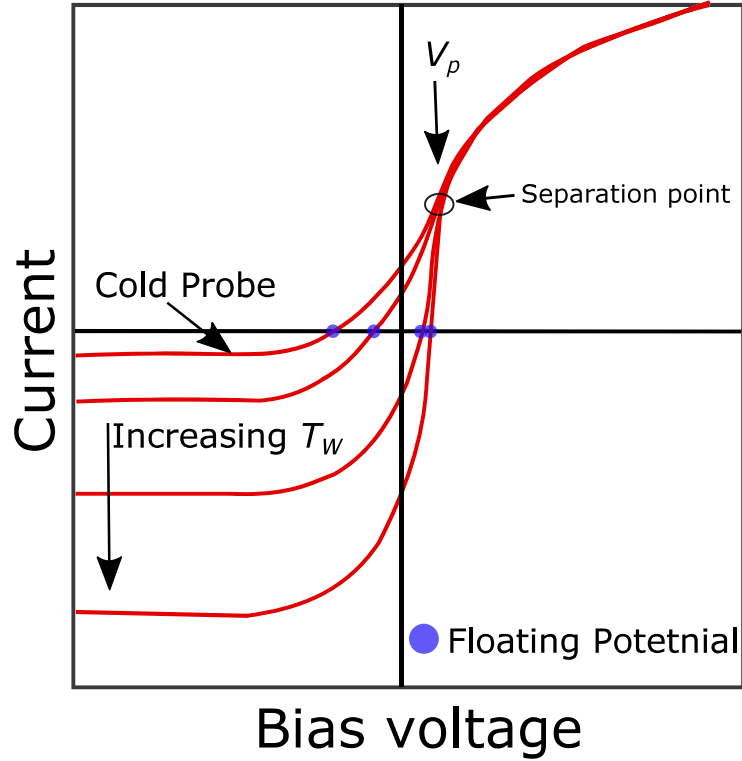
Figure 3.13: *Schematic of typical Emissive probe I-V traces with increasing wire (emissive probe) temperature. The cold probe characteristic is similar to the single Langmuir probe, increasing current increases the emission current for voltages below the plasma potential. For bias voltage above the plasma potential the emission current is reduced to zero and the I-V traces of cold and emissive probe are equivalent.*
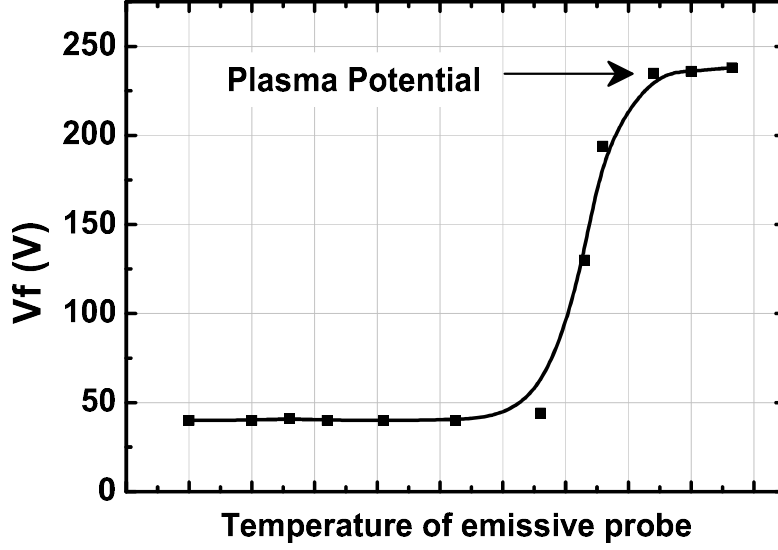
Figure 3.14: *The floating potential of emissive probe is measured for increasing probe (wire) temperature. The temperature is controlled by controlling the current flowing through the tungsten wire loop (the emissive probe). Increasing the current through the emissive probe does not affect floating potential until it starts emitting. Once emission starts, the floating potential quickly rises and saturates at the local plasma potential.*

The first use of emissive probe was reported by Langmuir [85], he argued that the lowest potential at which the collected current is same for emitting and none-mitting probe is the plasma potential. Figure 3.13 shows the I-V characteristic of typical emissive probe for increasing wire temperature.

First major step towards the practical and widespread use of emissive probe was a work done by Kemp and Sellen Jr [86]. They exploited the fact that with increasing temperature the floating potential of the emissive probe approaches the plasma potential, see figure 3.13. In practice, the emission of the emissive probe is increased by increasing the wire (probe) temperature until the floating potential saturates. this is demonstrated in the data taken from our device in figure 3.14. We used this technique to obtain the plasma potential. For each measurement the heating of the emissive probe is increased until the floating potential is saturated.

This method is most widely used for the measurement of plasma potential.
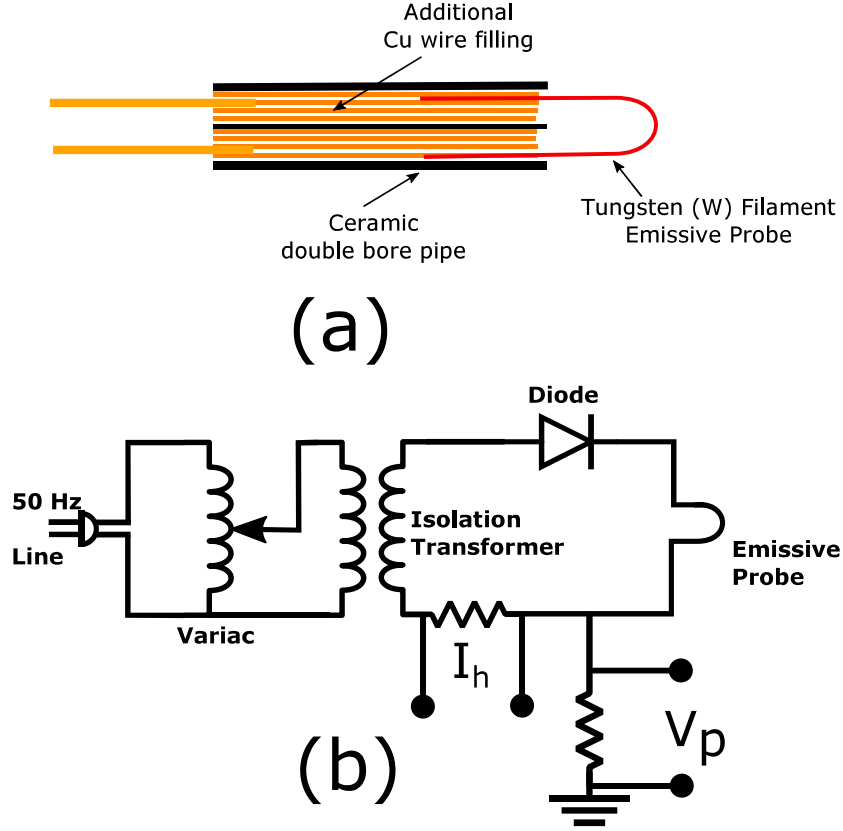
Figure 3.15: *(a) The schematic of the Emissive probe construction. 0.125 mm thin Tungsten (W) wire is taken and formed a loop, which is simply press fit in to the double bore ceramic tube. The ceramic tube is filled with many thin copper threads to increase the conductivity inside the ceramic. (b) Circuit used for heating the Emissive probe and the measurement of the plasma potential.*

Designing and implementation of Emissive probe

Emissive probes are most commonly made of thin Tungsten wire because it has highest melting point for any metal (3695 K). There are different methods to heat the probe e.g. Joule heating, Laser heating, Indirect heating etc. The Joule heating is one of the most widely used technique. Tungsten wire is made into a loop, which is fixed into the double bore ceramic tube. Current is run through the
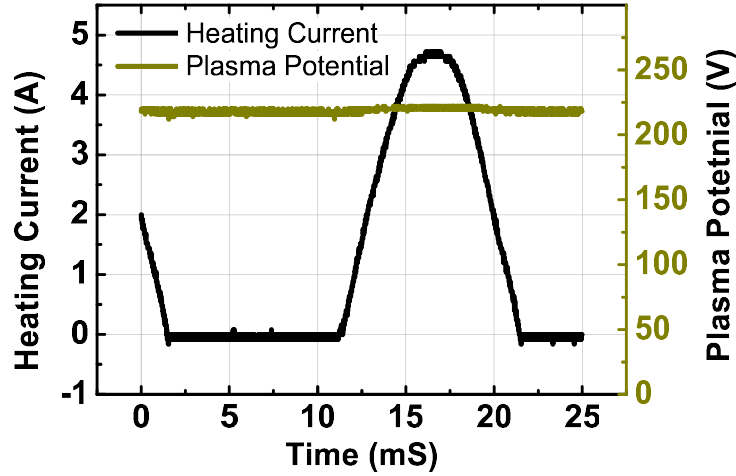
Figure 3.16: *Trace of emissive probe heating current and the floating potential of emissive probe identified as the plasma potential. The heating current is half wave rectified AC current run through the emissive probe.*

very thin emissive probe (wire) and for few amperes of current the emissive probe heats upto a temperature suitable for thermionic emission.

Passing a current through the emissive probe results in some voltage drop across the length of the probe, this may introduce additional errors in measurements. To avoid this, a half wave rectifier circuit is implemented (see figure 3.15(b)), the out put of this circuit remains on for half of the period of the input current and remains off for the other half. For a 50 Hz supply, the emissive probe does not cool down within the off period and allow us to measure the plasma potential when the source is effectively off. The output is measured with a floating digital oscilloscope and the trace is shown in figure 3.16. The emissive probe is very fragile to disturbance and tends to break easily, especially after few operations. Dorf et al. [87] have suggested that filling additional conducting wires inside the ceramic tube would increase the conductivity inside the tube and would prevent unnecessary heating. We used this technique and have found that there is significant improvement in the life span of a the probe.
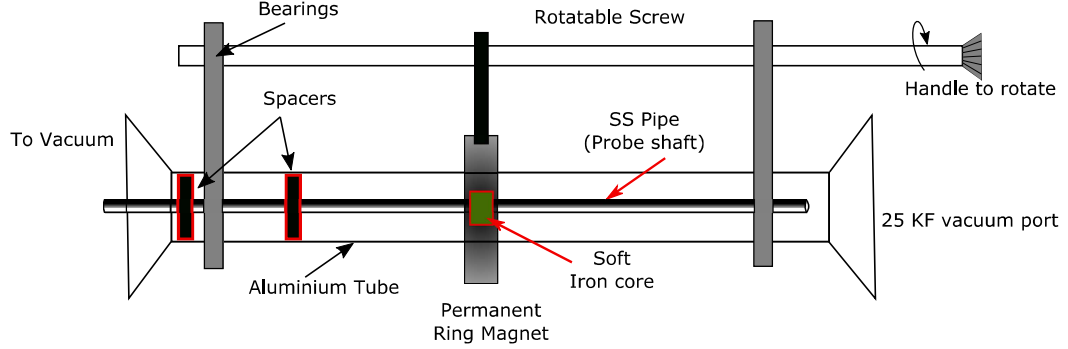
Figure 3.17: *The magnetically coupled linear translator. The outer ring magnet can slide on the aluminium pipe, the magnets couple with the iron ring fixed on the probe shaft. As the magnet slides on the shaft, the magnetically coupled ring inside the vacuum chamber moves the probe.*

3.5 Magnetic Translator

To measure the plasma parameters spatially one needs to move the probe in a reliably repeatable way. The usual vacuum feed through uses a 25 KF coupler with matching port, the probe shaft is sent through the coupler which uses a set of O-rings so that the probe shaft can be moved. This method though versatile does not offer the accuracy and repeatability of a mechanical translator. There are various options of both motorized and manual translators.

We adopted a magnetic coupling type design that was fabricated at our lab. The schematic of the design is shown in figure 3.17. The aluminium pipe is chosen to reduce the weight of the translator system. A permanent ring magnet is mounted on the pipe, this magnet can freely slide on the outer surface. After mounting the magnet the 25KF vacuum coupler is welded on both ends of the pipe. The probe shaft remains in the center of the pipe and has one soft iron ring fixed on it. The probe shaft can move freely on the two ring spacers placed inside the pipe. Various probes are mounted on the SS shaft (pipe) using a teflon coupler and ceramic holders. The electrical connections are taken out with a vacuum electric

feed through designed in the lab. To move the probe precisely, the outer ring magnet is rigidly connected to a rotatable screw. When the screw is manually rotated, the nut on the screw slides very precisely which in turn moves the ring magnet on the aluminium pipe. The moving magnet couples with the iron ring on the probe shaft and hence the motion is coupled inside the vacuum. In this manner the probe is moved in $\hat{R}$ and $\hat{Z}$ direction in the range of 10 cm.

4

Anode double layer and electron sheath formation

As discussed in the previous chapter, DC glow discharge is formed by applying high voltage between the grounded chamber and the anode. The discharge is formed with a bright anode glow visible from the view port, and no visible glow near the cathode. The shape of the anode fireball is that of an "inverted droplet". The typical glow and its characteristic dimensions are shown in figure 4.1. This droplet shaped glow appears at the center of the anode and is termed as C-Mode glow in contrast to the P-Mode glow that will be discussed in the next chapter. Formation of this glow and its suggested mechanism is discussed in this chapter. The potential structure is also discussed which is found to have an ionizing double layer near the visual boundary of the fireball.
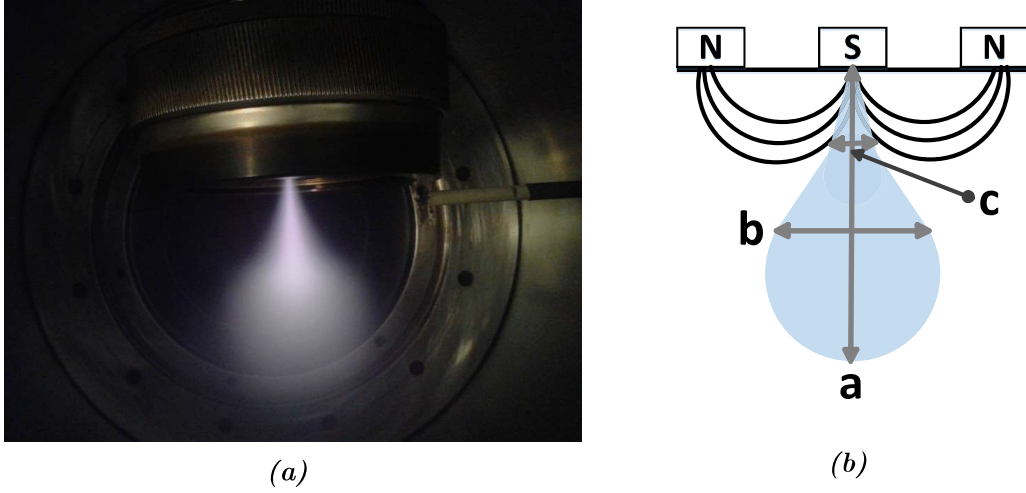
Figure 4.1: *Droplet shaped anode glow of the discharge. (a) Digital image of the droplet shaped anode glow showing bright anode fireball at pressure of 1×10^{-3} mbar and 450 V discharge voltage. No other visible glow is present elsewhere in the chamber. (b) Glow schematics and different lengths used in measurements. Magnetic field profile near the cusp plays a crucial role for the droplet shape of the anode glow.*

4.1 Current voltage characteristics

The discharge exhibits two distinct modes of operation. As shown in figure 4.2 the discharge at low pressure (below 1×10^{-2} mbar) has low values of current (~ 20 mA) and rises moderately with the applied voltage, where as for high pressures (above 1×10^{-1} mbar) the current is large (~ 100 mA) and it rises steeply with the discharge voltage. For low pressure, discharge cannot be sustained below a certain voltage which is evident from the figure 4.2. The low current mode corresponds to the C-Mode glow as shown in figure 4.1, where as the high current mode corresponds to the P-Mode and will be discussed in the next chapter. The C-Mode glow and P-Mode glow clearly follow different power laws. For the pressure in the range of $\sim 3 - 8 \times 10^{-2}$ mbar, the transition occurs from the C-Mode to the P-Mode, which is also evident in the I-V relationship. Our discussion in the
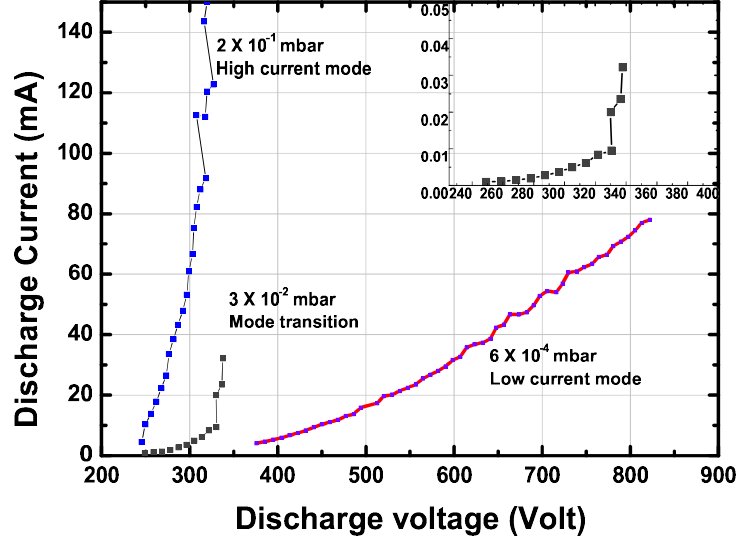
Figure 4.2: *Current-voltage characteristic of the discharge. There clearly exist two branches with distinct I-V relationship. One with high voltage and low current is identified as the low current C-Mode and the other with high current at low voltage is identified as the high current P-Mode. They both are present in different pressure regimes with mode transition in the intermediate pressure. Inset shows the intermediate pressure range, the jump in the discharge current is due to the glow transition*

present chapter is largely focused on the low current mode of the discharge.

4.2 Potential structure of the fireball

Plasma potential obtained using emissive probe in the two mutually perpendicular directions is shown in figure 4.3. Coordinate system is same as discussed earlier for the measurement of the magnetic field in chapter 3 (see figure 3.5 on page 29). Low discharge voltage cannot sustain the glow at low pressure whereas higher voltage makes the C-Mode unstable. Hence, the discharge voltage is kept at $300V$ as it provides widest stable range of operation for present C-Mode discharge. Emissive probe was mounted on the port exactly below the anode as shown in figure 3.1. Plasma is mainly classified in two categories *viz.* anode glow (fireball) and bulk

plasma which fills the remaining volume of the chamber. Anode glow or fireball is the bright visible glow near the anode as shown in figure 4.1. For measurement along the $\hat{Z}$ direction, probe was moved from the bulk plasma to the anode glow. Data in figure 4.3a shows plasma potential measured along the central $\hat{Z}$ axis. For $Z > 4$ cm plasma potential has flat region which we call bulk plasma potential. Bulk plasma potential for 1×10^{-2} $mbar$ is 252 V where as for 5×10^{-2} $mbar$ is 235 V. This reduction is due to the enhanced discharge current which increases potential drop across the ballast resistor, hence decreasing the effective discharge voltage and plasma potential. As we move the probe from bulk plasma region towards the anode, plasma potential remains almost constant up to $Z = 4$ cm and then rises sharply to a new value before again being constant. This sharp rise also marks the visible boundary of the anode fireball. The fall in the plasma potential for $Z > 14$ cm in 1×10^{-2} $mbar$ case is due to the presence of the cathode sheath, which shrinks for higher pressure and hence does not appear in 5×10^{-2} $mbar$ case. The bulk plasma in our case is produced by cathode fall as in the normal glow discharge. However, we do not see any glow near cathode or in bulk plasma, this may be due to the fact that our cathode area is unusually large. For our current range (3 to 10 mA) the cathode current density is only 0.54 to 1.8 $\mu A/cm^2$. This low current density leads to a low electron density, which does not produce any visible cathode glow at lower pressure. We however observe the cathode glow at higher discharge current (above 20 mA) and higher pressure (above 1×10^{-1} $mbar$), though faint with respect to the anode glow at those parameters.

Figure 4.3b shows plasma potential measured along the $\hat{R}$ direction using emissive probe. The scan was performed at $Z = 2$ cm. Here the bulk plasma potential for $R > 2$ cm is ~ 236 V. Again the boundary of the visible glow is marked with a steep rise in the plasma potential. In $\hat{R}$ direction the plasma potential rises to 252 V at boundary of the visible glow. The potential jump of 15.6 V from the bulk plasma to the anode glow, in both the cases ($\hat{R}$ and $\hat{Z}$) closely corresponds to
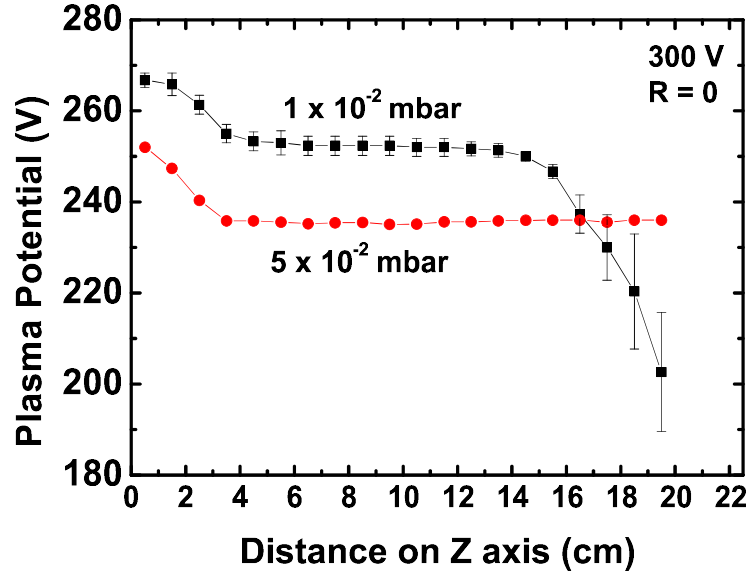
(a)
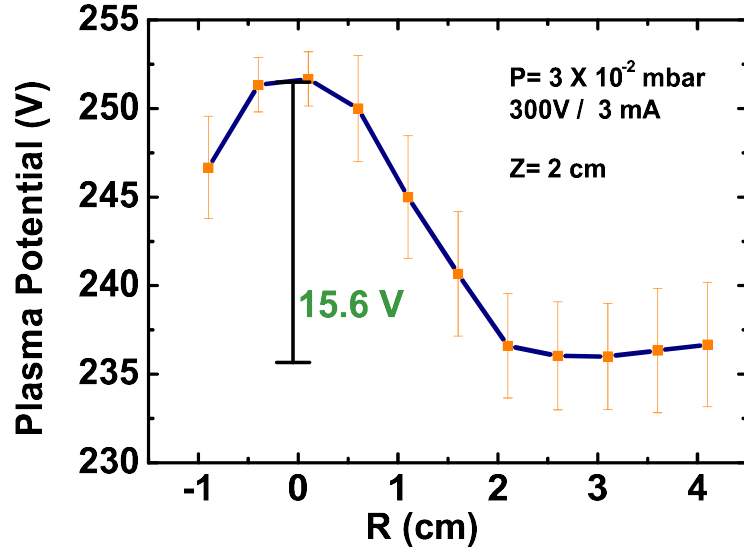
(b)

Figure 4.3: *Plasma potential measured using emissive probe. At visible boundary plasma potential jumps by 15.6 V in both the cases, which is close to the ionization potential of Ar gas used in the experiment. (a) Plasma potential along Z axis. Anode is at Z = 0. (b) Plasma potential along R axis at z = 2 cm.*

the ionization potential of Argon gas (15.7 eV). It has been noted by a number of authors [3, 65] that the anode double layer potential tends to be close to ionization potential of the gas used in the experiment. The physical understanding of this can be given as follows: The electron sheath near the anode is in response to excessive current requirement imposed by the external circuit. The electron sheath sustains the voltage to carry the extra current but as the voltage reaches above the ionization potential it causes ionization. This ionization in the sheath can provide the required current and hence potential usually does not rise above the ionization potential. The rise in the potential from bulk value, in both $\hat{R}$ & $\hat{Z}$ directions coincides with the visible boundary of the anode glow which results from the electrons accelerating uphill from the bulk plasma potential to the anode. This clearly indicates existence of double layer at the droplet shaped anode glow boundary.

4.3   Mechanism of discharge

Results in figure 4.3 and visible glow in figure 4.1 show the formation of anode glow or fireball near the anode. This glow is essentially due to the acceleration of electrons through the double layer of the anode glow. Figure 4.1a shows the anode glow (plasma ball) attached to the anode at the center via a narrow channel formed by the magnetic field. The difference between the discharge of a similar device used as a cathode (sputter magnetron) and our experiment is striking. The main difference in our experiment is that the magnetized electrode acts as an anode instead of the cathode as in a conventional sputter magnetron. Secondly, the origin of electrons beside ionization, is in the bulk plasma in contrast to the cathode surface of a sputter magnetron. In our case the anode acts as a sink for electrons in contrast to the conventional magnetron where it acts as a source. In a conventional magnetron, electrons are trapped in a magnetic field, which originates and ends on the cathode. Apart from closed $\vec{E} \times \vec{B}$ drift, electrons are trapped

electro-statically at the ends of the magnetic field lines. This can be clearly seen in the simulation performed by Sheridan *et.al.* [88], particularly figure 4(a) and 4(b) of their paper. In our case the magnetic field guides electrons directly to the anode where they sink. Much like Earth's magnetic field which blocks and guide solar wind to poles (for beautiful auroras!), our plasma is guided to the central pole of the magnetron. The cusp magnetic field profile on the central magnet pole dictates the shape of the glow as a droplet.

Plasma potential data in figure 4.3 shows potential jump equivalent to the ionization potential of the argon. This is associated with the anode double layer [3, 65], which necessarily requires electron sheath at lower potential side. Electron sheath can be easily formed near a small probe if it is biased more positive than the local plasma potential. Electron rich sheath can aslo be formed with a spherical grid that can be biased independently [31]. In our case, the bulk plasma potential remains below the anode potential which makes electron sheath possible. Conde *et.al.* [39] has numerically shown that electron sheath can collapse into a double layer due to ionization in the sheath induced by increased background pressure. Anode glow is not always present in DC glow discharge and in fact one has to carefully design the experiment to study it. Generally any object in contact with plasma receives thermal electron flux as given in equation 4.1, where q is electron charge, n is plasma density, T_e is electron temperature and m is electron mass.

$$j_e = \frac{1}{4} q n \sqrt{\frac{8kT_e}{\pi m}} \tag{4.1}$$

This is also the saturation electron current that the plasma can supply. Probes at floating potential charge themselves negatively in order to reduce the thermal electron flux. Current given by equation 4.1 multiplied by the area of the anode gives the maximum current that the discharge can carry. If external power supply imposes larger current than this, anode develops electron sheath which increases

the effective collection area of the anode. Below we summarize the criteria for the formation of different sheaths by examining the relationship between discharge current I_d and electron current I_e. Here $I_e = j_e \times A$, where A is anode area.

$$I_d < I_e \qquad\qquad \text{Ion sheath} \qquad\qquad (4.2a)$$

$$I_d = I_e \qquad\qquad \text{No sheath} \qquad\qquad (4.2b)$$

$$I_d > I_e \qquad\qquad \text{Electron sheath} \qquad\qquad (4.2c)$$

Here we have neglected the contribution of ions to the current. Equation 4.1 specifies the maximum current plasma is capable of delivering. If condition 4.2c is satisfied, anode develops electron sheath which in turn increases the effective area to support the current. Electrons being highly mobile, it is impractical to satisfy condition 4.2c for larger anode areas hence it is usually achieved using a small area anode. Our anode is of 76 mm diameter corresponding to the area 4534.16 mm^2, multiplying this by equation 4.1 with $q = -e$, $n = 1 \times 10^9\ cm^{-3}$ and $T_e = 3\ eV$ gives total electron current of 839 mA. This is much larger than our typical discharge current of 10 mA (see figure 4.2).

Our discharge current (typically ~ 3 to 10 mA) clearly does not satisfy equation 4.2c, though the potential profile requires it. This suggests that the magnetic field near the anode significantly restricts the available anode area to the discharge. Considering only the glow area in the center where plasma connects to the anode can explain the result. The central visible area measured as "c" (section 4.5, figure 4.10) varies but can be taken as $\sim 5\ mm$ in radius. This gives total area of 78.5 mm^2 multiplying it by equation 4.1 as earlier gives electron current as 3.63 mA, which can now satisfy equation 4.2c.

This point can also be proved using argument of Baalrud *et.al.* [9]. This includes ion current as well. They discuss the scenario where all ions are being lost from system to one surface and all electrons are being lost to the other, thus

establishing "Global nonambipolar flow". This can be applicable in our case as the chamber is having mostly just two surfaces namely the chamber wall (cathode) and the anode, both presumably collect only one kind of particle. In that case electron sheath requires

$$\frac{A_e}{A_w} < \mu \tag{4.3}$$

Where A_e is total electron collection area (here anode) and A_w is total ion collection area (here chamber wall) and μ is

$$\mu = \sqrt{2.3\frac{m_e}{m_i}} \tag{4.4}$$

where m_e and m_i are electron and ion mass respectively. This result was obtained by balancing global ion and electron losses. Our chamber area is 5557.8 cm^2 where as anode area is 45.34 cm^2 which makes $\frac{A_e}{A_w} = 8.1 \times 10^{-3}$ which is higher than μ, which is 5.59×10^{-3}. These values obviously do not satisfy equation 4.3. If we take anode area as the effective area due to the cusp magnetic field which is 0.78 cm^2 then $\frac{A_e}{A_w} = 1.4 \times 10^{-4}$, which is much smaller than μ. Here also we require smaller effective area as previously discussed.

We have seen that bright anode glow forms near the anode. Its shape is determined by the magnetic field. Sharp visual boundary and plasma potential indicate double layer and electron sheath. Magnetic field reduces the effective area of the anode. Magnetic field effectively constricts the anode, thus making electron sheath, double layer and formation of the fireball possible which otherwise would not have been possible for a 75 mm diameter anode.

4.4 Plasma density and temperature of the fireball

Visually bright anode glow is due to the acceleration of electrons through the double layer. These electrons create secondary plasma with a different plasma

potential than the bulk plasma. This anode glow plasma usually has a higher density than the bulk plasma and high electron temperature due to the energetic electrons of double layer. We measured the plasma density, electron temperature, floating potential and plasma potential at magnetic null on the central $\hat{Z}$ axis at $Z = 3\ cm$. As shown in figure 4.4 plasma density increases more or less linearly with the discharge voltage. The glow boundary acts as a virtual anode with size larger than the effective constricted anode. As we have noticed similar increase in the discharge current but the double layer potential and the size of the anode glow (virtual anode) does not increase with the discharge voltage, hence increased plasma density in the anode glow is associated with the increased bulk plasma density.

Electron temperature remains constant at about 15 eV, this is due to electrons accelerated through similar double layer potential. These electrons does not have sufficient length inside the anode glow (see Appendix table 7.1) to thermalise with the native electron population. Floating potential and plasma potential curves are not parallel which suggest variation in the electron temperature. At lower end the difference in the plasma potential and the floating potential indicate electron temperature of $\sim 8\ eV$. This is calculated form the well-known relation for Maxwellian electrons $V_p - V_f \sim 5T_e$ for Argon, where V_p, V_f and T_e are plasma potential, floating potential and electron temperature, respectively.

Axial measurements on the $\hat{Z}$ axis using a single Langmuir probe are shown in figure 4.5 and 4.6. Discharge current is kept constant at 8 mA for two different pressure ($2.5 \times 10^{-2}\ mbar$ and $4 \times 10^{-3}\ mbar$). Discharge voltage specified in figure 4.5 and 4.6 is the anode voltage with respect to the grounded chamber (cathode). Anode is at $Z = 0$ in figures 4.5 and 4.6. For high pressure ($10^{-2}\ mbar$), the plasma potential shows a clear jump near the anode glow boundary. This result is identical to the measurement shown in figure 4.3a. Electron temperature in the bulk region is near 5 eV for $2.5 \times 10^{-2}\ mbar$ whereas it is 15 eV for $4 \times 10^{-3}\ mbar$
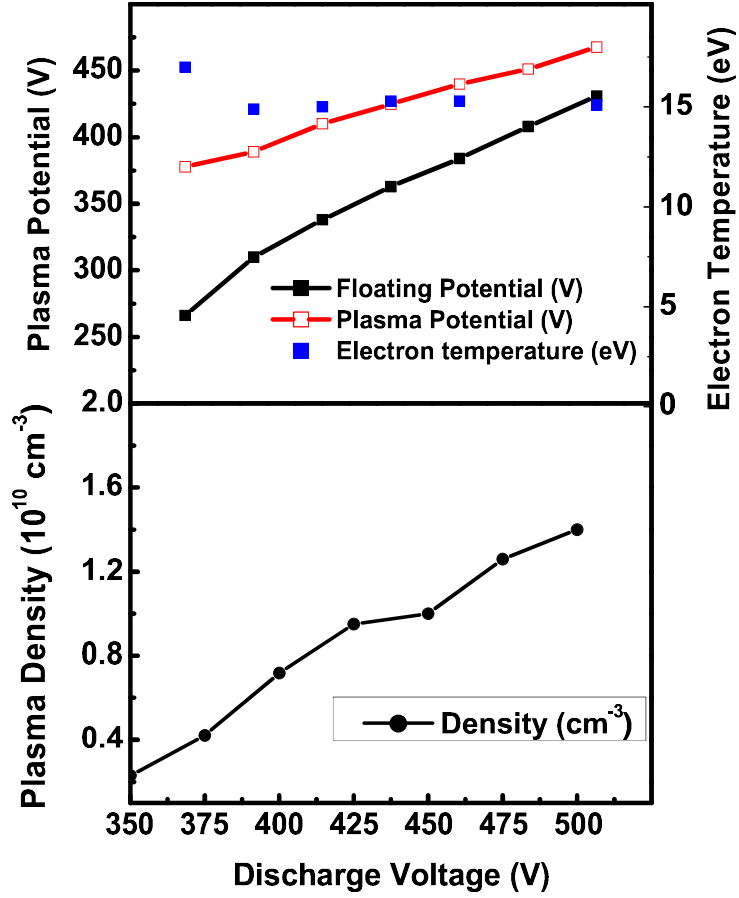
Figure 4.4: *Electron temperature, floating potential, plasma potential and plasma density at $Z = 3$ cm. Discharge voltage is varied over a wide range for pressure of 3×10^{-3} mbar. Data was acquired using a single Langmuir probe.*

case. Plasma density is 1×10^{10} cm^{-3} near the anode for both pressures at 8 mA discharge current. In case of high pressure of 2.5×10^{-2} $mbar$ the anode glow consists of a double layer as discussed earlier. Such a double layer has two temperature electrons on the high potential side. A semi-log plot of Langmuir probe characteristic shown in figure 4.7b shows two temperature electrons. High temperature electrons originate from acceleration of electrons across the double layer potential where as the low temperature component is result of the electrons produced due to the ionization in the glow which is trapped by the double layer
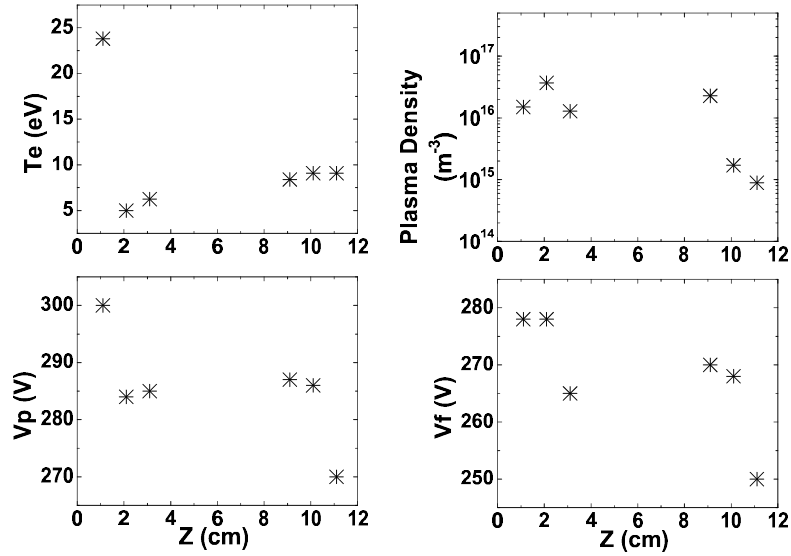
Figure 4.5: *Single Langmuir probe measurements along the $\hat{Z}$ axis. 310 V discharge voltage and 8 mA discharge current at 2.5×10^{-2} mabr pressure*
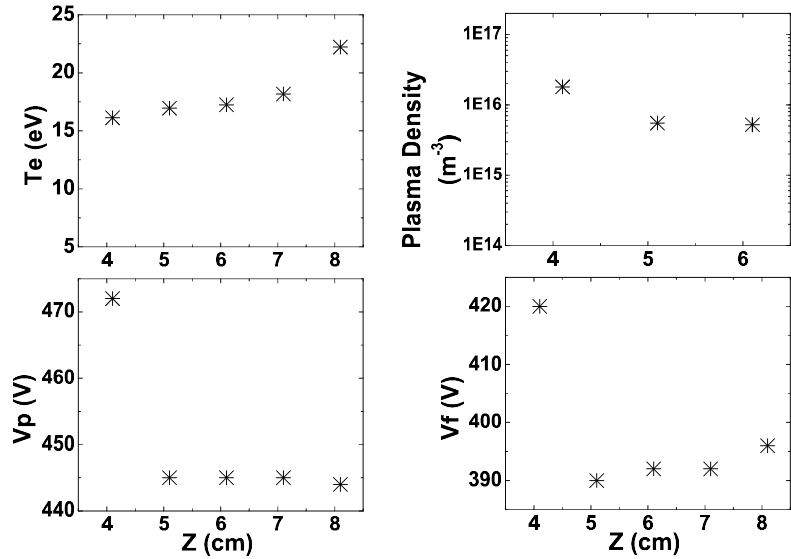
Figure 4.6: *Single Langmuir probe measurements along the $\hat{Z}$ axis. 485 V discharge voltage and 8 mA discharge current at 4×10^{-3} mbar pressure*
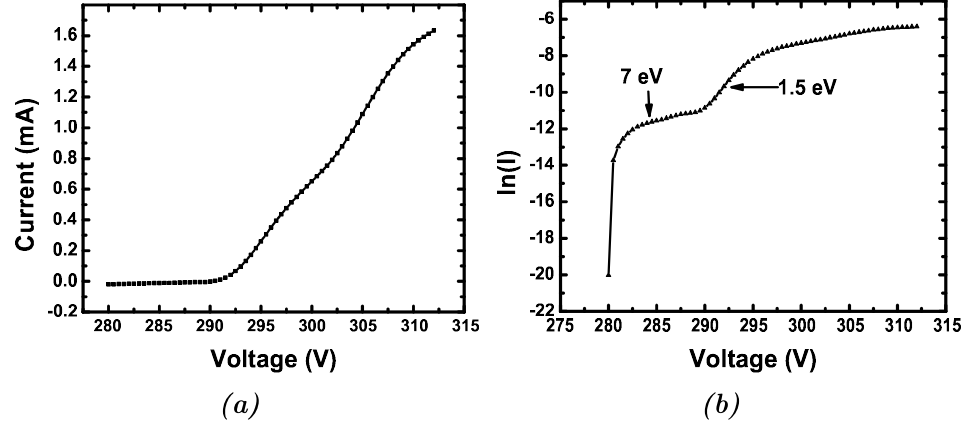
Figure 4.7: *Langmuir probe I-V trace and its semi-log plot at Z = 2 cm for discharge current of 8 mA at 2.5×10^{-2} mbar pressure, showing two distinct slopes corresponding to the two different temperatures in the anode glow plume (a) Single Langmuir probe trace, (b) Semi-log plot*

potential.

The extent to which electrons can be considered magnetized depend upon the pressure. This is one of the reasons why shape of the fireball shrinks at high pressure. For low pressure of 4×10^{-3} *mbar* the anode glow is relatively large so is the mean free path (see Appendix table 7.1). If we go closer to the anode, the probe cast its "shadow" in the glow. This is due to the draining of the particular field lines by the probe. This restricts the measurements closer to the anode and hence we have restricted our measurements at 4 *cm* from the anode (figure 4.6).

4.5 Variation in the dimension of the fireball

The size of the anode glow is a function of the discharge parameters such as pressure and voltage (see figure 4.8 and 4.9). To quantify expansion or contraction of the double layer boundary we have analysed digital images of the glow taken with a commercially available digital camera. Raw images were processed using ImageJ software [89, 90]. Diameter of the anode is used to scale the images. We adopt

to measure three lengths as shown in figure 4.1b. The anode glow (fireball) near the anode is predictably cylindrical in shape, diameter of this part is "c". Length "a" is the fundamental length of the droplet shaped anode glow and is determined by the double layer and the secondary plasma that it produces. Length "b" is measured where effect of the magnetic field appears to vanish and fireball starts becoming spherical. The results are summarized in figure 4.10.

(a) 2×10^{-3} *mbar*   *(b)* 5×10^{-3} *mbar*   *(c)* 8×10^{-3} *mbar*

(d) 1×10^{-2} *mbar*   *(e)* 5×10^{-2} *mbar*
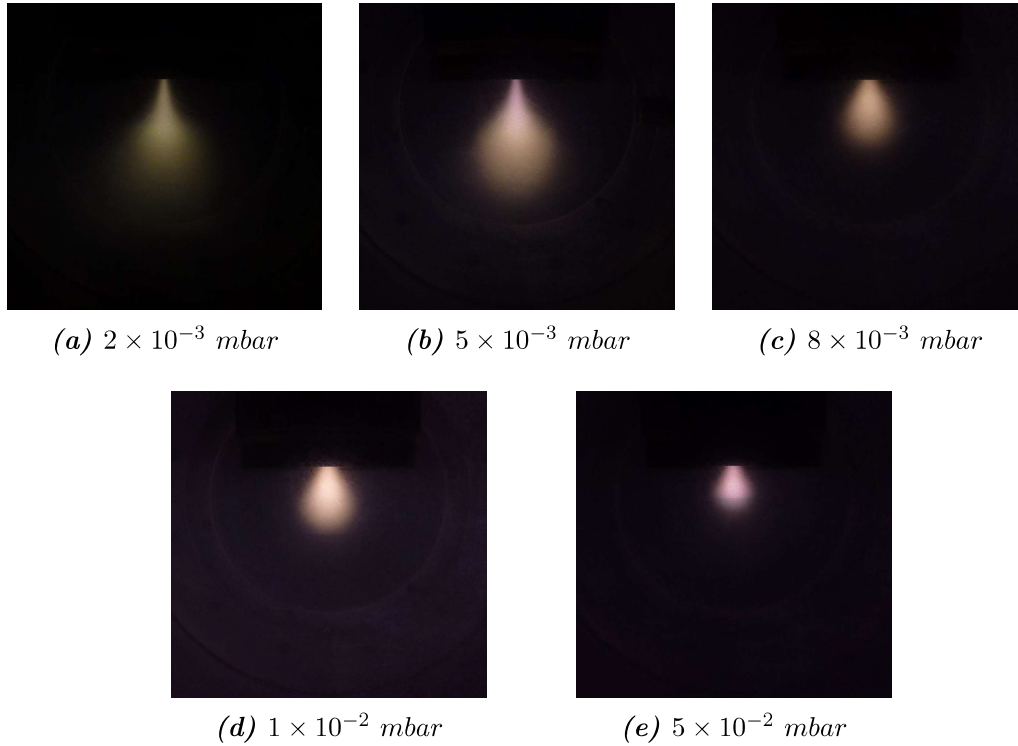
Figure 4.8: *Figure showing variation in the anode glow with pressure at constant discharge voltage of 300 V.*

Figure 4.10a represents various lengths for different pressure at 300 V of discharge voltage (see figure 4.8). Value of "a" is 55 mm at low pressure of 2×10^{-3} *mbar*, and decreases with increase in the pressure. It reduces to 27 mm for 1.6×10^{-2} *mbar*. Length "b" follows the similar trend reducing from $\sim$ 35 mm to 20 mm, this is expected as whole structure is funnelled down to a stronger magnetic field. Length

(a) 350 V   (b) 400 V   (c) 450 V

(d) 500 V   (e) 550 V
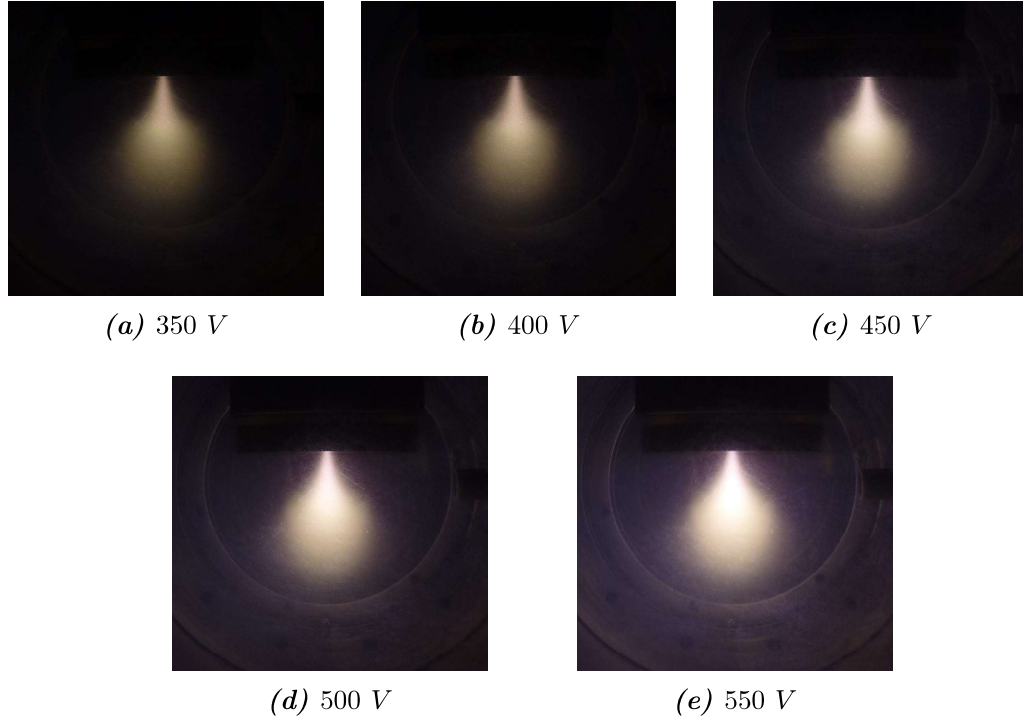
Figure 4.9: *Figure showing the effect of discharge voltage at constant pressure of 2×10^{-3} mbar. Discharge voltage mainly changes the intensity of the glow whereas pressure shrinks (Fig. 4.8) the glow at a given voltage.*

"c" unlike others increases with pressure. This is the diameter of the root of the anode glow. This diameter increases from 3 mm to 13 mm. This is due to the increased collisions at high pressure. In the absence of collision, plasma particle follows the magnetic field lines. With increase in the pressure collision frequency increases. With every collision particles can diffuse normal to the magnetic field. Increased diffusion across the magnetic field makes the channel root wider at higher pressure.

Dimension of the anode glow varies with the discharge voltage as well. Figure 4.10b shows data for different voltage at 2.5×10^{-3} mbar of pressure. Length "a" increases form $\sim$ 80 mm to $\sim$ 120 mm, as discharge voltage is varied from 300 to 400 V, respectively. Above 400 V it does not increase any further. However
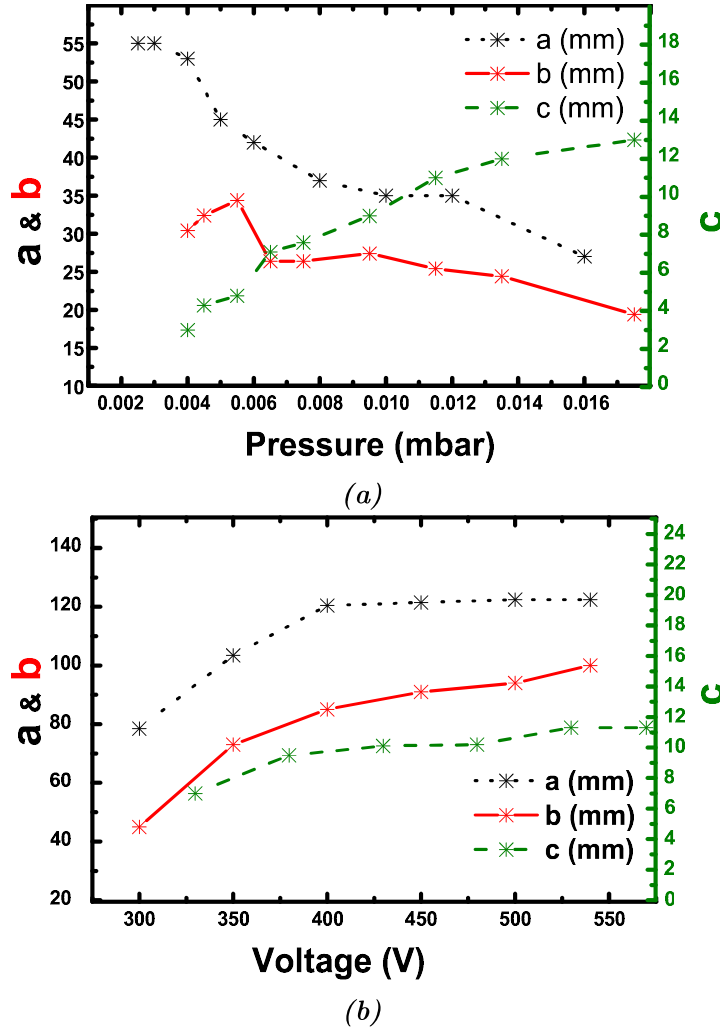
Figure 4.10: *Dimension of fireball. Left axis shows a and b, right axis shows c. All lengths are in mm. (a) For different pressure at discharge voltage of 300 V, (b) For different discharge voltages at pressure of 2.5×10^{-3} mbar.*

the intensity of the anode fireball and discharge current (figure 4.2 and figure 4.9) increases with voltage above 400 V as well. Similar is the case with length "*b*". Length "*c*" remains more or less constant, as it is dependent on the cross field diffusion which does not depend on the discharge voltage.

In summary, the fireball structure diffuses to the stronger magnetic field region with increasing pressure which shrinks the fireball. Increasing voltage on the other

hand increases the intensity of the glow but does not affect its size considerably. Volume of the fireball is related to the discharge current which continuously increases as shown in figure 4.2. This suggests that additional current is due to the increase in the bulk plasma density which in turn increases the ionization inside the fireball.

4.6   Summary

Magnetic field resulting from the use of permanent magnets is mapped in two dimensional plane. The magnetic field is strong near the anode surface but falls rapidly within about 2 cm, this gives advantage of magnetic field without interfering with measurements. Magnetic field constricts the anode area sufficiently to produce the droplet shaped anode glow. The plasma formed is of "inverted droplet" shape, which is primarily due to the presence of a highly non-uniform magnetic field near the anode.

Plasma potential profile is measured which shows that the bulk plasma potential is below anode potential, indicating the presence of an electron sheath. Potential measurements along with the sharp visual boundary at the anode glow establish the existence of the current driven anode double layer at the glow boundary. The plasma is observed to have the anode glow in all possible parameter range and the fireball particularly at low pressures can be as large as $\sim 8 - 12 \ cm$ in length. The dimension of this anode glow is measured with digital photography and it scales with pressure and voltage as explained. The effect of the magnetic field and the pressure is clearly observed. The anode double layer generates energetic ions which escape the fireball radially outward and can be utilized as low energy ion beam. The ions in the chamber cannot cross the measured potential barrier hence all the ions inside the fireball must have formed by ionization due to electrons accelerated through the anode double layer.

The role of magnetic field in establishing the anode glow has been qualitatively discussed. Magnetic field constricts the area of the anode sufficiently to produce an electron sheath and an anode double layer for relatively large anode.

5

Mode transition and oscillations

In the previous chapter we have investigated the details of the C-Mode discharge. This discharge is however not stable at higher pressure, it is observed that above a critical pressure typically $\sim 5 \times 10^{-2}$ $mbar$ the C-Mode switches to P-Mode discharge. This new P-Mode discharge connects the plasma to the outer peripheral region of the anode. This region is the location of the poles of the peripheral magnets. In the present chapter the discharge is operated at higher pressure and the characteristic of such transition form C-Mode to P-Mode is studied. The P-Mode shows oscillations of global nature in plasma parameters.

5.1 Observation

As shown in figure 5.1a and 5.1b two distinct modes of discharge namely C-Mode and P-Mode are observed. The C-Mode glow (figure 5.1a) connects the bulk plasma to the center of the anode, whereas the P-Mode glow (figure 5.1b) connects the bulk plasma to the peripheral region, both are the locations of the magnetic poles. It is interesting to investigate these two modes and their switching behaviour as it

is directly related to the diffusion of plasma in the magnetic field. For interesting insights into the diffusion in magnetic field, one may refer to Simon's short circuit effect [91] and a review by D. Curreli [92]. As mentioned earlier the glow switches from central to peripheral mode as the pressure is increased beyond a certain critical value. It is clear that the anode glow or fireball forms at a particular location due to the presence of the magnetic field.

<div align="center">(a)   (b)</div>

Figure 5.1: *Images of (a) C-Mode (3×10^{-2} mbar) and (b) P-Mode discharge (8×10^{-2} mbar).*

The magnetic field guides the electrons which originate from cathode or bulk plasma to the magnetic poles, hence making the bright C-Mode glow at the center of the anode. However as can be seen from figure 5.2 there are two locations of the magnetic poles on the surface. One is at the center (figure 5.2b) and other at the periphery. After a certain critical pressure and voltage, the discharge abruptly jumps towards the peripheral region. The critical pressure is typically between 5×10^{-2} mbar to 9×10^{-2} mbar, depending upon the discharge voltage. Discharge voltage is typically in the range of 250 V to 350 V and discharge current is in the range of 10 to 80 mA. The higher discharge voltage requires lower critical pressure
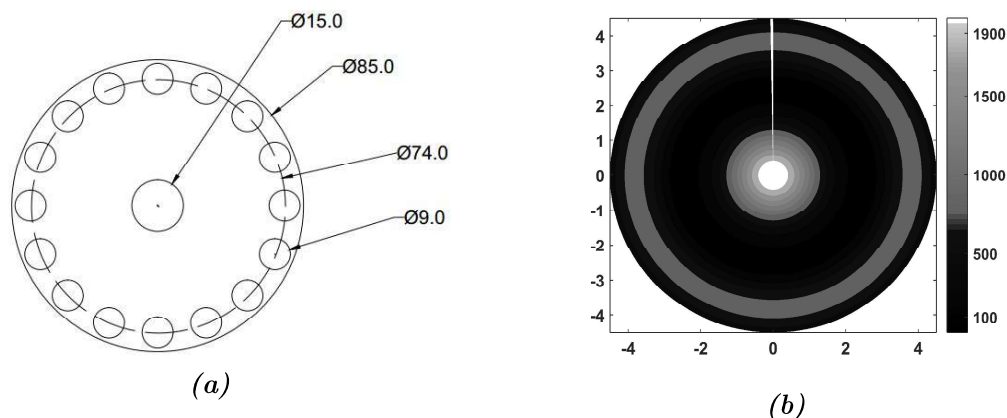
Figure 5.2: *(a) The dimensions of the anode and the magnets used in the experiments. Possible locations of plasma contact with anode coincides with central or peripheral magnet poles hence are called as C-Mode or P-Mode.(b) Representation of $B_\perp$ on the anode surface. Values of contour (gray scale bar) are in gauss. Light area is where the magnetic field connects with the anode. Clearly there are two sites where plasma can form near the anode corresponding to the central and peripheral magnetic poles.*

to switch from C-Mode to P-Mode. The discharge appears to operate in either of the modes depending upon the pressure. In the present set-up and experimental parameter range, both modes have never been observed simultaneously. We further examine the behaviour and general properties of each modes.

5.2 Mode transition

The C-Mode discharge is present below the critical pressure of 5×10^{-2} *mbar*. We start with low pressure in the range of 10^{-3} *mbar* and gradually increase it until the transition to P-Mode occurs. The formation of the anode glow and the fireball can be explained as follows. The magnetic field severely reduces the available anode area to the discharge. In fact, only central and peripheral regions are available to the plasma (see figure 5.2). The actual width of this area available to an electron is further limited by the collsions. This makes accessible area even smaller at low

background pressure (white area in figure 5.2b). Thus the plasma forms an electron sheath near the anode. This electron sheath is transformed into the anode double layer due to the current requirement imposed by the external circuit. Background gas pressure or the neutral number density is an important parameter to induce the transition form electron sheath into the double layer [39]. Neutral density also determines the rate of ionization in the electron sheath and total charge balance [3, 9]. The electron sheath precipitates ions due to the collisional ionizations, these ions are then swept away from the glow into the bulk plasma by the double layer. If the rate of production of these ions is higher than the loss of ions, the electron sheath turns into a quasi neutral plasma with different plasma potential than bulk plasma hence establishing the double layer and the fireball.

We have found the length of C-mode discharge to be reducing with an increase in the pressure. Increasing the pressure above a critical limit causes the C-Mode discharge to become unstable and it abruptly jump to the peripheral mode (P-Mode) as shown in the figure 5.1b. This transition is marked by a discrete jump in the discharge current as shown in figure 5.3a. For a given pressure, there also exists a critical discharge current for this transition to occur.

Figure 5.3 shows I-V characteristics of the discharge. Depending upon the background pressure the I-V curve has different slopes. For pressure below 10^{-3} $mbar$ the current remains very low, below 40 mA for voltage as large as 600 V. This low pressure low current branch shows a moderate increase in the current with the discharge voltage, whereas for pressure above 1×10^{-1} $mbar$, the current increases significantly for even a small increase in discharge voltage. For the pressure in the range of 1 to 9×10^{-2} $mbar$, the I-V shows the behaviour of both of the discharge modes. For this pressure it can be seen from figure 5.3 that the slope of I-V follows that of low pressure branch upto a voltage close to 350 V at which point the glow suddenly switches to P-Mode and the slope of I-V becomes very steep. The low pressure low current branch is hence associated with C-Mode discharge where as
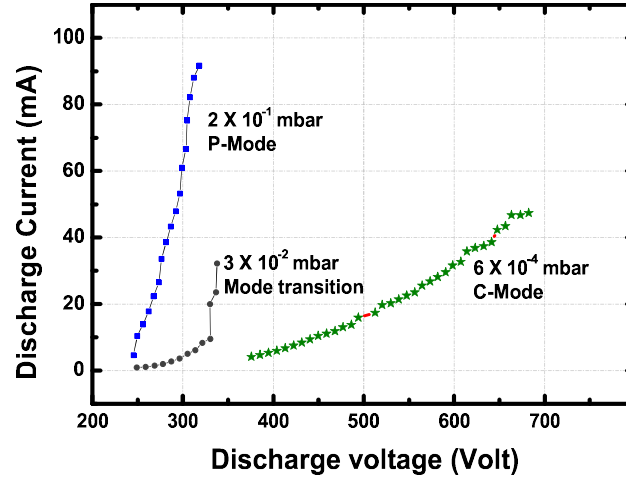
(a)
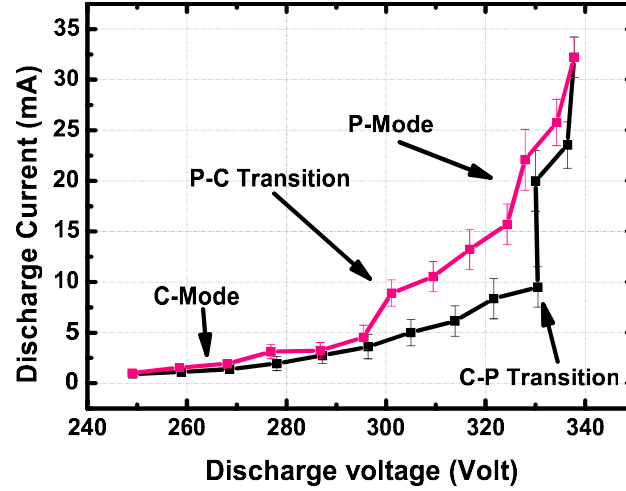
(b)

Figure 5.3: *I-V characteristics of the discharge (a) For different pressure regime. In low pressure only C-Mode is observed where as in high pressure only P-Mode is observed. Mode transition is observed in the intermediate pressure range. (b) The mode transition form C-Mode to P-Mode and back.*

high current branch is associated with that of P-Mode. For low pressure regime (below 10^{-3} *mbar*) only C-Mode discharge is observed where as for high pressure regime (above 10^{-1} *mbar*) only P-Mode discharge is observed. In the intermediate pressure the discharge undergoes the transition form C-Mode to P-Mode with a

hysteresis in the discharge current as shown in the figure 5.3b.

We have seen from figure 5.3 that for intermediate pressure range there exist a critical discharge voltage and a discharge current for the transition to occur. Increase in the discharge voltage from 250 V leads to a smooth increase in the discharge current to about 10 mA upto 330 V of discharge voltage. At discharge voltage of 330 V the discharge abruptly jumps from C-Mode to P-Mode. While returning to lower voltage the I-V curve takes a different path and P-Mode plasma is sustained upto 300 V. Figure 5.4 shows the critical discharge current values which trigger the transition. Figure 5.4(b) shows the values of the current at which the transition from stable central mode (C-Mode) to peripheral mode (P-Mode) occurs. For pressure below 8.5×10^{-2} $mbar$ the discharge current upto which the central mode can be maintained is $\sim$ 8 mA, after that pressure the central mode becomes much less sustainable. Figure 5.4(a) shows the critical discharge values for triggering P-C mode transition. These values are much lower than one required to induce the P-Mode. With increasing pressure the discharge current at which P-Mode transforms in to the C-Mode decreases.

The mode transition is very sensitive to the background pressure. For low pressure in the range of 10^{-3} $mbar$ the anode glow remains exclusively in central mode (C-Mode). It was shown earlier that this C-Mode anode glow changes its dimensions, its length shrinks with the pressure for a given voltage. Most importantly its width where it connects with the anode is observed to increase with pressure. As shown in figure 5.5 this width starts to saturate as it approaches the diameter of the central magnet. Now it is clear that the plasma can only penetrate into the magnetic field at the poles of the magnets. With increasing pressure, the plasma penetrates deeper into the magnetic field, hence the increased width (see figure 5.5). According to our understanding when this width of the fireball near the surface of the anode reaches the diameter of the central magnets, (where the magnetic field stars to deviate from being perpendicular to the anode) the anode glow
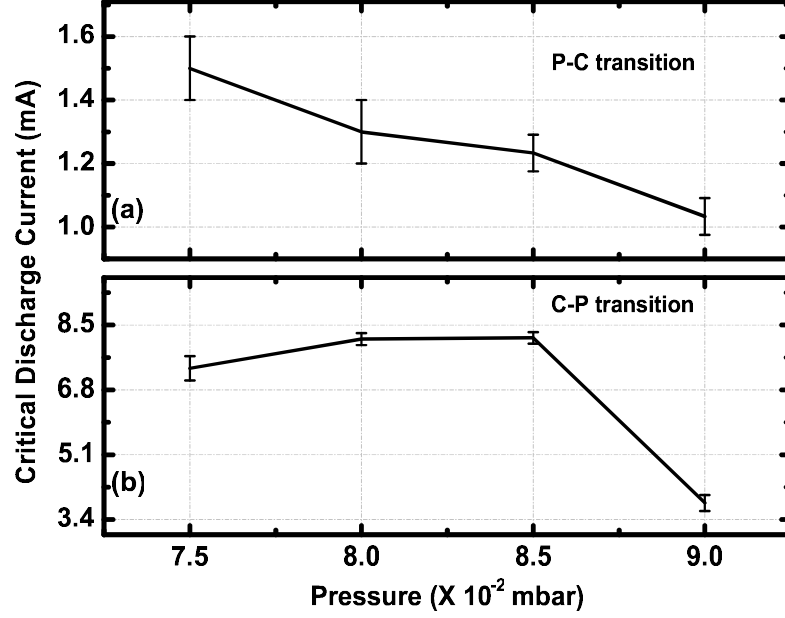
Figure 5.4: *Critical values of the discharge current for transition to occur. (a) The critical current up to which the P-Mode remains stable, below this current C-Mode is re-established. (b) Critical current above which C-Mode becomes unstable and discharge switches to P-Mode.*

abruptly jumps to the outer peripheral region. As discussed earlier in Chapter 4 the width of the column is only $2 - 3$ *mm* in low pressure regime and gradually increases to about $14 - 15$ *mm* at high pressure. This is about the diameter of the central magnet. Any further increase in the pressure forces the plasma to go beyond the limit of the central magnet but the magnetic field does not connect to the anode beyond the diameter of the magnet. This triggers the transition.

5.3   Global oscillations of P-Mode plasma

The C-Mode is stable in the low pressure regime but as soon as the transition occurs from C-Mode to P-Mode, the plasma shows global oscillations in the discharge current and the floating potential. The oscillation frequency is typically in the range of few kHz.
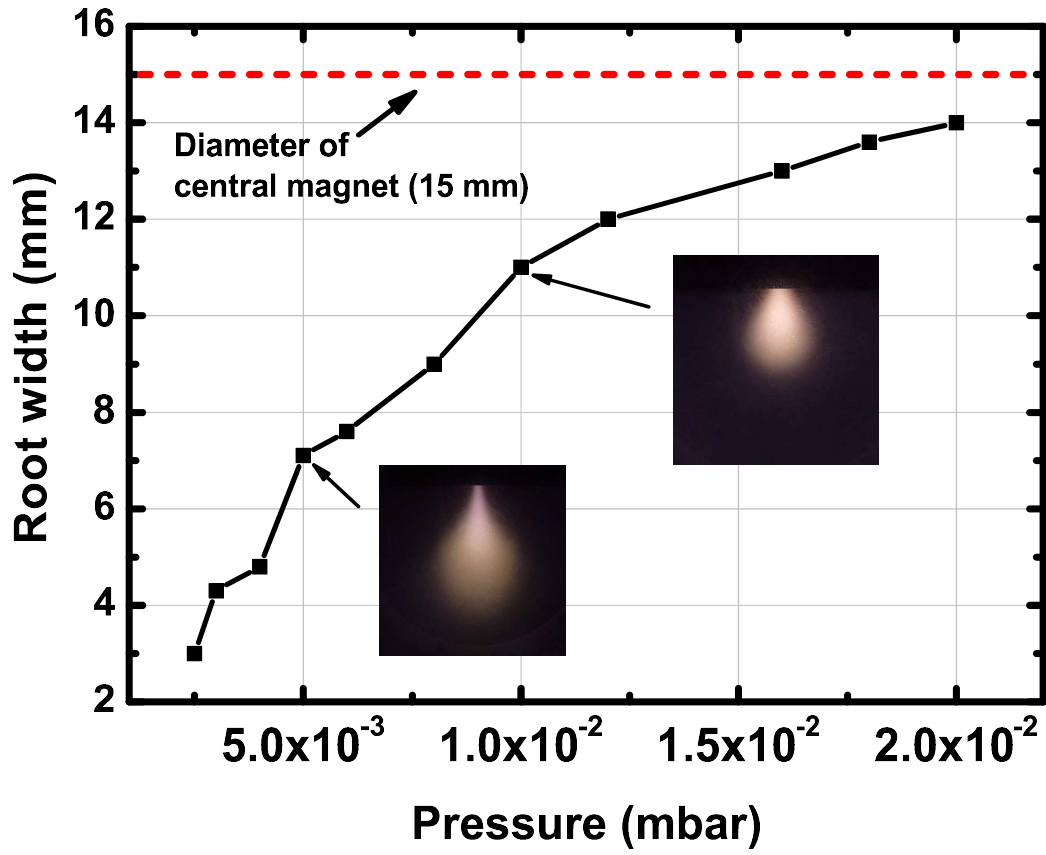
Figure 5.5: *The width of the C-Mode glow at its root where it connects with the anode. The horizontal line represents the diameter of the central magnet.*
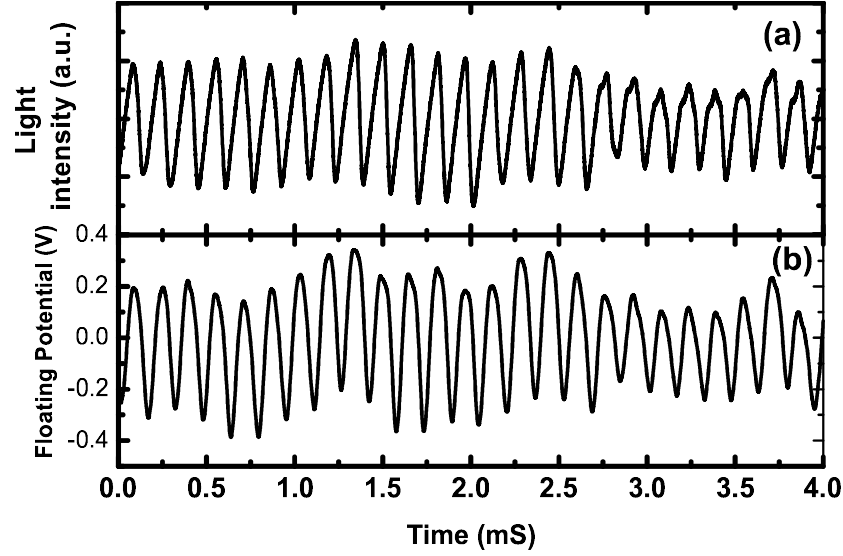
Figure 5.6: *Oscillations measured at 8×10^{-2} mbar and $300\ V$. (a) Light oscillations measured with photo diode. (b) Floating potential oscillations.*

Figure 5.6 shows the oscillations present in the light intensity and floating potential. Similar oscillations are also observed in the discharge current. Light emission is measured with a photo diode. It is worth noting that the light oscillations are only detected in the anode glow, light captured from any other location, including cathode glow does not show any oscillations. This is in contrast to the global nature of the floating potential oscillations, which are present in both the anode glow and the bulk plasma. Absence of light oscillations in the bulk plasma is possibly due to the lower intensity of light as compared to the bright anode region. The oscillation frequency depends upon the plasma parameters and varies within a few kHz. Time series of oscillations are obtained for different pressure and discharge voltage. The floating potential oscillation frequency and that of light oscillation are same within the errors of measurements. Figure 5.7a shows that the oscillation frequency decreases with increasing pressure, while keeping the discharge voltage constant. Initially the trend of frequency is linear, however, more rapid decay is observed at higher pressure. In the same figure it can be seen that,
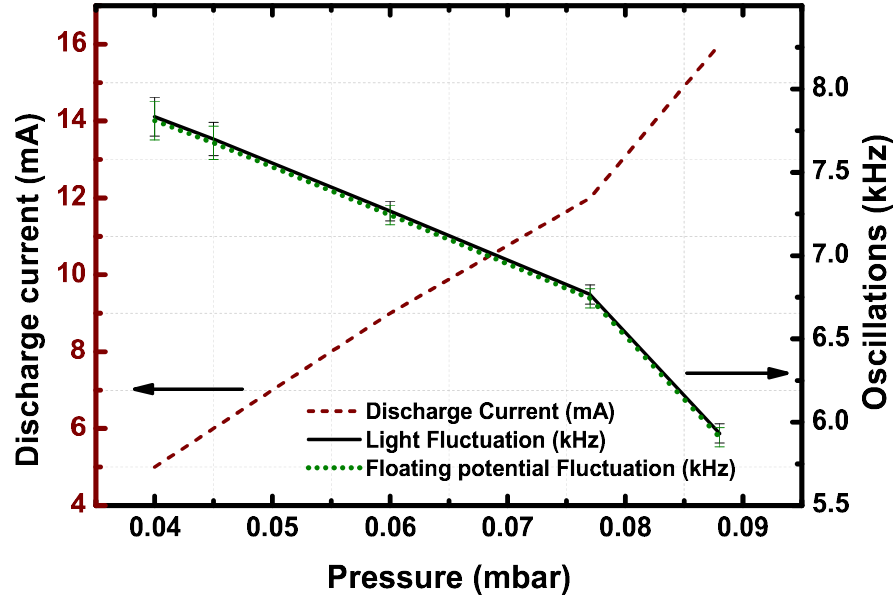
(a)
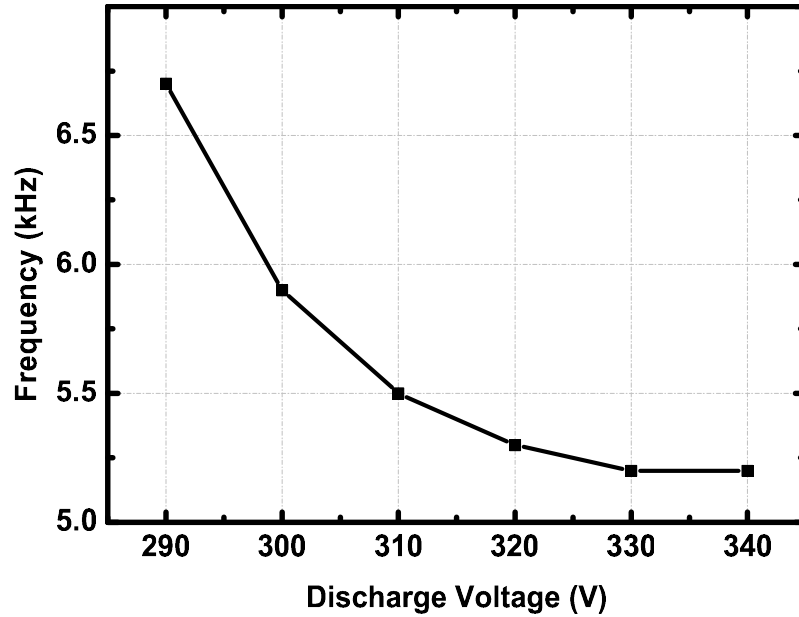
(b)

Figure 5.7: (a) Variation of the frequency of oscillations and discharge current with the background pressure, for constant applied voltage. (b) Oscillation frequency of the floating potential fluctuations with discharge voltage for background pressure of 8×10^{-2} mbar.

the discharge current also tend to rise more rapidly in the same region. Figure 5.7b shows that frequency of oscillations reduces with discharge voltage. Changing the voltage changes the plasma density, while keeping the background gas pressure constant. Hence these both plots suggest that the oscillation frequency depends upon plasma density as well as the neutral density.

The time scale of the oscillations eliminate any mechanism involving electron or ion in the anode double layer. These oscillations may be explained by predator-prey [93, 94] behaviour as reported in the case of plasma thrusters, however this is outside the scope of the present work.

5.4   Summary

The magnetically constricted anode device is shown to have two stable modes of discharge. In the low pressure mode it remains in the center of the anode, which is identified as C-Mode plasma. As the pressure increases the cross field diffusion pushes the plasma deeper in to the magnetic field, this brings the plasma closer to the electrode as more and more magnetic field lines become accessible to the plasma due to collisions. This also leads to the increased width at the root of the plasma column in contact with the anode. When this width reaches the critical value defined primarily by the physical size of the central magnet, the anode glow becomes unstable and abruptly switches to the P-Mode. This P-Mode also exhibits global oscillations in the discharge current, floating potential and light emission in kHz range. These oscillations are postulated to be possible predator prey cycle in the anode glow region, which witness intense ionization due to the double layer and the magnetic field. Absence of oscillations in light emitted from any other region in the chamber indicate anode glow as the source of those oscillations.

6

Application of Anode fireball

In this chapter, we explore possible applications of the fireball device in nanofabrication. The anode fireball observed in Chapter 4 can be utilized as a localized high density plasma source. Plasma technology has been the work force of silicon chip industry. Plasma has unique properties which can be utilized for various applications e.g. thin film growth, materials modification, nanopatterning, etching etc. Due to the ease of fabrication and cost effectiveness plasma based planar magnetron sputtering systems are commonly used in R&D labs and in industries for the thin film and nanoparticles growth [95–99]. On the other hand expensive ion sources are used for nanopatterning and are not easily accessible in research labs. Rapid developments in metal/semiconductor nanofabrication technologies has seen an exciting and emerging trend towards the development of periodic nanostructures due to their superior properties as against non ordered configurations [100–104]. Normally a two step approach is followed to make regular arrays of metal nanoparticles; first to pattern the surface using an ion source and then the patterned template is used for the deposition of the metal nanoparticles so as to tune the plasmonics and magnetic properties of the materials. This two-step process sometimes require two

different experimental systems. In the present Chapter, we demonstrate a single step technique using a commercial DC planar magnetron sputtering system that can be used for nanopatterning in one mode and as a normal sputter magnetron in the other mode. Plasma physics and the operating regime of the planar magnetron sputtering systems for the thin film and nanoparticles growth are widely reported [96–99], therefore in this work we have focused on the properties of the same device used for nanopatterning. Facscko et al. [105] showed for the first time in 1999 that the surface of a binary semiconductor (GaSb), when irradiated by normal incidence low energy ion beam ($< keV$) forms short range hexagonally ordered pattern (nanodots) on the surface. Since then numerous research groups have focused on ion-solid interaction so as to understand the fundamental mechanisms involved in the formation of nanodots [106, 107]. Such nanodots like structures appear on the surface due to the preferential sputtering of one atomic specie over the other [108, 109]. Along with the above phenomena, incident ion fluence and ion energy play key role in the formation of nanodots which can alter the periodicity as well as the height/thickness of the nanostructure. Literature survey shows that the developed nanodots template can be extremely useful for applications in the optoelectronic devices [110], high density magnetic memory [111], deep space photovoltaics [112] and broadband light harvesting [113, 114]. Therefore, as a proof of concept, we describe the experimental procedure that can be replicated with any conventional DC sputter magnetron source to form regular nonodots on GaSb without an additional ion source. The choice of GaSb was dictated by the promising applications shown by the nanostructure as mentioned above. Unique surface wettability properties and increased anti reflective nature of such nanoarchitecture are also reported as the application of the work.

6.1   Experiment

We used the same experimental setup used in earlier Chapters for this experiment. The DC sputter magnetron is equiped with Ag sputter source. As shown in figure 6.1 the magnetron is biased positive with respect to the ground. The bright fireball is formed in the center. The working pressure is kept low at 5×10^{-3} $mbar$, which reduces ion neutral collisions and also avoids the so called P-Mode discharge as described in Chapter 5. The sample is kept 15 mm away from the visual boundary of the fireball to minimise possibility of collisions between ions coming from the fireball and background gas. The discharge current was monitored for each experiment, which is indicative of the ion density in the fireball. When the sample placed near the fireball is connected to the ground, which is also the cathode of the discharge, the ion bombardment starts. The energy of the ion hitting the surface depends on the discharge voltage. No additional power supply is used for biasing the sample, it is simply connected to the ground which is negative terminal of the discharge power supply and hence is a cathode of the system.

The following procedure was followed to develop nanodots on an epi-polished GaSb wafer by making use of the innovative technique of inverted anode fireball. The GaSb wafer (110) has band gap of $\sim$ 0.7 eV and face to face resistance of $\sim$ 3 $k\Omega$ at room temperature and $\sim 100 - 300$ Ω in the temperature range of $\sim 300\,^{\circ}C$. Non inclined vertical GaSb nanodots were grown on a clean epi-polished GaSb (100) substrate by bombarding the bulk wafer at normal incidence with Ar^{+} ions using a bias from 400 to 1000 V, at a pressure of $1 - 5 \times 10^{-3}$ mbar. The ion fluence was maintained at a constant value of $\sim 6 \times 10^{18}/cm^2$. After the completion of ion irradiation, the topography of the sample was observed through Scanning Electron Microscope (SEM) followed by the measurement of contact angle.
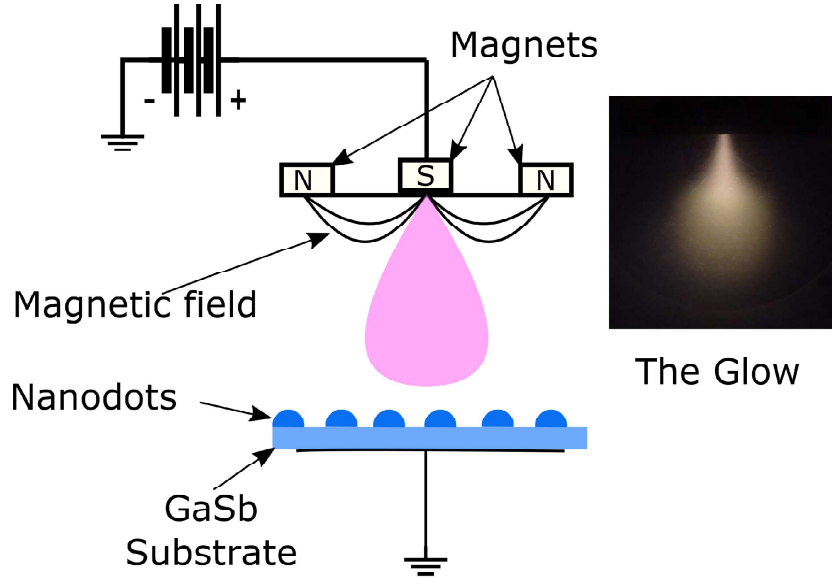
Figure 6.1: *Nanodots are formed using the fireball of magnetron. Ions from the fireball are accelerated in the sheath towards the sample.*

6.2 Results and discussion

We extract the ions from the bright droplet shaped glow for nanopatterning. Figure 6.1 shows the droplet like glow at the surface of the anode, this in fact is an anode fireball [6] as discussed in Chapter 4. Since we are using the bright droplet shaped anode fireball for nanopatterning, the impact of introducing the sample holder and the sample near the fireball needs to be taken into account. When the floating sample holder is moved towards the fireball its size increases by a small amount but no appreciable increase in the discharge current is observed. However, when the sample holder is grounded it becomes a part of the cathode which causes the discharge current to increase. The increase in the current is due to the extra cathode surface that is introduced in the vicinity of the fireball. The fireball also shows increase in brightness, this suggests an increase in the plasma density in the fireball. Figure 6.2(a) and (b) shows the discharge current for different pressure values of 1×10^{-3} *mbar* to 8×10^{-3} *mbar*. These two discharge curves are the basis

P (mbar)	V_d (V)	I_d (mA)	V_f (V)	n (cm^{-3})
1×10^{-3}	600	6	539	6×10^9
1×10^{-3}	800	12	724	3.2×10^{10}
3×10^{-3}	500	6	455.5	1.4×10^9
3×10^{-3}	450	4	406	8.5×10^8
5×10^{-3}	400	7	360.5	1.8×10^{10}
5×10^{-3} (*)	400	7	354	3×10^9

Table 6.1: *Some of the relevant plasma parameters measured with Langmuir probe. Electron temperature is in the range of $\sim 4 - 5\ eV$. Location of the measurement for the last column marked with (*) is outside the fireball, for all others the measurement is made inside the fireball on the Z axis, at $Z \sim 3\ cm$, $R = 0$.*

for deciding the operating regime of the device i.e. for choosing optimum energy and fluence for the formation of nanopattern. Fig. 6.2 (a), shows that at a pressure of $1 - 2 \times 10^{-3}\ mbar$ the discharge current could reach upto $\sim 10\ mA$ for the voltage in range of $600\ V$. A slight difference in the current value is observed when the sample holder is part of the circuit. Fig. 6.2 (b) shows that in the pressure range of $5 - 8 \times 10^{-3}\ mbar$, $8\ mA$ current could be achieved at much lower voltage of 400 V. Therefore based upon the above curve, the energy and proper current can be decided to make different types of nanodot pattern in the same given time.

Plasma parameters for the pressure and discharge voltage used in the present work are mentioned in table 6.1. These values depend upon the cathode of the discharge, hence they may differ depending upon the surface area and the size of the vacuum chamber . As can be seen from the last two rows, the plasma density inside the fireball is $1.8 \times 10^{10}\ cm^{-3}$ whereas outside the fireball it is $3 \times 10^9\ cm^{-3}$ for $400\ V$ discharge voltage at $5 \times 10^{-3}\ mbar$. This is why we need to place our sample as close to the fireball as possible, without disturbing the discharge. The plasma density is related to the discharge current, for a similar discharge current the plasma density is expected to be similar. This fact can be used to optimize the process. The fluence is dependent on the plasma density and the energy of the ions depends upon the discharge voltage. As mentioned in the introduction
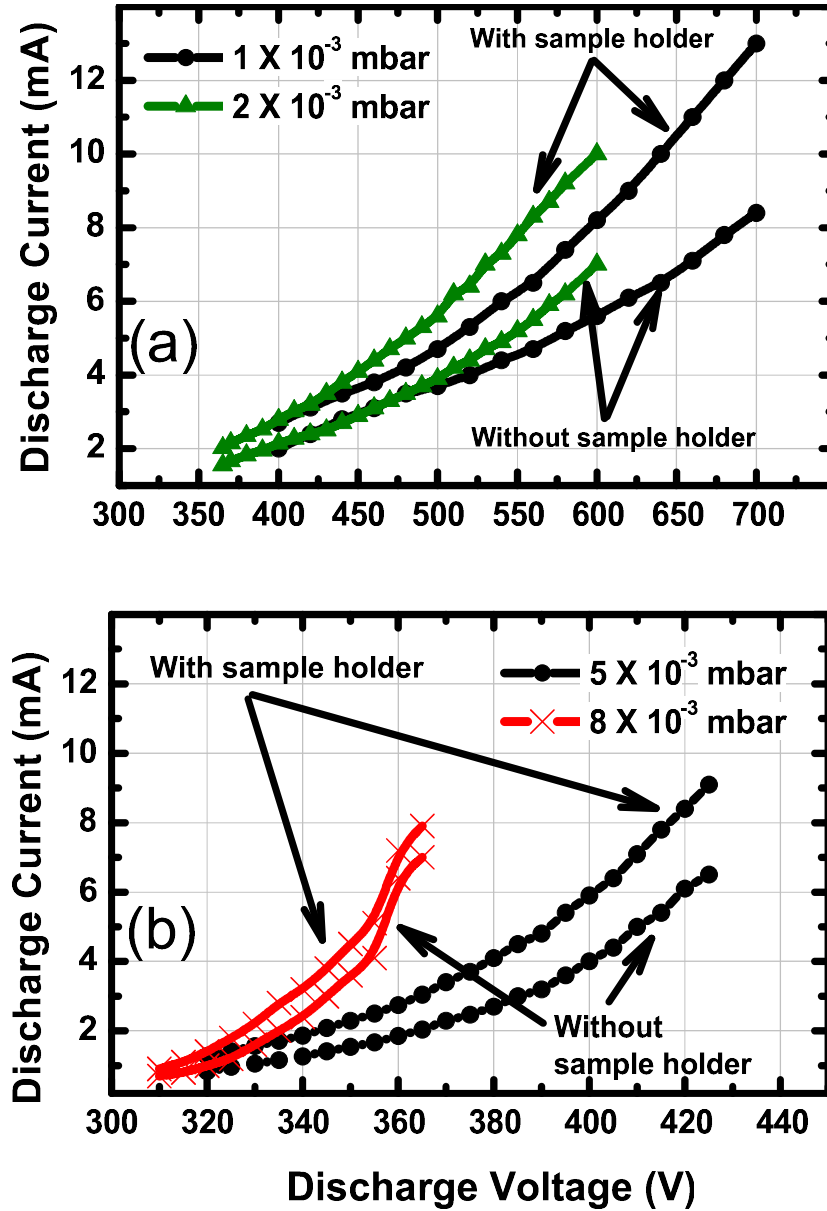
Figure 6.2: *Discharge current for different pressure, with and without the sample holder connected to the ground. In the selected pressure regime the discharge current increases in the presence of sample holder, however the increase is most significant for the low pressure range.*

the two main parameters that determine the structure of the nanopattern are the ion energy and fluence. Estimation of each of these parameters can be done in the following manner.

6.2.1 Ion energy

The source of ion energy is in the sheath that is formed around the sample and the holder. Since both are grounded along with the wall of the vacuum chamber, they all act as the cathode of the device. A visible cathode sheath forms near the sample and its holder. This cathode sheath typically has a large potential fall of the order of the discharge voltage. From earlier experiments [6] it is known that the anode of our discharge is about 50 V above the plasma potential, hence the cathode fall in our case would be ~ 50 V less than the applied discharge voltage.

Ions in the plasma will accelerate down the cathode sheath to form an almost monoenergetic beam. This beam forms the nanopattern as observed on the GaSb sample. Formation of the sheath ensures that the angle of incident is always 90° (parallel (0°) to surface normal). Accurate estimation of the ion energy when the sample is kept very close to the fireball can be determined by measuring the plasma potential inside the fireball.

6.2.2 Fluence

It is necessary to estimate the duration of the exposure of the sample to the incident ion beam as the formation of nanodots also depend upon the fluence of the ions which is defined as the number of ions hitting a surface over the specific period of time. Depending upon the flux, the time required for a particular fluence can be calculated as below.

$$Fluence = flux \times time \tag{6.1}$$
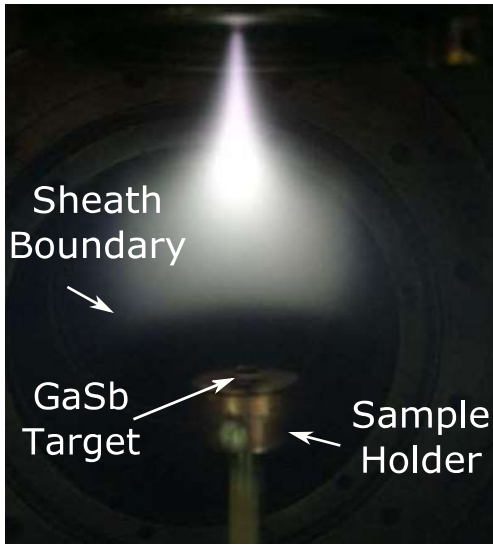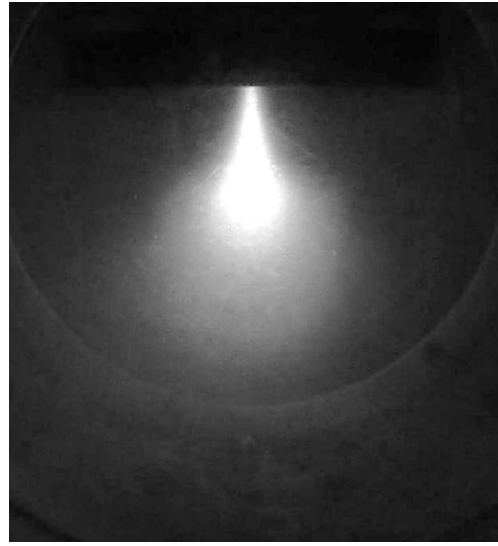
(a)   **(b)**

Figure 6.3: *(a) The sample and holder act as part of the cathode and a high voltage sheath forms near the sample. The sheath voltage depends upon the discharge voltage, and is typically few tens of volts below the discharge voltage. (b) A fireball in absence of the sample.*

The flux of the ions can be calculated by measuring the plasma density and electron temperature of the fireball, since this fireball is essentially in contact with the substrate and forms an ion sheath. Taking the plasma parameters from earlier chapters, for plasma density of the order of $\sim 1 \times 10^{10}$ cm^{-3} and electron temperature of 4 eV, using the Bohm criterion of sheath formation, the flux is given by,

$$flux = 0.6n\sqrt{\frac{KT_e}{M_i}} \qquad (6.2)$$

where, n is plasma density, K is Boltzmann constant, T_e is electron temperature and M_i is the mass of the Argon ion. For our case, the flux is $\sim 1.8 \times 10^{15}$ $cm^{-2}s^{-1}$ for fluence to be $\sim 6 \times 10^{18}$ ions$/cm^2$ the time turns out to be ~ 60 minutes. These values lie within the range of the fluence and the flux reported in the literature for making nanodot structure using conventional ion sources [115]. The flux is a weak function of the electron temperature, hence, accurate measurement of plasma density inside the fireball is very important to quantitatively estimate the duration for the process.

6.2.3   Surface materials properties

SEM images of the observed structure of nanodots prepared at 400, 600, 800 and 1000 V are shown in Fig. 6.4. The regular nanodot structures are clearly visible, prepared using our technique without the use of any additional ion source. The effect of incident ion energy is clearly seen in the micrographs; reduced diameter and inter-dot spacing at lower bias voltage is consistent with earlier reports. The observed trend is found to be in agreement with other published results [114]. The SEM images clearly demonstrate that this technique can be utilised to develop periodic nanostructures.

To test the hydrophobicity of our nanodot structures, we performed contact angle measurements and compared against the untreated wafer. The contact angle
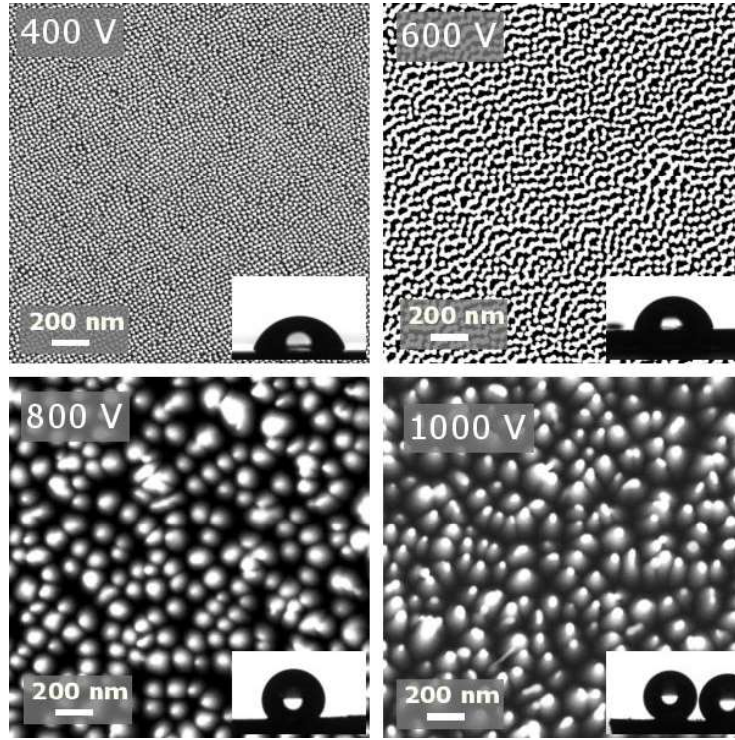
Figure 6.4: *SEM images of nanodots formed with at 400, 600, 800 and 1000 V. Insets shows the contact angle of water droplet on the patterned surface.*

of water measured on the nanopatterned surface of GaSb is shown in figure 6.5. For bias voltage of 400 V and 600 V, the contact angle is $\sim 74°$ and $\sim 81°$, respectively. Nanodot structures formed on the substrates biased at 800 V and 1000 V show clear hydrophobic nature with contact angle of $\sim 126°$ and $\sim 150°$, respectively. This is also an interesting result, since hydrophobic coatings are needed for many applications, and through our process it can be done in a single step by making nanopattern. This may be utilized as a property in many applications where hydrophobic materials are preferred.
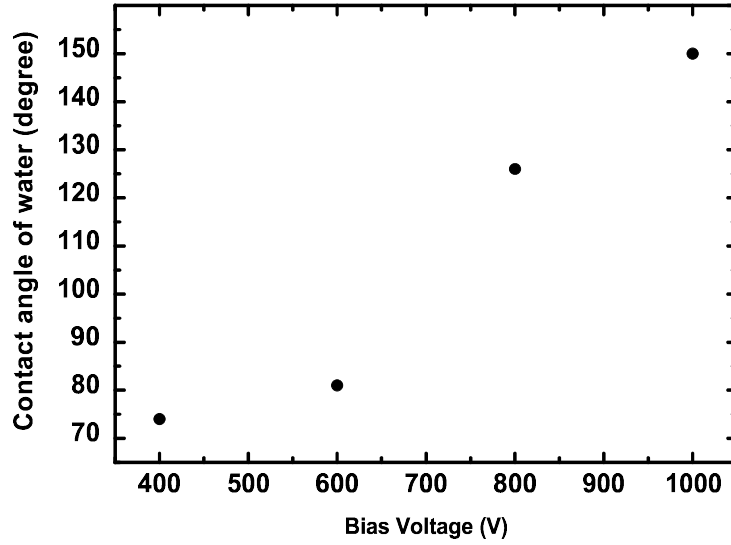
Figure 6.5: *Contact angle of water measured on the nanodots formed at 400, 600, 800 and 100 V bias, on the GaSb wafer.*

6.3   Anode stops

We have seen in Chapter 5 that the C-Mode glow was not stable during high pressure and switched to the so called P-Mode. In the present chapter we have analysed a possible application of the C-Mode discharge of the device. At low pressure, the discharge current and plasma density is low compared to high pressure discharge, the trade off of high pressure besides the switching of the glow is possible arcing in the device and frequent collisions. To limit the switching of the glow we have developed Anode Stops, the term is used in analogy with optics where the peripheral region of lens is blocked using optical stops to avoid aberration. Annular ring made of insulating Teflon is made which blocks the peripheral regions of the anode, as shown in figure 6.6. The opening of the annular ring selectively exposes central region of various diameter to the plasma.

For low pressure ($< 2 \times 10^{-2}$ $mbar$) there is no visual difference in the C-Mode discharge even when only 12 mm opening was kept in the center, which is smaller

Figure 6.6: *The photograph of actual anode stop, it is mounted on the surface of the anode, the peripheral region is hence blocked from the plasma*

than the diameter of central magnet. Figure 6.7 shows the I-V of the discharge for two different pressure and openings including the full anode without any anode stops. As can be seen, for low pressure and low voltage the I-V curve are almost identical, hence we can conclude that the anode stops do not affect the discharge in the low pressure low voltage discharge i.e. the C-Mode glow. This also backs our earlier claim that only the small central area of the anode is exposed in the C-Mode glow. The electrons guided by the magnetic field naturally go to the central region and the anode stops have no effect, however, this changes when we go to the high voltage or higher pressure. The pressure we have chosen $(4 \times 10^{-2} \ mbar)$ is on the verge of critical pressure required for the C-Mode to P-Mode transition, hence we can clearly see the effect when the voltage is raised. As can be seen form figure 6.7, there is no transition of the anode fireball from C-Mode to P-Mode, even for the pressure above the critical pressure.
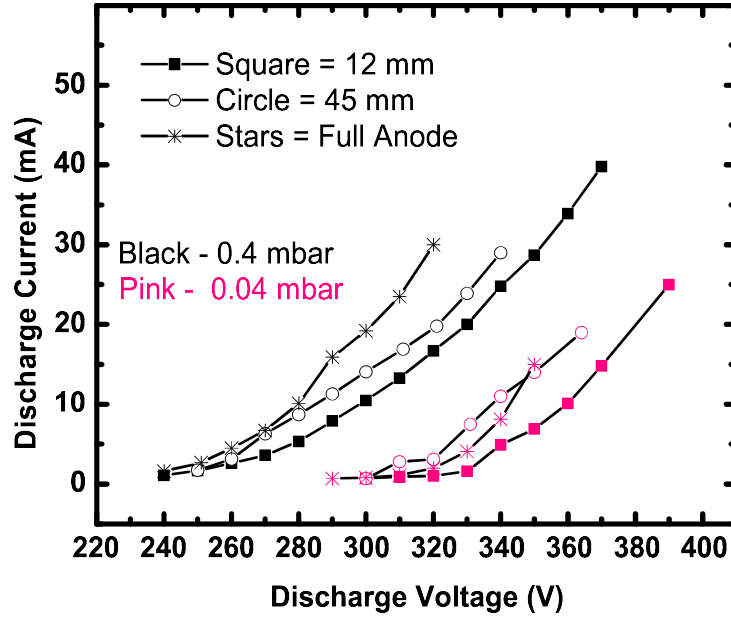
Figure 6.7: *The I-V of the discharge for two different pressures using anode stops with different openings.*

6.4 Summary

In the present chapter we have outlined two important aspects of the C-Mode and P-Mode discharge. The device is demonstrated for use in nanopatterning. The structured nanodots on GaSb are formed by preferential sputtering by ions. Such an experiment is usually assisted by a dedicated ion beam source which is complicated, usually requiring a separate setup. Our use of DC sputter magnetron for the formation of nanodots may open new research windows. The ion beam is formed due to the presence of the cathode sheath near the GaSb substrate. The fireball formed in the C-Mode helps to achieve very low pressure operation and a localized high density plasma, which otherwise would not have been possible. Ion energy and fluence are two important aspect of the process, the ion energy can be controlled by applied voltage. Once the energy is fixed, the fluence can be calculated from the local plasma density and the electron temperature in the

fireball. The fluence depends upon the flux of the ions, which in turn is proportional to the plasma density. The plasma density can be related to the discharge current. Hence by controlling the discharge current, the flux and fluence can be controlled. For constant voltage, the pressure may be varied to change discharge current and flux. Lastly, the fluence can also be controlled by changing the duration of the exposure of the sample to the plasma.

The anode stops are used to restrict the plasma in C-Mode discharge. As expected in the low pressure regime the behaviour of the plasma remained the same. Even for higher pressure above the critical value, the C-Mode is sustained.

7

Conclusions and future scopes

7.1 Conclusions

Fireballs are mostly produced by a physically small anode used as a secondary electrode, also known as the auxiliary electrode. In the present thesis we have reported a novel concept of magnetically constricted anode to produce relatively large sized fireball without using any auxiliary electrode. Though the device uses strong permanent magnets that create complicated magnetic field with large gradients and curvature near the surface of the anode, the fireball is produced largely in the weak magnetic field region. We have observed two stable modes of operation, mainly depending on background pressure, called as the C-Mode and P-Mode. The anode glow is a result of the electron sheath near the anode, the potential profile clearly indicates the accelerating region for the electrons. The anode double layer is formed near the boundary of the anode glow or fireball. The electrons gain energy from this double layer profile and cause ionization and excitation in the fireball, resulting in the bright glow. In the prsent work, the discharge properties and the fireball characteristics are studied and reported in detail.

It is observed that the plasma potential measured with respect to the laboratory ground is very high, on the range of few hundreds of volts. This is due to the experimental constraint which requires us to ground the cathode of the DC discharge. Since the plasma potential and the floating potential are generally closer to the anode it appears on the order of full discharge voltage. This puts serious limitations for a single Langmuir probe measurement as the sweeping voltage has to have a range comparable to discharge voltage. This limitation was overcome with the use of double Langmuir probe, which does not require a ground and can be biased with respect to each other. Standard single and double Langmuir probes and Emissive probe are used for measuring various plasma parameters. It is revealed that the fireball is separated by a potential double layer from the bulk plasma. This double layer has potential difference equivalent to the ionization potential of the Argon gas. It is argued that such a fireball cannot form if the whole surface of the anode is in contact with the plasma. Using various arguments mostly related to the loss of the particles, it is established that the plasma must be restricted only to the central region of the anode to explain the observed phenomena.

It is observed for the first time that the fireball can be attached to two different locations on the anode, depending upon the background pressure. It was qualitatively explained on the basis of collisional diffusion of plasma into the magnetic field. This transition from one place to another is a very interesting observation and sets a bedrock for the future investigation of similar device, especially because the device may have a commercial value as described in Chapter 6.

The device provides a localized plasma at very low pressure, which is otherwise very difficult to achieve. This can effectively be used as a broad beam ion source for various applications and also for thin film growth or nanofabrication by utilizing a DC sputter magnetron. We have demonstrated the example of nanodot formation on the GaSb substrate using our device, the reflection spectra and surface wettability is measured and shown to have marked effect.

The main results of the thesis can be highlighted as follow,

- Large size fireball can be formed on the large anode using the magnetic field to restrict the area of the anode. The fireball harbours the potential double layer at the visible boundary of the glow.

- Measured potential profile proves that the origin of all of the ions inside the fireball is due to the ionization by the electrons accelerated in the double layer. No ions from the background plasma can cross the potential barrier of the fireball.

- The plasma makes contact with the anode at different locations depending upon the pressure. The two locations produce the C-Mode and P-Mode anode fireball.

- C-Mode glow is not stable at high pressure and a transition is observed from C-Mode to the P-Mode. The transition is marked with a sudden rise in the discharge current and global oscillations of the plasma parameters such as floating potential, light and the discharge current.

- The transition from C-Mode to P-Mode is triggered when the root width of the glow reaches the physical diameter of the central magnet, beyond which the magnetic field does not penetrate the surface of the anode and hence the plasma cannot make contact with the anode. Near the surface the magnetic field is very high and plasma remains magnetized for highest pressure reached in experiment.

- The transition can be stopped using anode stops, which forces the discharge to remain in the C-Mode.

- C-Mode can potentially be used for nanopatterning. Sputter magnetron can be used for both nanopatterning and nanoparticle growth opening up unique

possibilities.

- P-Mode is accompanied by global oscillations in the discharge current, floating potential and light emission. They are typically in the range of $\sim$ $5 - 7 \ kHz$.

The thesis also outline the problems that can be studied in future, e.g. the transition and oscillation mechanism, application as ion source, fireball dynamics under various gases and the diffusion of the electron into magnetic field in presence of an electron sheath. The setup can be used for getting insights into ultra low pressure DC glow discharge which remains an unexplored problem. The use of RF power supply can also be studied in future.

7.2 Future Scopes

7.2.1 Effect of different gases on the glow transition

It is clear by now that the transition from C-Mode to P-Mode is due to the increased width of the root of the plasma in contact with the anode. This broadening is due to the collisional diffusion of the electrons in the magnetic field. In presence of the magnetic field the electrons strictly follow the field line. The cross field diffusion of the electrons is of prime importance in many cross field devices, for a deeper insight the reader may refer to the recent tutorial by Boeuf [116] and references therein. One of the important mechanisms for cross field diffusion in our case is the electron neutral collision. The collision can abruptly change the momentum of the electrons and allow them to diffuse to a different area in the magnetic field.

For all of our experiments in the present thesis we have used the Argon gas. The collision cross section of the electron with Argon atom is $\sim 1 \times 10^{-15} \ cm^2$. If we use a different gas the collision cross section and hence the mean free path would vary, this has a significant effect on the critical pressure of the transition.
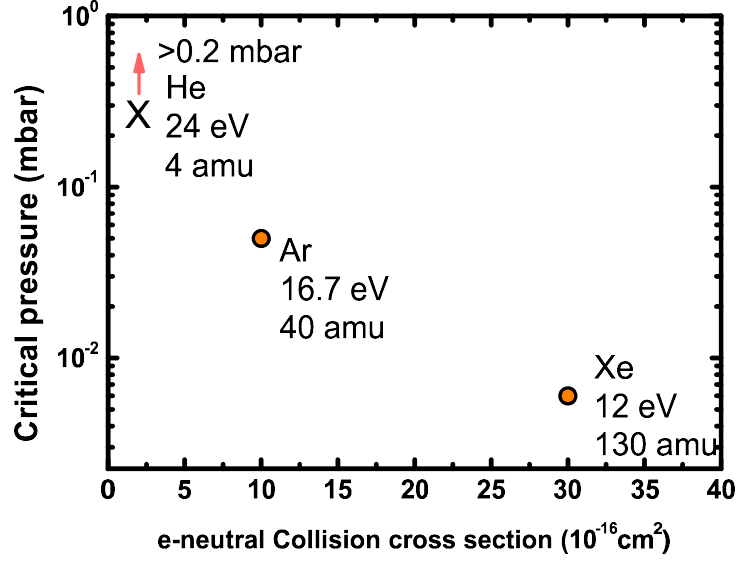
Figure 7.1: *Effect of various gases on the critical pressure for the transition. For Helium the transition did not occur for pressure as high as 7×10^{-1} mbar. Xenon, on the other hand showed transition at a much lower pressure than Argon.*

We have performed few experiments, the results of which are plotted in figure 7.1. For Xenon gas which has a larger cross section than Argon, the critical pressure is found to be $\sim 6 \times 10^{-3}$ *mbar*, above which the glow switches to the P-Mode. This is significantly lower than the critical pressure for Argon which is 5×10^{-2} *mbar*. On the other hand, for Helium with a much lower cross section, the transition never occurs upto the pressure of 2×10^{-1} *mbar* which is the limit of our experimental setup.

This work can be expanded in future to gain a deeper understanding of the transition, the role of collisions and the effect of different gas mixture. This can also shed light on the leakwidth of the magnetic cusp in the presence of different gases. Extensive experiments may lead to a proper modelling or an empirical relation between the critical pressure and the collision cross section. It is to be noted that there are other variables as well, such as the mass of the ion and the ionization potential of individual gas which can be properly investigated for their

role in the transition.

7.2.2 Effect of the Magnetic field

For our experiments we have exclusively used permanent magnets, however such a device can also be fabricated with an electro magnet. This design would be significantly more complex and time consuming but would offer absolute control over the magnetic field. By varying the magnetic field the contact area of the anode can be varied and various sheath formations can be studied. Such experiments would compliment the measurement presented in the thesis and the idea presented in Section 7.2.1. The strength of the magnetic field may also play a crucial role and the pressure, currently not accessible by the C-Mode may become viable.

7.2.3 Modelling of the transition

In continuation of the above mentioned ideas, a physical model may be developed to understand and control the transition. If the role of magnetic field and the effect of different gases is investigated, it may greatly aid the modelling part. Models developed by Song et al. [37] and Baalrud et al. [3] can be extended for the present case. Simulation of the anode region may also be performed by simplifying the problem as follows. The fireball boundary may be taken as an electron emitting cathode with the electrons having certain initial energy. The current may be specified on the boundary to let the problem evolve self consistently. A detailed simulation will go a long way to understand the mechanism of the transition. This may be of interest to the research groups working in the domain of cusp magnetic fields.

7.2.4   Detailed investigation of the P-Mode oscillations

The P-Mode is accompanied by the presence of the global oscillations in the discharge parameters. The origin of these oscillations is not fully understood in the context of our experiment. The time scale of the oscillations suggest possible predator-prey cycle in the intense ionization zone of the P-Mode glow. In Chapter 6 (Section 6.3, page 91) we have seen that the oscillations are present even when the P-Mode is blocked by the means of the anode stops. Hence, any P-Mode specific mechanism is ruled out. If the C-Mode is forced by the anode stops, the oscillations still appear when the pressure reaches the typical P-Mode value. These oscillations can also be studied by the techniques of the non-linear dynamics [117].

7.2.5   Development of ion source

The device used in C-Mode can be adapted to be used as an ion source. Multiple extraction grids can be employed near the anode to harness ions from the C-Mode fireball. We have planned to use two grid ion extraction system to obtain the ions of desired energy. First grid would screen the electrons by forming the sheath, second grid would be biased to various voltages to extract the ions. The voltage on the second grid would control the ion energy. The housing of the grid can be differentially pumped to control the collisions and loss of the plasma.

Appendix

Some of the practical formulas are listed below for obtaining various length and frequency related to plasma. Units used for various quantities are as follow, Plasma density n_e is in cm^{-3}, Electron temperature T_e is in eV, Magnetic field B_0 in $gauss$, Mass of Ion A_R in amu.

- Debye length

$$\lambda_d = 740\sqrt{\frac{T_e}{n_e}}\ cm \qquad (7.1)$$

- Plasma frequency

$$\frac{\omega_p}{2\pi} = f = 9000\sqrt{n_e}\ Hz \qquad (7.2)$$

- Electron Gyrofrequency

$$f_{ce} = \frac{\omega_{ce}}{2\pi} = 2.8B_0\ MHz \qquad (7.3)$$

- Electron Gyroradius

$$r_{ce} = \frac{3.37\sqrt{E}}{B_0}\ \ cm\ \ (E\ \text{ is energy or temperature in eV}) \qquad (7.4)$$

- Ion Gyrofrequency

$$f_{ci} = \frac{\omega_{ci}}{2\pi} = \frac{1.52B_0}{A_R}\ KHz \qquad (7.5)$$

- Ion Gyroradius

$$r_{ci} = \frac{144\sqrt{EA_R}}{B_0}\ \ cm\ (E\ \text{ is energy or temperature in eV}) \qquad (7.6)$$

- Ion-neutral mean free path

$$\lambda_i \approx \frac{1}{330p} \quad cm \quad (p \text{ in torr}) \tag{7.7}$$

This ion-neutral mean free path approximate value using the order of magnitude for typical ion neutral collision cross section($\sigma \approx 10^{-14} \ cm^2$) of a *typical* ion in its parent gas. (For details see chapter 3, page 80 of Lieberman and Lichtenberg [83]).

The tables given below outlines some of the length and time scales related to the plasma condition outlined in the thesis.

All length scales listed below are for Argon gas. Pressure range is 10^{-2} to $10^{-3} \ mbar$, plasma density $\sim 10^8$ to $10^{10} \ cm^{-3}$, magnetic field $\sim 100 - 500 \ G$, unless otherwise specified. The energy of thermal ion is 0.025 eV and for sheath ion it is 15 eV. Electron temperature is taken as 4 eV. CT- Charge transfer, MT - Momentum transfer.

Table 7.1: *Table of length scales*

Length	
Debye length - λ_d	0.16 - 1.6 mm
Electron gyro radius - r_e	0.1 - 1 mm
Ion (Thermal) gyro radius - r_i	3 - 14 mm
Ion (Sheath) gyro radius - r_i	57 - 288 mm
Ion - Neutral mfp (Elastic)	12 - 124 mm
Ion - Neutral mfp (CT)	7.4 - 74 mm
Electron - Neutral mfp (MT)	38- 380 mm

Table 7.2: *Table of frequency scales*

Frequency	
plasma frequency - f_p	284.6 *MHz*
Electron gyro frequency - ω_{ce}	280 *MHz* - 1.4 *GHz*
Ion gyro frequency - ω_{ci}	3.8 - 19 *KHz*
Ion - Neutral collision frequency (Elastic)	0.2 - 2.8 *KHz*
Ion - Neutral collision frequency (CT)	0.4 - 4 *KHz*
Electron – Neutral collision frequency (MT)	3.8 -38 *MHz*

Bibliography

[1] EV Barnat, GR Laity, and SD Baalrud. Response of the plasma to the size of an anode electrode biased near the plasma potential. *Phys. Plasmas*, 21 (10):103512, 2014. doi:10.1063/1.4897927.

[2] Brett Scheiner, Scott D Baalrud, Benjamin T Yee, Matthew M Hopkins, and Edward V Barnat. Theory of the electron sheath and presheath. *Phys. Plasmas*, 22(12):123520, 2015. doi:10.1063/1.4939024.

[3] S D Baalrud, B Longmier, and N Hershkowitz. Equilibrium states of anodic double layers. *Plasma Sources Sci. Technol.*, 18(3):035002, 2009. doi:10.1088/0963-0252/18/3/035002.

[4] M A Mujawar, S K Karkari, and M M Turner. Properties of a differentially pumped constricted hollow anode plasma source. *Plasma Sources Sci. Technol.*, 20(1):015024, 2011. URL http://stacks.iop.org/0963-0252/20/i=1/a=015024.

[5] J Gruenwald, J Reynvaan, and P Knoll. Creation and characterization of inverted fireballs in h 2 plasma. *Physica Scripta*, 2014(T161):014006, 2014. doi:10.1088/0031-8949/2014/T161/014006. URL http://stacks.iop.org/1402-4896/2014/i=T161/a=014006.

[6] S Chauhan, M Ranjan, M Bandyopadhyay, and S Mukherjee. Droplet shaped anode double layer and electron sheath formation in magnetically constricted anode. *Phys. Plasmas*, 23(1):013502, 2016. doi:10.1063/1.4939029.

[7] J P Sheehan and N Hershkowitz. Emissive probes. *Plasma Sources Sci. Technol.*, 20(6):063001, 2011. doi:10.1088/0963-0252/20/6/063001.

[8] J P Sheehan, Yevgeny Raitses, Noah Hershkowitz, Igor Kaganovich, and N J Fisch. A comparison of emissive probe techniques for electric potential measurements in a complex plasma. *Phys. Plasmas*, 18(7):073501, 2011. doi:10.1063/1.3601354.

[9] S D Baalrud, N Hershkowitz, and B Longmier. Global nonambipolar flow: Plasma confinement where all electrons are lost to one boundary and all positive ions to another boundary. *Phys. Plasmas*, 14(4):042109, 2007. doi:10.1063/1.2722262.

[10] S. Chauhan, M. Ranjan, M. Bandyopadhyay, and S. Mukherjee. Observation of mode transition and low-frequency oscillations in magnetically constricted anode. *Physics of Plasmas*, 23(12):123524, 2016. doi:10.1063/1.4972533.

[11] F.F. Chen. *Introduction to Plasma Physics and Controlled Fusion*. Number v. 1 in Introduction to Plasma Physics and Controlled Fusion. Springer, 1984. ISBN 9780306413322. doi:10.1007/978-1-4757-5595-4.

[12] Yuri P Raizer and John E Allen. *Gas discharge physics*, volume 2. Springer Berlin, 1997. URL http://www.springer.com/in/book/9783642647604.

[13] Jean-Pierre Boeuf and E Marode. A monte carlo analysis of an electron swarm in a nonuniform field: the cathode region of a glow discharge in helium. *Journal of Physics D: Applied Physics*, 15(11):2169, 1982. doi:10.1088/0022-3727/15/11/012.

[14] T. J. Sommerer, W. N. G. Hitchon, and J. E. Lawler. Self-consistent kinetic model of the cathode fall of a glow discharge. *Phys. Rev. A*, 39:6356–6366, Jun 1989. doi:10.1103/PhysRevA.39.6356. URL http://link.aps.org/doi/10.1103/PhysRevA.39.6356.

[15] T. J. Sommerer, J. E. Lawler, and W. N. G. Hitchon. A framework for modeling the cathode fall illustrated with a single beam model. *Journal of Applied Physics*, 64(4):1775–1780, 1988. doi:10.1063/1.341774. URL http://dx.doi.org/10.1063/1.341774.

[16] DA Doughty, EA Den Hartog, and JE Lawler. Current balance at the surface of a cold cathode. *Physical review letters*, 58(25):2668, 1987. doi:10.1103/PhysRevLett.58.2668.

[17] AV Phelps, BM Jelenković, and LC Pitchford. Simplified models of electron excitation and ionization at very high e/n. *Physical Review A*, 36(11):5327, 1987. doi:10.1103/PhysRevA.36.5327.

[18] Brian N Chapman. *Glow discharge processes*. Wiley, 1980. URL http://as.wiley.com/WileyCDA/WileyTitle/productCd-047107828X.html.

[19] Michael A Lieberman and Alan J Lichtenberg. *Principles of plasma discharges and materials processing*. John Wiley & Sons, 2005. doi:10.1002/0471724254.

[20] André Anders and Simone Anders. The working principle of the hollow-anode plasma source. *Plasma Sources Science and Technology*, 4(4):571, 1995. doi:10.1088/0963-0252/4/4/008.

[21] Benjamin T Yee, Brett Scheiner, Scott Baalrud, Ed Barnat, and Matthew Hopkins. Electron presheaths: The outsized influence of positive boundaries on plasmas. *Plasma Sources Science and Technology*, 2017. URL http://iopscience.iop.org/10.1088/1361-6595/aa56d7.

[22] B E Cherrington. The use of electrostatic probes for plasma diagnosticsâĂŤa review. *Plasma Chem. Plasma Process*, 2(2):113–140, 1982. doi:10.1007/BF00633129.

[23] Joseph E Borovsky. The dynamic sheath: Objects coupling to plasmas on electron-plasma-frequency time scales. *Phys. Fluids*, 31(5):1074–1100, 1988. doi:10.1063/1.866788.

[24] Nobie H Stone, W J Raitt, and K H Wright Jr. The tss-1r electrodynamic tether experiment: Scientific and technological results. *Adv. Space Res.*, 24 (8):1037–1045, 1999. doi:10.1016/S0273-1177(99)00551-7.

[25] David L Cooke and I A KATZ. Ionization-induced instability in an electron-collecting sheath. *J. Spacecr. Rockets*, 25(2):132–138, 1988. doi:10.2514/3.25961.

[26] Nagendra Singh and Ashford Jaggernauth. Ionization-driven plasma dynamics in a high voltage sheath of a conducting body in the ionosphere. *J. Geophys. Res.: Space Phys.*, 101(A8):17229–17242, 1996. doi:10.1029/96JA00925.

[27] R A Filatov, A E Hramov, Yu P Bliokh, A A Koronovskii, and J Felsteiner. Influence of background gas ionization on oscillations in a virtual cathode with a retarding potential. *Phys. Plasmas*, 16(3):033106, 2009. doi:10.1063/1.3080200.

[28] Yu A Kalinin, A A Koronovskii, A E Khramov, E N Egorov, and R A Filatov. Experimental and theoretical investigations of stochastic oscillatory phenomena in a nonrelativistic electron beam with a virtual cathode. *Plasma Phys. Rep.*, 31(11):938–952, 2005. doi:10.1134/1.2131130.

[29] Staffan Torvén and Dag Andersson. Observations of electric double layers in a magnetised plasma column. *J. Phys. D: Appl. Phys.*, 12(5):717, 1979. doi:10.1088/0022-3727/12/5/012.

[30] Tomaž Gyergyek, Milan Čerček, R Schrittwieser, and C Ionita. Experimental study of the creation of a fire-rod i: Temporal development of the electron energy distribution function. *Contrib. Plasma Phys.*, 42(5):508–525, 2002. doi:10.1002/1521-3986(200208)42:5<508::AID-CTPP508>3.0.CO;2-B.

[31] R L Stenzel, C Ionita, and R Schrittwieser. Dynamics of fireballs. *Plasma Sources Sci. Technol.*, 17(3):035006, 2008. doi:10.1088/0963-0252/17/3/035006.

[32] RL Stenzel, J Gruenwald, B Fonda, C Ionita, and R Schrittwieser. Transit time instabilities in an inverted fireball. i. basic properties. *Physics of Plasmas*, 18(1):012104, 2011. doi:10.1063/1.3533437.

[33] R L Stenzel. High-frequency instability of the sheath-plasma resonance. *Phys. Fluids B: Plasma Phys.*, 11(1):2273, 1989. doi:10.1063/1.859042.

[34] Neeraj Chaubey, S Mukherjee, A N Sekar Iyengar, and A Sen. Synchronization between two coupled direct current glow discharge plasma sources. *Phys. Plasmas*, 22(2):022312, 2015. doi:10.1063/1.4913227.

[35] Satoru Iizuka, Poul Michelsen, Jens Rasmussen, Roman Schrittwieser, Rikizo Hatakeyama, Koichi Saeki, and Noriyoshi Sato. Double layer dynamics in a collisionless magnetoplasma. *J. Phys. Soc. Jpn.*, 54(7):2516–2529, 1985. doi:10.1143/JPSJ.54.2516.

[36] Mircea Sanduloviciu and Erzilia Lozneanu. On the generation mechanism and the instability properties of anode double layers. *Plasma Phys. Controlled Fusion*, 28(3):585, 1986. doi:10.1088/0741-3335/28/3/005.

[37] Bin Song, N D'Angelo, and R L Merlino. On anode spots, double layers and plasma contactors. *J. Phys. D: Appl. Phys.*, 24(10):1789, 1991. doi:10.1088/0022-3727/24/10/012.

[38] Tomaž Gyergyek, Milan Čerček, Roman Schrittwieser, C Ionita, G Popa, and V Pohoata. Experimental study of the creation of a fire-rod ii: Emissive probe measurements. *Contrib. Plasma Phys.*, 43(1):11–24, 2003. doi:10.1002/ctpp.200310002.

[39] L Conde, C Ferro Fontan, and J Lambás. The transition from an ionizing electron collecting plasma sheath into an anodic double layer as a bifurcation. *Phys. Plasmas*, 13(11):113504, 2006. doi:10.1063/1.2388265.

[40] Codrina Ionitİğă, Dan-Gheorghe Dimitriu, and Roman W Schrittwieser. Elementary processes at the origin of the generation and dynamics of multiple double layers in dp machine plasma. *Int. J. Mass Spectrom.*, 233(1):343–354, 2004. doi:10.1016/j.ijms.2004.01.009.

[41] D G Dimitriu, M Aflori, L M Ivan, C Ionita, and R W Schrittwieser. Common physical mechanism for concentric and non-concentric multiple double layers in plasma. *Plasma Phys. Controlled Fusion*, 49(3):237, 2007. doi:10.1088/0741-3335/49/3/004.

[42] Matthew M. Hopkins, Benjamin T. Yee, Scott D. Baalrud, and Edward V. Barnat. The onset of plasma potential locking. *Physics of Plasmas*, 23(6): 063519, 2016. doi:10.1063/1.4953896. URL http://dx.doi.org/10.1063/1.4953896.

[43] Yeong-Shin Park, Yuna Lee, Kyoung-Jae Chung, and Y. S. Hwang. Characterization of plasma ion source utilizing anode spot with positively biased electrode for stable and high-current ion beam extraction. *Review of Scientific Instruments*, 82(12):123303, 2011. doi:10.1063/1.3664616. URL http://dx.doi.org/10.1063/1.3664616.

[44] L Oksuz and Noah Hershkowitz. First experimental measurements of the plasma potential throughout the presheath and sheath at a boundary in

a weakly collisional plasma. *Physical review letters*, 89(14):145001, 2002. doi:10.1103/PhysRevLett.89.145001.

[45] Li Yi-Ren, Ma Jin-Xiu, Zheng Yao-Bang, and Zhang Wen-Gui. Experimental studies of plasma sheath near meshes of different transmissivity. *Chinese Physics B*, 19(8):085201, 2010. doi:10.1088/1674-1056/19/8/085201.

[46] RN Franklin. The plasma–sheath boundary region. *Journal of Physics D: Applied Physics*, 36(22):R309, 2003. doi:10.1088/0022-3727/36/22/R01.

[47] K-U Riemann. The bohm criterion and sheath formation. *Journal of Physics D: Applied Physics*, 24(4):493, 1991. doi:10.1088/0022-3727/24/4/001.

[48] D Bohm. *The characteristics of electrical discharges in magnetic fields ed. By A. Guthrie and R.K. Wakerling.* National nuclear energy series: Electromagnetic Separation Project. McGraw-Hill, 1949. URL https://books.google.co.in/books?id=KyRRAAAAMAAJ.

[49] Irving Langmuir. The interaction of electron and positive ion space charges in cathode sheaths. *Physical Review*, 33(6):954, 1929. doi:10.1103/PhysRev.33.954.

[50] K-U Riemann. The influence of collisions on the plasma sheath transition. *Physics of plasmas*, 4(11):4158–4166, 1997. doi:10.1063/1.872536.

[51] Noah Hershkowitz. Sheaths: More complicated than you think a. *Physics of plasmas*, 12(5):055502, 2005. doi:10.1063/1.1887189.

[52] Jin-Yuan Liu, Zheng-Xiong Wang, and Xiaogang Wang. Sheath criterion for a collisional sheath. *Physics of Plasmas*, 10(7):3032–3034, 2003. doi:10.1063/1.1584048.

[53] L Oksuz and N Hershkowitz. Plasma, presheath, collisional sheath and collisionless sheath potential profiles in weakly ionized, weakly collisional plasma. *Plasma Sources Science and Technology*, 14(1):201, 2005. doi:10.1088/0963-0252/14/1/022.

[54] Scott Robertson. Sheaths in laboratory and space plasmas. *Plasma Physics and Controlled Fusion*, 55(9):093001, 2013. doi:10.1088/0741-3335/55/9/093001.

[55] S Mukherjee and PI John. Dynamics of a collisional ion sheath. *Pramana*, 44(1):55–66, 1995. doi:10.1007/BF02898212.

[56] TE Sheridan and J Goree. Collisional plasma sheath model. *Physics of Fluids B: Plasma Physics*, 3(10):2796–2804, 1991. doi:10.1063/1.859987.

[57] Jin-Yuan Liu, Zheng-Xiong Wang, and Xiaogang Wang. Sheath criterion for a collisional sheath. *Physics of Plasmas*, 10(7):3032–3034, 2003. doi:10.1063/1.1584048. URL http://dx.doi.org/10.1063/1.1584048.

[58] MS Benilov. The child–langmuir law and analytical theory of collisionless to collision-dominated sheaths. *Plasma Sources Science and Technology*, 18(1): 014005, 2008. doi:10.1088/0963-0252/18/1/014005.

[59] VA Lisovskiy, KP Artushenko, and VD Yegorenkov. Child–langmuir law applicability for a cathode sheath description of glow discharge in hydrogen. *Physica Scripta*, 91(8):085601, 2016. doi:10.1088/0031-8949/91/8/085601.

[60] CD Child. Discharge from hot cao. *Physical Review (Series I)*, 32(5):492, 1911. doi:10.1103/PhysRevSeriesI.32.492.

[61] Irving Langmuir. The effect of space charge and residual gases on thermionic currents in high vacuum. *Physical Review*, 2(6):450, 1913. doi:10.1103/PhysRev.2.450.

[62] Irving Langmuir. The effect of space charge and initial velocities on the potential distribution and thermionic current between parallel plane electrodes. *Phys. Rev.*, 21:419–435, Apr 1923. doi:10.1103/PhysRev.21.419.

[63] Bin Song, N D'Angelo, and Robert L Merlino. Stability of a spherical double layer produced through ionization. *Journal of Physics D: Applied Physics*, 25(6):938, 1992. doi:10.1088/0022-3727/25/6/006.

[64] Mircea Sanduloviciu, Catalin Borcia, and Gabriela Leu. Self-organization phenomena in current carrying plasmas related to the non-linearity of the current versus voltage characteristic. *Physics Letters A*, 208(1-2):136–142, 1995. doi:10.1016/0375-9601(95)00715-F.

[65] Silviu Gurlui, Marcel Agop, Mitachi Strat, Georgeta Strat, and Simona Bācāiţā. Experimental and theoretical investigations of anode double layer. *Jpn. J. Appl. Phys., Part 1*, 44(5R):3253, 2005. doi:10.1143/JJAP.44.3253.

[66] M Strat, Georgeta Strat, and S Gurlui. Basic processes in discharge plasma double layers. *Journal of Physics D: Applied Physics*, 32(1):34, 1999. doi:10.1088/0022-3727/32/1/007.

[67] Deli Tang and Paul K Chu. Anode double layer in magnetized radio frequency inductively coupled hydrogen plasma. *Journal of applied physics*, 94(3):1390–1395, 2003. doi:10.1063/1.1589592.

[68] L Conde. Ionization instability by energized electrons in weakly ionized unmagnetized plasmas. *Physics of Plasmas*, 11(5):1955–1959, 2004. doi:10.1063/1.1705651.

[69] V Lapuerta and E Ahedo. Dynamic model of a plasma structure with an intermediate double-layer, formed outside an anodic plasma contactor. *Physics of Plasmas*, 7(6):2693–2703, 2000. doi:10.1063/1.874113.

[70] RL Stenzel, J Gruenwald, B Fonda, C Ionita, and R Schrittwieser. Transit time instabilities in an inverted fireball. ii. mode jumping and nonlinearities. *Physics of Plasmas*, 18(1):012105, 2011. doi:10.1063/1.3533440.

[71] Steven L Cartier and Robert L Merlino. Anode-type double layers in a nonuniform magnetic field. *Phys. Fluids*, 30(8):2549–2560, 1987. doi:10.1063/1.866093.

[72] Tao An, RL Merlino, and N D'Angelo. Cylindrical anode double layers ('firerods') produced in a uniform magnetic field. *Journal of Physics D: Applied Physics*, 27(9):1906, 1994. doi:10.1088/0022-3727/27/9/014.

[73] Yuna Lee, Kyoung-Jae Chung, and YS Hwang. Feasibility study on high current ion beam extraction from anode spot plasma for large area ion implantation. *Current Applied Physics*, 15(12):1599–1605, 2015. doi:10.1016/j.cap.2015.09.020.

[74] SK Nema, PM Raole, S Mukherjee, P Kikani, and PI John. Plasma polymerization using a constricted anode plasma source. *Surface and Coatings Technology*, 179(2):193–200, 2004. doi:10.1016/S0257-8972(03)00822-3.

[75] M Mayer, J Reynvaan, J Gruenwald, K Krenn, T Schoeberl, S Surnev, and P Knoll. Diamond like carbon deposition by inverted fireballs. *Materials Today: Proceedings*, 3:S184–S189, 2016. doi:10.1016/j.matpr.2016.02.031.

[76] J Gruenwald, J Reynvaan, and P Knoll. Creation and characterization of inverted fireballs in h2 plasma. *Physica Scripta*, 2014(T161):014006, 2014. doi:10.1088/0031-8949/2014/T161/014006.

[77] C. S. Corr and R. W. Boswell. High-beta plasma effects in a low-pressure helicon plasma. *Physics of Plasmas*, 14(12):122503, 2007. doi:10.1063/1.2802080.

[78] S. P. Banerjee, V. P. Anitha, G. Ravi, and S. K. Mattoo. A laboratory produced extremely large beta plasma. *Physics of Plasmas*, 13(9):092503, 2006. doi:10.1063/1.2338022.

[79] I. H. Hutchinson. *Principles of Plasma Diagnostics:*. Cambridge University Press, Cambridge, 2 edition, 007 2002. ISBN 9780511613630. doi:10.1017/CBO9780511613630. URL https://www.cambridge.org/core/books/principles-of-plasma-diagnostics/93578947341481B0F9169D598D535E76.

[80] Noah Hershkowitz. 3 - how langmuir probes work. In Orlando Auciello and Daniel L. Flamm, editors, *Plasma Diagnostics*, pages 113 – 183. Academic Press, 1989. ISBN 978-0-12-067635-4. doi:http://dx.doi.org/10.1016/B978-0-12-067635-4.50008-9. URL http://www.sciencedirect.com/science/article/pii/B9780120676354500089.

[81] R.H. Huddlestone and S.L. Leonard. *Plasma diagnostic techniques*. Pure and applied physics. Academic Press, 1965. URL https://books.google.co.in/books?id=Eb08AAAAIAAJ.

[82] E. O. Johnson and L. Malter. A floating double probe method for measurements in gas discharges. *Phys. Rev.*, 80:58–68, Oct 1950. doi:10.1103/PhysRev.80.58.

[83] Michael A Lieberman and Alan J Lichtenberg. *Principles of plasma discharges and materials processing*. John Wiley & Sons, 2005. URL http://as.wiley.com/WileyCDA/WileyTitle/productCd-0471720011.html.

[84] Muhammad Yasin Naz, Abdul Ghaffar, NU Rehman, S Naseer, and Muhammad Zakaullah. Double and triple langmuir probes measurements in inductively coupled nitrogen plasma. *Progress In Electromagnetics Research*, 114: 113–128, 2011. doi:10.2528/PIER10110309.

[85] Irving Langmuir. The pressure effect and other phenomena in gaseous discharges. *Journal of the Franklin Institute*, 196(6):751–762, 1923. doi:10.1016/S0016-0032(23)90859-8.

[86] Robert F Kemp and JMs Sellen Jr. Plasma potential measurements by electron emissive probes. *Review of Scientific Instruments*, 37(4):455–461, 1966. doi:10.1063/1.1720213.

[87] L Dorf, Y Raitses, and NJ Fisch. Electrostatic probe apparatus for measurements in the near-anode region of hall thrusters. *Review of scientific instruments*, 75(5):1255–1260, 2004. doi:10.1063/1.1710698.

[88] Terrence E Sheridan, Matthew John Goeckner, and J Goree. Model of energetic electron transport in magnetron discharges. *J. Vac. Sci. Technol., A*, 8(1):30–37, 1990. doi:10.1116/1.577093.

[89] M.D. Abramoff, P.J. Magalhaes, and S.J. Ram. Image processing with imagej. *Biophotonics International*, 11:36–42, 2004. URL https://dspace.library.uu.nl/handle/1874/204900.

[90] W.S. Rasband. Imagej. URL https://imagej.nih.gov/ij/.

[91] Albert Simon. Ambipolar diffusion in a magnetic field. *Physical Review*, 98(2):317, 1955. URL http://journals.aps.org/pr/pdf/10.1103/PhysRev.98.317.

[92] Davide Curreli and Francis F Chen. Cross-field diffusion in low-temperature plasma discharges of finite lengththis article is part of the special issue âĂŸtransport in b-fields in low-temperature plasmasâĂŹ, published in plasma sources sci. technol. vol 23, issue 4 (http://iopscience. iop. org/0963-0252/23/4). *Plasma Sources Sci. Technol.*, 23(6):064001, 2014. doi:10.1088/0963-0252/23/6/064001.

[93] Serge Barral, Eduardo Ahedo, Hans-Jürgen Hartfuss, Michel Dudeck, Jozef Musielok, and Marek J Sadowski. On the origin of low frequency oscillations in hall thrusters. In *AIP Conference Proceedings*, volume 993, page 439, 2008. doi:10.1063/1.2909170.

[94] Ch Wang, L Wei, and D Yu. A basic predator-prey type model for low frequency discharge oscilations in hall thrusters. *Contrib. Plasma Phys.*, 51 (10):981–988, 2011. doi:10.1002/ctpp.201100040.

[95] Edgar Alfonso, Jairo Olaya, and Gloria Cubillos. 15 - thin film growth through sputtering technique and its applications. In Marcello Rubens and Barsi Andreeta, editors, *Crystallization - Science and Technology*, pages 397 − 432. InTech, 2012. ISBN 978-953-51-0757-6. doi:10.5772/2395.

[96] PJ Kelly and RD Arnell. Magnetron sputtering: a review of recent developments and applications. *Vacuum*, 56(3):159–172, 2000. doi:10.1016/S0042-207X(99)00189-X.

[97] H Sato, T Minami, S Takata, and T Yamada. Transparent conducting p-type nio thin films prepared by magnetron sputtering. *Thin solid films*, 236(1): 27–31, 1993. doi:10.1016/0040-6090(93)90636-4.

[98] Klaus Ellmer. Magnetron sputtering of transparent conductive zinc oxide: relation between the sputtering parameters and the electronic properties. *Journal of Physics D: Applied Physics*, 33(4):R17, 2000. doi:10.1088/0022-3727/33/4/201.

[99] I Safi. Recent aspects concerning dc reactive magnetron sputtering of thin films: a review. *Surface and Coatings Technology*, 127(2):203–218, 2000. doi:10.1016/S0257-8972(00)00566-1.

[100] DK Ball, S Günther, M Fritzsche, K Lenz, G Varvaro, S Laureti, D Makarov, A Mücklich, S Facsko, M Albrecht, et al. Out-of-plane magnetized cone-shaped magnetic nanoshells. *Journal of Physics D: Applied Physics*, 50(11): 115004, 2017. doi:10.1088/1361-6463/aa5c26.

[101] David Grosso, Cédric Boissière, Bernd Smarsly, Torsten Brezesinski, Nicola Pinna, Pierre A Albouy, Heinz Amenitsch, Markus Antonietti, and Clément Sanchez. Periodically ordered nanoscale islands and mesoporous films composed of nanocrystalline multimetallic oxides. *Nature materials*, 3(11):787–792, 2004. doi:10.1038/nmat1206.

[102] Michael C McAlpine, Habib Ahmad, Dunwei Wang, and James R Heath. Highly ordered nanowire arrays on plastic substrates for ultrasensitive flexible chemical sensors. *Nature materials*, 6(5):379–384, 2007. doi:10.1038/nmat1891.

[103] Mukesh Ranjan and Stefan Facsko. Anisotropic surface enhanced raman scattering in nanoparticle and nanowire arrays. *Nanotechnology*, 23(48):485307, 2012. doi:10.1088/0957-4484/23/48/485307.

[104] Ioannis Papadas, Joseph A Christodoulides, George Kioseoglou, and Gerasimos S Armatas. A high surface area ordered mesoporous bifeo 3 semiconductor with efficient water oxidation activity. *Journal of Materials Chemistry A*, 3(4):1587–1593, 2015. doi:10.1039/C4TA05272B.

[105] S. Facsko, T. Dekorsy, C. Koerdt, C. Trappe, H. Kurz, A. Vogt, and H. L. Hartnagel. Formation of ordered nanoscale semiconductor dots by ion sputtering. *Science*, 285(5433):1551–1553, 1999. doi:10.1126/science.285.5433.1551. URL http://www.sciencemag.org/content/285/5433/1551.abstract.

[106] S. Facsko, T. Bobek, T. Dekorsy, and H. Kurz. Ordered quantum dot formation by ion sputtering. *physica status solidi (b)*, 224(2):537–540, 2001. ISSN 1521-3951. doi:10.1002/1521-3951(200103)224:2<537::AID-PSSB537>3.0.CO;2-F. URL http://dx.doi.org/10.1002/1521-3951(200103)224:2<537::AID-PSSB537>3.0.CO;2-F.

[107] T Allmers, M Donath, and G Rangelov. Pattern formation by erosion sputtering on gasb: Transition from dot to ripple formation and influence of impurities. *Journal of Vacuum Science & Technology B*, 24(2):582–586, 2006. doi:10.1116/1.2170100.

[108] O El-Atwani, SA Norris, K Ludwig, S Gonderman, and JP Allain. Ion beam nanopatterning of iii-v semiconductors: consistency of experimental and simulation trends within a chemistry-driven theory. *Scientific reports*, 5, 2015. doi:10.1038/srep18207.

[109] Francis C Motta, Patrick D Shipman, and R Mark Bradley. Theory of nanoscale pattern formation produced by oblique-incidence ion bombardment of binary compounds. *Physical Review B*, 90(8):085428, 2014. doi:10.1103/PhysRevB.90.085428.

[110] Manijeh Razeghi, Aaron Gin, Yajun Wei, Junjik Bae, and Jongbum Nah. Quantum sensing using type ii inas/gasb superlattice for infrared detection. *Microelectronics journal*, 34(5):405–410, 2003. doi:10.1016/S0026-2692(03)00035-1.

[111] C Teichert, JJ De Miguel, and T Bobek. Ion beam sputtered nanostructured semiconductor surfaces as templates for nanomagnet arrays. *Journal of Physics: Condensed Matter*, 21(22):224025, 2009. doi:10.1088/0953-8984/21/22/224025.

[112] Lorenzo Rosa, Mukesh Ranjan, Mukul Bhatnagar, Daryoush Mortazavi, Subroto Mukherjee, and Saulius Juodkazis. Simulation and measurement of solar harvesting enhancement of silver plasmonic nanoparticles on gasb nanodots. *Journal of Photonics*, 2014, 2014. doi:10.1155/2014/327586.

[113] Chenglin Yan, Xiaopeng Li, Keya Zhou, Anlian Pan, Peter Werner, Samuel L Mensah, Alexander T Vogel, and Volker Schmidt. Heteroepitaxial growth of gasb nanotrees with an ultra-low reflectivity in a broad spectral range. *Nano letters*, 12(4):1799–1805, 2012. doi:10.1021/nl203857h.

[114] Mukul Bhatnagar, Mukesh Ranjan, and Subroto Mukherjee. Silver nanoparticles on gasb nanodots: a lspr-boosted binary platform for broadband light harvesting and sers. *Journal of Nanoparticle Research*, 17(2):100, 2015. doi:10.1007/s11051-015-2913-9.

[115] T. Allmers, M. Donath, and G. Rangelov. Pattern formation by erosion sputtering on gasb: Transition from dot to ripple formation and influence of impurities. *Journal of Vacuum Science & Technology B: Microelectronics and Nanometer Structures Processing, Measurement, and Phenomena*, 24(2): 582–586, 2006. doi:10.1116/1.2170100.

[116] Jean-Pierre Boeuf. Tutorial: Physics and modeling of hall thrusters. *Journal of Applied Physics*, 121(1):011101, 2017. doi:10.1063/1.4972269.

[117] MD. Nurujjaman. *Nonlinear dynamics experiments in glow discharge plasma.* PhD thesis, Homi Bhabha National Institute, Mumbai, 2009.